Lab on fiber technology: a nanospectroscopic approach for biochemical sensing

Author

Ángel Ortega Gómez

Universidad del País Vasco
Euskal Herriko Unibertsitatea

Bilbao, 2021

“If you trust in yourself…and believe in your dreams…and follow your star…you'll still get beaten by people who spent their time working hard and learning things and weren't so lazy”

T. Pratchett

“…por un mundo donde seamos socialmente iguales, humanamente diferentes y totalmente libres”

R. Luxemburgo

Agradecimientos

Esta tesis es el fruto de un duro trabajo de cuatro años en los que he aprendido, disfrutado, y también sufrido, puesto que la investigación no es una tarea fácil, y muchas veces genera frustración, pero el día que las cosas encajan te llena de una inmensa alegría, y tengo la sensación de que ha quedado un trabajo bonito del que sentirme orgulloso.

Gracias a mi madre y a mi padre por todo el cariño que siempre me han dado, a mi madre por enseñarme el valor del esfuerzo y ser un ejemplo de sacrificio y trabajo, y a mi padre por enseñarme que, en esta vida, lo más importante es sentirse orgulloso de uno mismo, sin esperar que el resto lo estén de ti.

Me gustaría agradecer a mis directores de tesis, Joel Villatoro y Joseba Zubia, el haberme dado la oportunidad de realizar la tesis doctoral en su grupo. En especial, a Joseba por darme libertad y confianza para afrontar la tesis y la investigación a mi manera, y a Joel por guiarme en todo momento, sobre todo al principio de la tesis, y enseñarme una metodología de trabajo en el laboratorio. Al fin y al cabo, cuando llegué nunca había realizado ningún trabajo experimental, y fueron comienzos difíciles, pero que con trabajo y dedicación se pudo superar.

También me gustaría agradecer a toda la gente del grupo *Applied Photonics Group (APG)* por su acogida. Ir a una ciudad nueva que está en la otra punta del país es difícil, pero ellos me lo han hecho sencillo. Especialmente con los que he compartido tanto tiempo en el laboratorio, Josu, Oskar, Eneko, Mikel, José, Rubén, Igor, etc. También a Ibon y Asun por dejarme impartir junto a ellos sus clases de laboratorio. Mila esker guztioi zure laguntzagatik.

Gracias también al grupo de la de Universidad de Mons (UMONS), por darme la oportunidad de aprender de la tecnología en la que son expertos en el mundo y acogerme tan bien, muchas gracias a Christophe, Méderic, Karima, Ivan, Tianbo y Maxime.

Esta tesis no hubiera sido posible sin el trabajo del grupo de *Microfluidic Cluster* de Vitoria. Ellos son la otra mitad sobre el que se sustenta este trabajo de investigación multidisciplinar tan apasionante. Gracias a todos por lo bien que me han tratado en todas las horas que he pasado en su laboratorio. A Alba, con la que he compartido tantas frustraciones, pero también alegrías, y que me ha ayudado siempre en todo lo que necesitaba. A Javi, por todo lo que me ha enseñado, por todas las horas de coche mostrándome lo que es la "buena" música, y todos los consejos que siempre me ha dado. Es un gran tipo a pesar de ser del Athletic. De esta tesis me llevo una bonita amistad de ambos.

Me gustaría agradecer a "Deustocracia" por todos los jueves de pintxo pote y los domingos de rabas. No hubiera estado tan a gusto en Bilbao si no hubiera sido por Carlos, Juan, Ana, Estela, Iván, etc. Muchas gracias por vuestra amistad. También a Lorena, Cristina y Lara por proporcionarme ese espacio en el que volcar las frustraciones de las semanas cerveza en mano y a Iker por no reírse tanto de los andaluces como podría.

Por último, gracias a Marta, por ser un apoyo incondicional desde el principio y hacerme la vida fácil. Nunca tendré suficiente tiempo en esta vida para agradecerte justamente todo lo que haces por mí.

Resumen

Hoy en día, gracias al uso de fibras ópticas, el desarrollo de sensores bioquímicos económicos y de altas prestaciones capaces de realizar medidas en tiempo real es posible, cambiando esta tecnología por la tradicional basada en equipamientos caros, grandes y complejos. Por esta razón, en esta tesis hemos desarrollado un sensor mediante nanopartículas de oro inmovilizadas en la cara de una fibra óptica. El sensor que proponemos combina las ventajas de las fibras ópticas con el efecto plasmón de las nanopartículas, que proporcionan gran sensibilidad a cambios en el medio externo. Sin embargo, la mayor novedad que esta tesis proporciona es el uso de la nano-espectroscopia. Esta técnica se basa en hacer coincidir las frecuencias de resonancia de las nanopartículas con el elemento bioquímico que se quiera detectar, consiguiendo altos niveles de selectividad y sensibilidad, en contraposición con los métodos convencionales que se basan en medir cambios en longitud de onda de la frecuencia de resonancia de las nanopartículas. Para demostrar la validez de la nano-espectroscopia en la punta de una fibra óptica, se han realizado medidas para detectar iones de cobre (II) y Citocromo c, consiguiendo unos límites de detección varios órdenes de magnitud por debajo de los sensores basados en nano-espectroscopia mediante microscopios. Además, esta tesis contribuye también a un mayor entendimiento del proceso de inmovilización de las nanopartículas en la fibra óptica gracias a la amplia caracterización que se ha realizado.

Abstract

Lab-on-fiber represents a promising technology for developing cost-effective and high-performance biochemical sensors to conduct *in vivo* measurements, unlike conventional sensors that require bulky, complex, and expensive equipment. For that reason, in this work, a sensor based on gold nanoparticles attached to the end face of a multimode optical fiber has been developed. This thesis contributes to a deep characterization of the gold nanoparticles immobilization process on the optical fiber end face. In addition, the novelty of this thesis radiates in the detection method: the nanospectroscopy. This technique relies on the match between the resonance frequency of the used gold nanoparticles and the biochemical target under study, modifying the intensity of the gold nanoparticles spectrum; in contrast to traditional methods based on monitoring the shift of the gold nanoparticles resonance frequency that may cause a lack of selectivity. In order to demonstrate the performance of the aforementioned detection method combined with optical fibers, copper ions (II) and Cytochrome *c* were measured, with limits of detection of 1 pM and 60 nM, respectively. These sensitivities are several orders of magnitude above other nanospectroscopic sensors that use microscopes as optical platforms. The proposed sensor combines the advantages of optical fibers, the localized surface plasmon resonance effect and nanospectroscopy as the detection method, which allows developing highly selective and sensitive sensors as we prove.

Table of contents

List of figures

List of tables

List of acronyms/abbreviations

3D	Three-dimensional
AFM	Atomic Microscope Force
AgNPs	Silver nanoparticles
apoE	Antipoliprotein E
APTES	Aminoproyltriethoxysilane
AuNPs	Gold nanoparticles
CCD	Charge Coupled Device
Cr	Chromium
Cu	Cooper
Cu^{2+}	Copper ions (II)
CLU	Cluster
Cytochrome c	Cyt c
EBL	Electron-Beam Lithography
EDTA	Ethylenediaminetetraacetic acid
FBGs	Fiber Bragg Gratings
FIB	Focus Ion Beam
FOC	Fiber Optical Coupler
FRET	Fluorescence Resonance Energy Transfer
H_2O_2	Hydrogen peroxide
H_2SO_4	Sulfuric acid
HCF	Hollow Core Fiber
HCl	Hydrochloric acid
Hg	Mercury
IoTs	Internet of Things
LPGs	Long Period Gratings
LED	Light-Emitting Diode
LoD	Limit of Detection

LSPR	Localized Surface Plasmon Resonance
MMFs	Multimode Optical Fibers
MPA	Mercaptopropionic acid
MS	Mass Spectrometry
NA	Numerical aperture
$Na_2S_2O_4$	Sodium dithionite
Ni	Nickel
Pb	Lead
PBS	Phosphate Buffered Saline
PCFs	Photonics Crystal Fibers
POC	Point-of-Care
PRET	Plasmon Resonance Energy Transfer
PSA	Prostate Specific Antigen
QCM	Quartz Crystal Microbalances
QD	Quantum dots
ROS	Reactive oxygen species
RSD	Relative standard deviation
SEM	Scanning Electronic Microscopy
SERS	Surface-Enhanced Raman Spectroscopy
SPR	Surface Plasmon Resonance
STD	Standard deviation
TFBGs	Tilted Fiber Bragg Gratings
TM	Transverse-magnetic
TMSen	N-[3-(trimethoxysilyl)propyl] ethylediamine
TNT	Trinitrotoluene
WHO	World Health Organization
XPS	X-ray Photoelectron Spectroscopy
ZnO	Zinc oxide

1. Introduction

The combination of optical fibers and metal nanoparticles has caught the attention of many researchers in the last decade, due to the potential that this technology provides to the field of biochemical sensing. This potentiality relies on the demanding necessities from the society, such as the detection in real time of diseases, contaminants, etc. In addition to this, it is mandatory to reduce the cost of the sensors to expand their usefulness to all society. To that end, optical fibers represent a promising platform to meet such necessities.

Several approaches based on this combination have been developed trying to resolve the next question: How could we increase the sensitivity of the sensors? In other words, how could we reduce the limit of detection (LoD) when we measure a certain sample? In this thesis, we will introduce our contribution to this field with a novel detection approach combined with optical fibers.

In this chapter, we will introduce the most relevant objectives proposed in this thesis, and, then, we will explain the structure of it, introducing the general idea of each chapter and the storyline.

1.1. Objectives of the thesis

The main objectives of the thesis are summarized in the following points:

- **To design and manufacture a biochemical sensor based on the lab-on-fiber technology to increase the sensitivity and reduce the LoD of current sensors.** To that end, the work proposed in this thesis is based on combining optical fibers and gold nanoparticles. On the one hand, the advantages that optical fibers provide are electromagnetic immunity, cost-effective, the possibility to measure remotely and in real

time, etc., and, on the other hand, gold nanoparticles provide, essentially, high sensitivity thanks to the plasmonic effect.

- **Study and characterization of the manufacturing process**. To develop the sensor, it is mandatory to characterize deeply the manufacturing process first. To that end, spectral characterization and image analysis were conducted. The main goal of both characterizations is to understand, and therefore, to control the immobilization of AuNPs on the optical fiber end face to increase the reproducibility of the manufacturing process.
- **Study of new approaches to developing selectivity sensors**. In order to address this objective, we propose a novel detection approach for optical fibers, the nanospectroscopy, which allows improving the selectivity of the sensors, as we will discuss in the results.
- **To prove that applying the nanospectroscopic approach by optical fibers, high-performance sensors can be developed.** According to that, the sensor developed was designed for a chemical and biological application, copper ions (II) Cu^{2+} and Cytochrome c (Cyt c) detection respectively.

1.2. Structure of the thesis

The thesis has been structured according to the objectives explained in the previous section. The intention is to expose a storyline with the aim to emphasize the novelty that this thesis provides. In this section, we explain the main idea of each chapter of the thesis, and thus, we can contribute to a better comprehension of this thesis by the following scheme:

- **Chapter 1. Introduction**. Here, the main objectives of the thesis are presented. Each one of these objectives is complemented with a brief idea about the manner to address it. In addition, a scheme of the

structure of the thesis is included with the aim of facilitating the comprehension of the thesis.

- **Chapter 2. State of the art.** In this chapter, the state of the art of biochemical sensors and, particularly, of lab-on-fiber technology, is detailed. First, we describe briefly the main features of biochemical sensors, and, then, we focus on optical sensors. Among all the different optical approaches, we focus on optical fibers and the combination of those with the plasmonic phenomena, which are explained as well. We finish the chapter analysing the novelty that this thesis brings to the state of the art.
- **Chapter 3. Fiber probe manufacturing.** A deep characterization of the manufacturing process of our lab-on-fiber-based probe is shown in this chapter. In particular, a study centre on the immobilization process of gold nanoparticles (AuNPs) on the optical fiber facet is done by a spectral characterization and image analysis. The impact of the temperature, the optical fiber used and the concentration of AuNPs on the immobilization process have been studied as well.
- **Chapter 4. Chemical sensing application: copper ions (II) detection.** This chapter is related to the chemical application of the sensor proposed in this thesis, in particular, for Cu^{2+} detection.
- **Chapter 5. Biosensing application: Cytochrome c detection.** Equivalent to Chapter 4, here we show the results of the sensors in a biological application. The main motivation to detect this protein is shown, and the results obtained are discussed as well.
- **Chapter 6. Conclusions and future directions**. In this chapter, the most relevant conclusions of the thesis are presented, related to the general idea of the thesis and with each chapter in particular. In addition, the principal future lines of work are described.
- **Chapter 7. Publications of the author.**

- **Appendix 1. Optical setup used in the experiments.**
- **Appendix 2. X-ray photoelectron spectroscopy.**

It is important to point out that the references are included at the end of each chapter, in order to facilitate the consulting of such references.

2. State of the art

Biochemical sensing has become an essential research field due to its importance and impact on the world. The relevance radiates in the necessity of monitoring pollutions and contaminants in the air, water and earth to protect the environment, and detect diseases in the human body improving the quality of life of people. These are just a few examples of the huge number of applications of biochemical sensors. To that end, different scientific fields work together on the development of biochemical sensors, as a multidisciplinary vision it is mandatory to go beyond the actual edge of science, improving the sensitivity and expanding the range of applications.

This thesis addresses the biochemical sensing from an optical approach based on lab-on-fiber technology. Such technology is the result of using optical fibers as probes for sensing by the integration of materials and components. In addition, the approach of this thesis is to incorporate a nanospectroscopic vision to the lab-on-fiber technology. Nanospectroscopy relates to monitoring changes in the nanoscale, that in our case are gold nanoparticles (AuNPs) immobilized chemically onto the end face of an optical fiber.

In order to introduce properly our approach described in the previous paragraph, we will show an overview of the state of the art of lab-on-fiber technology for biochemical applications. According to that, the fundamentals and the operating principle of biochemical sensors will be shown, as well as the impact of such devices in the world and their classification concerning the transducer and the labelling used. Then, we will focus on the lab-on-fiber technology, explaining the three different approaches, lab-in-fiber, lab-around-fiber, and lab-on-tip, and its combination with plasmonic effects, emphasizing, specially, in the use of plasmonic macro- and nano- structures, and the surface plasmon resonance

(SPR) and localized surface plasmon resonance (LSPR) phenomena. Finally, we will focus on the nanospectroscopic approach proposed in this thesis explaining the working principle and the background.

2.1. Biochemical sensors

In this section, a brief overview of biochemical sensors is shown, with an emphasis on the fundamentals and operating principle of biochemical sensors, the economic, social and research impacts, the different classifications of such sensors depending on if it is labelled or label-free, and the mechanism applied as transductors. At this point, we will focus on optical transductors and, more in particular, in optical fibers.

2.1.1. Fundamentals and operating principles

Sensors are devices whose purpose is to detect and quantify physical or chemical variations in the environment, generating a signal, an electrical one generally, which can be read in a receptor. Nowadays, the Internet of Things (IoT) has caused a huge growth in the developments of sensors, which are located in many cities controlling and monitoring many different parameters. With the feedback of such sensors, we are able to predict pollution levels, climate conditions, etc. Moreover, these sensors can be used for other applications, such as distance sensors, which are very useful, for instance in cars to prevent accidents.

According to this, biochemical sensors are devices capable to detect biological and/or chemical samples, such as proteins, enzymes, metal ions, chemical contaminants, etc. The first biosensor was developed by Leland Clark in 1962 for glucose detection by an electrochemical reaction[1], and, nowadays,

biochemical sensors are used daily for several applications, such as pregnancy tests or diabetes detection.

Biochemical sensors are not only able to detect a specific sample, in many cases they are also able to estimate the concentration of such sample, quantifying the aforementioned sample. This is a crucial point, as, in many examples, the capacity to know the quantity of some targets means the difference between applying one diagnosis or other. For this reason, one of the most important features of biochemical sensors is the limit of detection (LoD), which indicates the minimum concentration of the sample that one given sensor is able to detect[2].

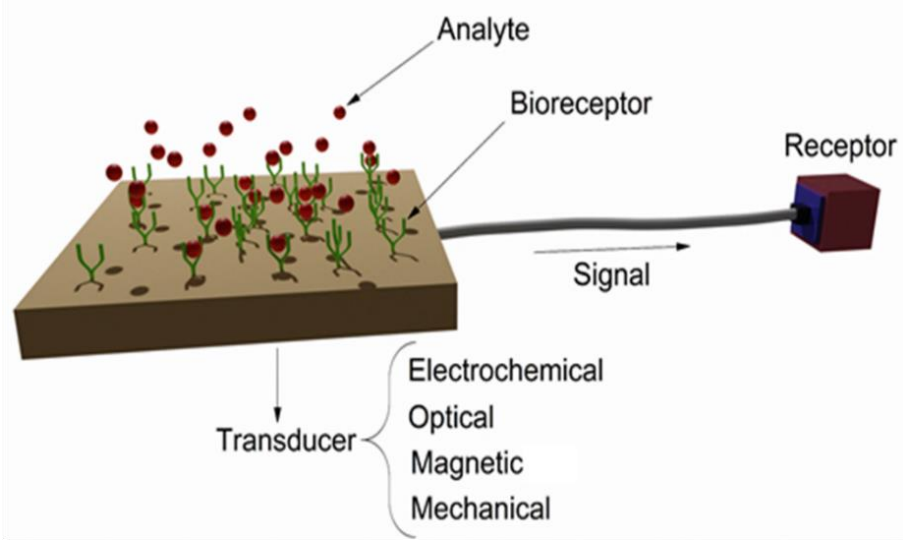

Figure 1. Scheme of a generic biosensor, which consists of the transducer, the bioreceptor, the analyte under study, and the receptor.

In contrast to generic sensors, the biochemical ones consist of two different parts, the bioreceptor and the transducer[3, 4]. The bioreceptor is the element that catches or interacts with the target of interest. This biological bond or interaction is transformed by the transducer in a signal that can be read properly in the receptor. A scheme of a generic biochemical sensor is depicted in Figure 1.

Generally, the working principle of such sensors is as follows: the interaction between the target or analyte and the bioreceptor causes a change in the transductor, which by a signal notifies to the receptor that the target has been detected. The quantification of the sample is given in the majority of cases by the “intensity” in the change of the transductor.

2.1.2. Impact of biochemical sensors

In the following paragraph, we present a few brief comments about the impact of biochemical sensors on the economy, society, and research. The potentiality of biochemical sensing and its usefulness has grown considerably in the last decades. An example of this is the market of biochemical sensors in the world, approximately USD 21.2 billion in 2019, but with expectations to reach USD 31.5 billion by 2025. Why are people investing money in biochemical sensors? From the scientific point of view, the answer relies on all the applications of such devices and their impact on humanity. A scheme of the different applications is shown in Figure 2. Some examples of their applications[6] are the following:

i) The food industry, to keep the food safe to eat or to detect unsafe food that could provoke any disease.
ii) Environmental monitoring, where biochemical sensors are capable to detect contaminants or elements such as metal ions harmful to the environment.
iii) The quantification of cancer biomarkers, that can be very helpful for early detection or to determine if a certain cancer treatment is useful or not.
iv) Medical diagnosis, where an early detection may be crucial to saving lives. Some examples could be cardiovascular diseases, cerebral ictus, etc.
v) Doping control or detection of drugs.

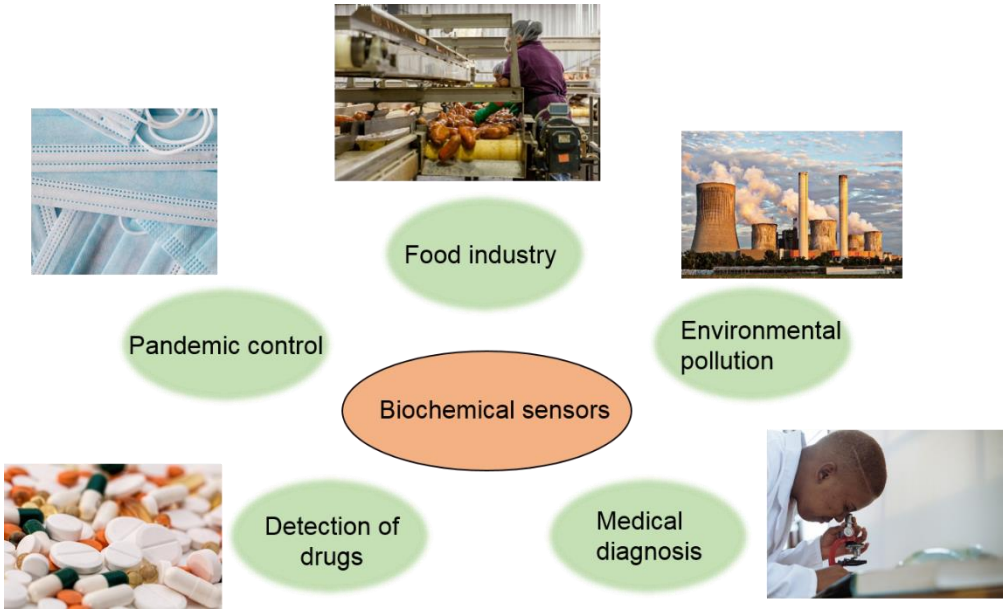

Figure 2. Scheme of the different applications of biochemical sensors.

Many of the applications mentioned previously need daily controlling and monitoring. Therefore, to research continuously on the development of cheap and reliable biochemical sensors improving the LoD have become a crucial challenge to globalize its profits. Therefore, researchers of many different scientific fields (i.e. physics, chemist, biologist, engineering…etc.) are working on developing specific, sensitive, and accurate biochemical sensors, due to the impact they provide to the industry, hospitals and our lives. The relevance of such a research line in the scientific community can be observed, for example, in the number of publications on this topic. Figure 3 shows the number of publications with concepts of “biosensors” and “biochemical sensors” in papers from 2000 to 2020. As it can be noticed, the number of publications has grown considerably in the last two decades, which is proof of its relevance.

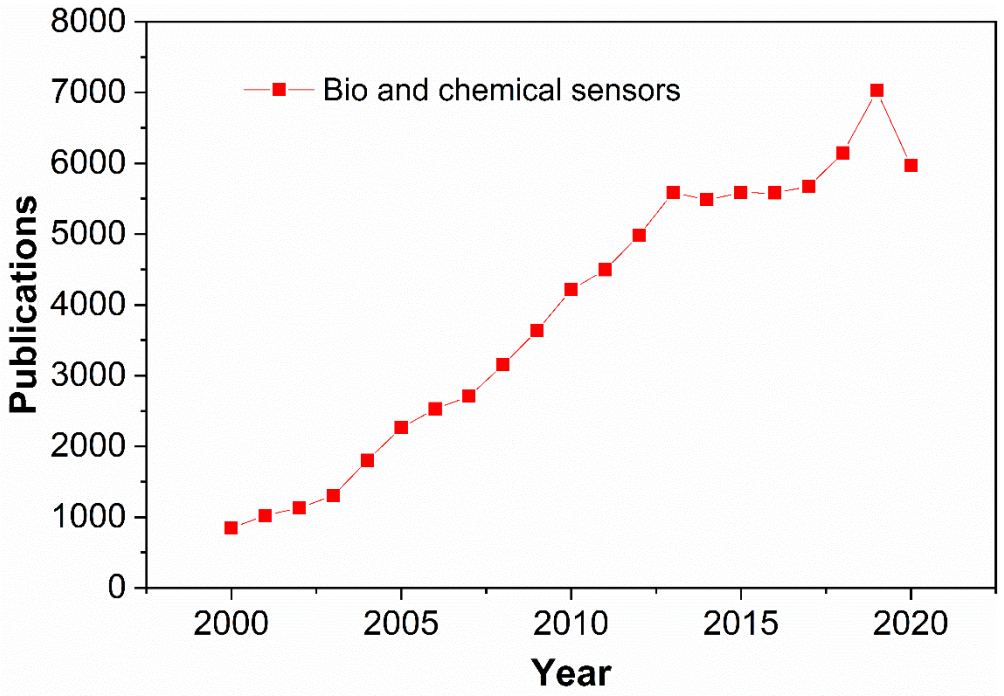

Figure 3. The number of publications with the words "biosensors" or "biochemical sensors" inside the article. The data was obtained from Pubmed.

2.1.3. Classification of biochemical sensors

Due to the impact and applications of biochemical sensors explained in the previous section, it is easy to understand that over the last decades, a vast variety of biochemical sensors have been developed. Such sensors can be grouped by different categories with respect to the features or the techniques applied, but in this section, we will focus on the two main groups, according to the transduction technique used, and depending on if it requires a label or not.

2.1.3.1. Labelled or label-free

Biochemical sensors can be classified depending on if a marker/label biomolecule is required for sensing or not. According to that, we can divide such sensors into two groups, labelled and label-free[7] (see Figure 4).

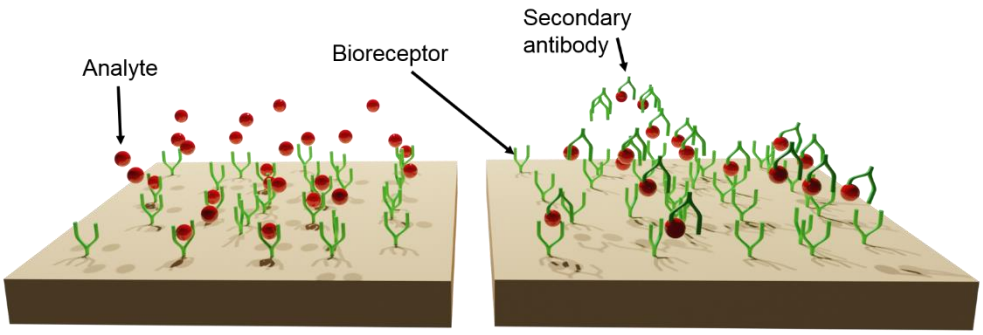

Figure 4. Scheme of a label-free biosensor (on the left), where only the interaction of the analyte with the bioreceptor is required, and a scheme of a labelled sensor (on the right) where a secondary antibody is necessary for the detection.

In labelled techniques, a secondary molecule has to be used to detect the target. In such cases, the molecule captures the analyte, and the presence of it can be verified by the information from such secondary molecule. Usually, those molecules have properties that change when they bind with the sample of interest, such as colorimetry, fluorescence, etc[8, 9]. Fluorescent detection, and, in particular, fluorescence resonance energy transfer (FRET)[10, 11], is one of the most common techniques used, due to the high resolution and sensitivity that this technique provides. The FRET effect has been exploited by different methods, like quantum dots (QD) or proteins with fluorescence features[12, 13], where many samples with such attributes can be selected depending on the brightness wavelength band required. Other labelled techniques have been developed, as isotopic labelling, where the detection of the analyte remains in the radioisotopes detection, electrochemical, or by metal nanoclusters[14-16]. Among the most relevant advantages of label-based methods, it highlights that the use of a secondary molecule reduces the reading of false-positives. However, labelled techniques require an extra time-consuming step, which may be a limitation for *in vivo* applications.

Conversely, label-free techniques are based on the detection of the analyte without any additional molecule. Due to this, faster measurements can be carried out, which is a very relevant advantage compared with label-based methods, as it allows the development of devices for biochemical sensing in real time. Among the most remarkable techniques we can emphasize on mass spectrometry (MS), atomic microscope force (AFM), quartz crystal microbalance (QCM), and Raman spectroscopy, where the operating principle of all of them is based on identifying the analytes by the molecular mass, acoustic waves, Raman signal, etc[17-21]. In other words, an extra marker is not required because the intrinsic features of such samples are exploited. However, label-free techniques usually require bulky and expensive devices. Plasmonic-based biochemical sensors have grown in the last decades, because it allows *in vivo* detection with a low-cost equipment compared with others label-free methods.

2.1.3.2. Transduction techniques

As we explained, the transducers are required to trigger a signal in the receptor when a certain sample is detected. Depending on the nature of the signal, we can divide biochemical sensors into many groups. First, we will comment briefly on the most relevant transduction techniques, which are electrochemical, magnetic, mechanical, and optical (see Figure 5). Finally, we will focus on the different techniques for optical-based biochemical sensing.

i) ***Electrochemical****:* Sensors based on the electrochemical method rely on the interaction between the bioreceptor and the analyte in an electrode surface[17, 22-24]. Normally, such interaction causes a reduction/oxidation reaction that produces an electronic variation, although there are examples where the electrical signal is caused by a molecular interaction as well. Electrochemical biosensors can be divided into three main types concerning the way the analyte is detected:

potentiometric, if it is measured by voltage difference in electrodes, amperometric, if the sensor detects the changes in the electrical current, or impedimetric, where a change in the electrode impedance is detected.

ii) ***Mechanical***: This type of transduction method works by detecting mechanical forces on the cellular scale. The main techniques rely on measuring forces, displacements, or mass variations. Some of these sensors are based on a nano-cantilever, where a stress caused in a surface due to the binding of the analyte of interest generates a deflection that is possible to measure. Other methods developed are the QCM or nanowire biosensors[25].

iii) ***Magnetic***: Normally, magnetic-based biosensors are labelled techniques, and their operating principle relies on the use of biomolecules as markers sensitive to magnetic fields, such as magnetic nanoparticles. Thus, it is possible to know if the marker is bound to the sample of interest when the system is exposed to an external magnetic field[26].

iv) ***Optica***l: Optical sensors are based on the interaction of the light with the analyte. Different detection methods have been developed by optics, which can be divided in labelled techniques, such as Raman spectroscopy, and label-free sensors, such as interferometers, plasmonic sensors, etc. Mainly, these sensors are based on measuring changes on the refractive index of the surrounding medium. Many optical platforms and structures can be used for this purpose, such as optical fibers and planar waves[27-29].

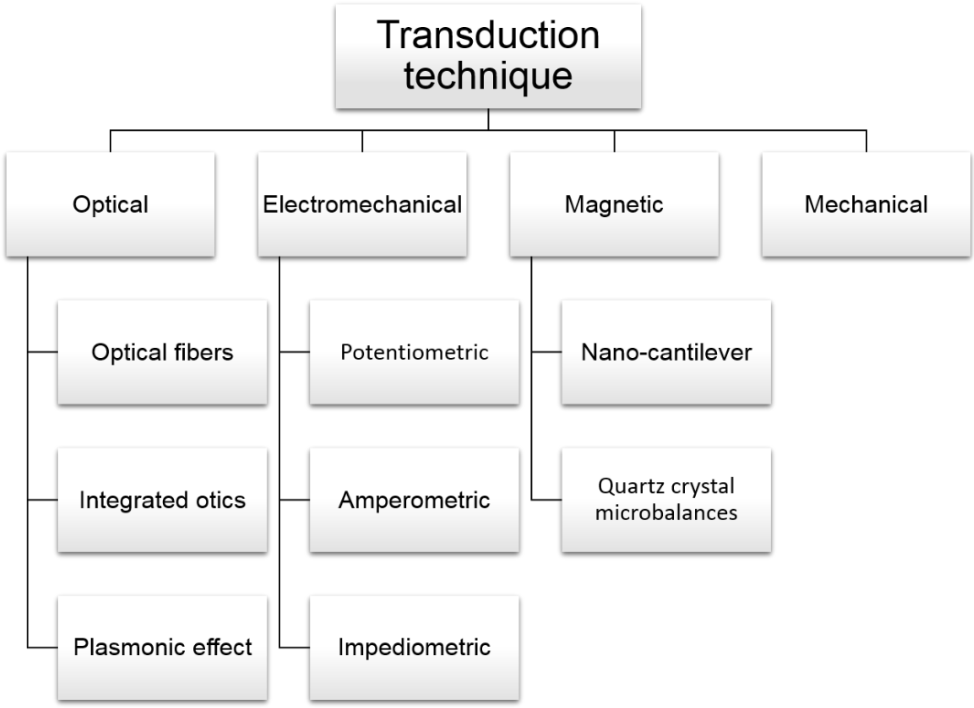

Figure 5. Scheme of the main transduction techniques and some examples of their most relevant sub-techniques.

2.2. Optical sensors for biochemical applications

Optical sensors for biochemical applications represent a promising technology to develop sensitive, reproducible, accurate, and low-cost sensors. As we mentioned, there are many optical label-based sensors, but we will focus on label-free sensors, as they are very useful for point-of-care (POC)[30] applications due to the possibility of measuring in real time and, in addition, the optical platforms are portable, which is very useful to conduct measurements outside the laboratory. Among such types of sensors, we point out two optical platforms, integrated optics, or in other words, planar waveguides, and optical fibers. In addition, such waveguides have been hugely developed in the last 50 years due

to their applications in telecommunications. For this reason, the price of the interrogation setups, the fabrication process, etc. has decreased considerably.

Regarding integrated optics, different structures for biosensing, such as resonators, interferometers, etc., have been developed in the last years for biochemical sensing[31-33]. Recently, the interest in applying this technology for gas sensing has increased due to its potential to work in the mid-infrared wavelength range (from 2 μm to 20 μm approximately) [29, 34]. In this range, the fingerprint spectral region of many gases is localized, thus the development of sensors on a chip based on the evanescence field absorption represents a promising technique.

Concerning optical fibers, this technology represents a promising field for biochemical sensing as well, due to the electromagnetic immunity, low cost, and the miniaturized size. In addition, compared with planar waveguides, the interrogation setup is less complex and, normally, all systems are connected among them easily. One of the most interesting features of this technology is that it allows *in vivo* applications at a remote location, because of the intrinsic low losses that optical fibers provide. Different configurations have been developed in the last decades to increase the performance of such sensors, amongst these are sensors based on fiber Bragg gratings (FBGs), Fabry-Perot interferometer, tapered fibers, etc[35-37]. However, the high performance of optical fibers for biochemical applications is a reality, in part, due to the combination of plasmonic structures with fiber technology. Such phenomena are the SPR and the LSPR[38]. In the following section, we will explain the fundamentals of both physical effects.

2.2.1. Fundamentals of surface plasmon resonance

A surface plasmon resonance is an electromagnetic wave that propagates on the edge of a metallic film and a dielectric[38]. This plasmonic effect is caused by the interaction of light and the metallic film. This wave is a transverse-magnetic (TM) one, which means that the magnetic field vector is perpendicular to the longitudinal axis, or, in other words, parallel to the metallic film-dielectric interface plane[39, 40]; however, the SPR only takes place at certain boundary conditions, where the propagation constant (β) of the SPR wave obeys the following expression:

$$\beta = \frac{\omega}{c}\sqrt{\frac{\varepsilon_D \varepsilon_M}{\varepsilon_D + \varepsilon_M}} \quad (1)$$

where ω corresponds to the angular frequency, *c* is the speed of the light in the vacuum, and ε_D, ε_M, are the dielectric constant of the dielectric and metal material respectively. The electromagnetic wave is mainly confined to the metal-dielectric interface boundary, but decays exponentially on the dielectric and metallic media. Nevertheless, as it is confined to the boundary it is very sensitive to the surrounding medium. Thus, according to Eq. 1, the electromagnetic waves can be modulated by the refractive index of the dielectric material, exploiting its behaviour for biochemical sensing. The most common setup for exciting the SPR wave in a metallic film is the Kretschmann-Raether configuration[41], which is depicted in Figure 6.

The working principle to excite the SPR wave is as follows: the light is launched towards a metal film surface, normally by a prism to control the incidence angle on the metal film. This angle is calculated in such a way that the angle must be larger than the critical one, which in itself is intrinsic to the prism-metal layer.

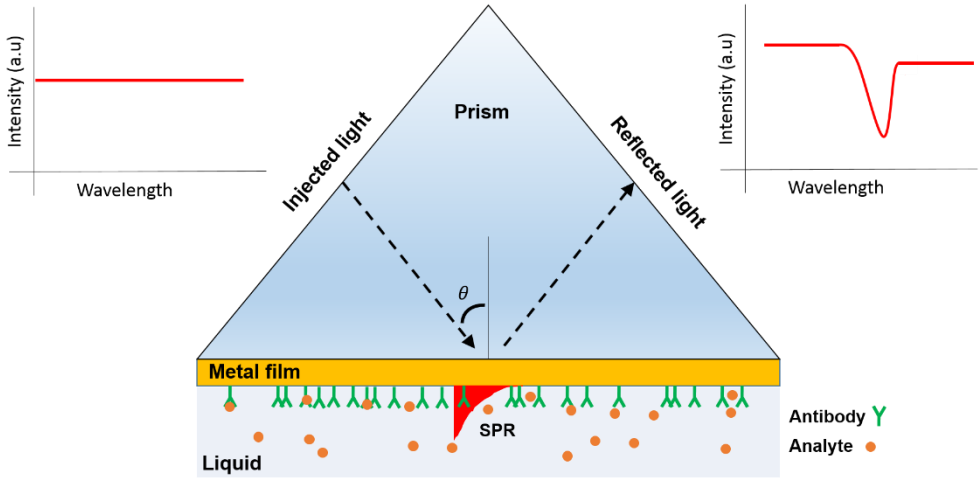

Figure 6. Scheme of the operating principle of the Kretschmann configuration.

Thus, the total reflection is obtained and recorded out of the prism. The evanescence wave that appears in the prism-metal interface due to the total internal reflection, transfers the energy to the metal-external boundary, exciting the SPR wave. This only occurs when the propagation constant of the evanescence wave is equal to the SPR wave, or in other words, it fulfils Eq. 1. The other condition is that the polarization of the launched light must be TM-like, this means, parallel to the plane of Figure 6 (perpendicular to the metal film). Such a dip at a certain wavelength depends on both, the refractive index of the surrounding medium and the angle of incidence (see Figure 6). This behaviour provides a high sensitivity and a variety of interrogation methods, such as spectral-based, tracking the shift of the peak when a molecular interaction occurs in the film, or angular-based interrogation, scanning the incidence light.

The Kretschmann-Raether configuration has been exported to the optical fiber technology[40], which allows the inclusion of the sensitivity of the SPR effect to the aforementioned advantages of the optical fibers. Moreover, it represents a

step forward in the miniaturization process. An example of such sensors is depicted in Figure 7.

The configuration of the sensor shown in Figure 7 corresponds to the called hetero-core structure[42], based on splicing two fibers with different diameters of the core to produce the propagation of the cladding modes that interact with the gold film. Covering the cylindrical external surface of the optical fiber with a metal layer, normally gold, allows changing the prism for an optical fiber, exciting the SPR wave by the cladding modes. Thus, only the cladding modes with the propagation constant of Eq. 1 are able to contribute to the excitation of the SPR wave. The different techniques to generate the cladding modes will be shown in the following sections, in particular, in the section of lab-on-fiber technology.

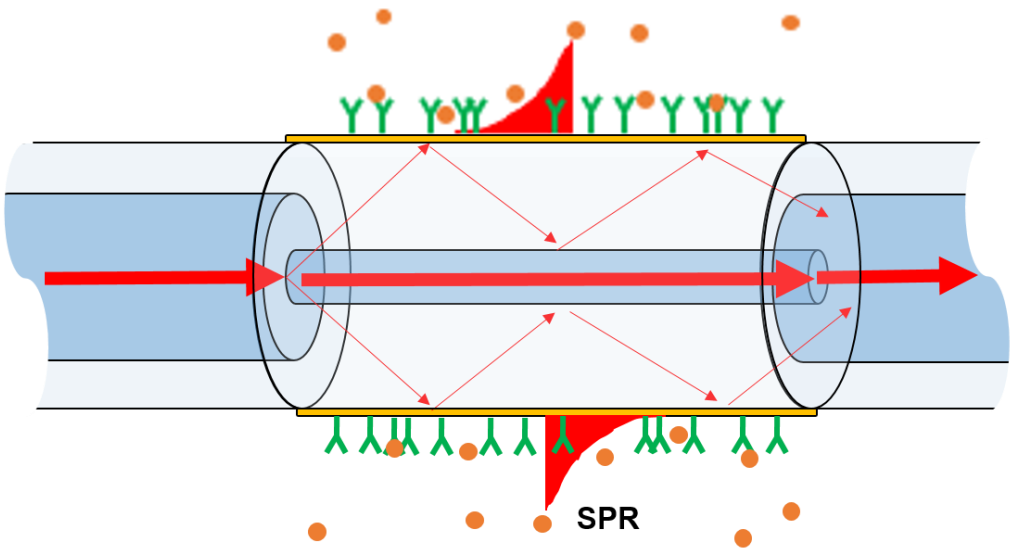

Figure 7. Example of the Kretschmann-Raether configuration applied in optical fibers. The structure shown is called hetero-core.

2.2.2. Fundamentals of localized surface plasmon resonance

SPR is an effect where a wave propagates through the boundary of a metal-dielectric structure, in contrast with LSPR, which is a physical phenomenon that relies on a strong electromagnetic field confined around metal nanoparticles. This optical effect takes place when metal nanoparticles are radiated by an external light with a wavelength shorter than the diameter of the nanoparticle. When the light hits the nanoparticle, the electrons of the metal surface are set in an oscillatory movement (see Figure 8)[43].

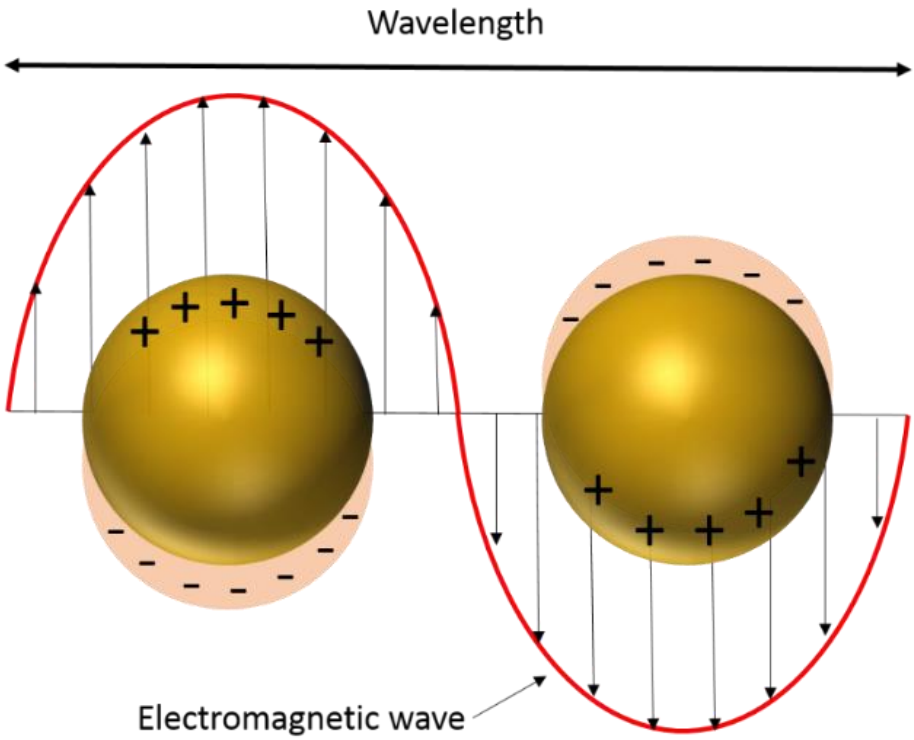

Figure 8. Sketch of the electrons oscillating movement in a gold nanoparticle when it is excited by an electromagnetic field of the incident light.

The mentioned periodical action causes two optical effects at certain wavelengths, scattering, when such electron movement provokes radiation of light, and absorption, when the energy from the incidence light is transformed into another different energy source, as for example, temperature[44]. The scattering and absorbance resonance of gold and silver nanoparticles, AuNPs and AgNPs respectively, are localized in the visible wavelength band. In fact, such wavelengths resonances are strongly related to the metal shape, size of the nanoparticle, and with the surrounding dielectric medium, which is the basis of the use of the LSPR effect for biochemical sensing[45].

The LSPR effect can be explained with the theory developed by the German physicist Gustav Mie (1868-1957)[46], wherein his famous work titled "*Contributions to the optics of diffuse media, especially colloid metal solutions"* solved Maxwell's equations analytically for the case of spherical nanoparticles excited by an incoming wave[47]. In Mie's problem, a smooth spherical particle was immersed in a dielectric medium, with a real refractive index. A detailed formulation of the Mie theory was derived after years by Bohren and Huffman[48]. Here, we will explain only the most relevant steps.

In order to solve the electromagnetic field in the problem, Mie introduced some relevant coefficients related to the optical effects previously explained, which are Q_{sca}, Q_{abs} and Q_{ext}. Such coefficients are called the Mie efficiencies and represent the cross-section normalized per area unit of the scattered, absorbed, and extinct power respectively[49]. The coefficients are described by the following equations:

$$Q_{sca} = \frac{\sigma_{sca}}{\pi R^2} = \frac{2}{x^2} \sum_{n=0}^{\infty} (2n+1) Re(a_n + b_n) \quad (2)$$

$$Q_{ext} = \frac{\sigma_{ext}}{\pi R^2} = \frac{2}{x^2} \sum_{n=0}^{\infty} (2n+1)(a_n + b_n) \quad (3)$$

$$Q_{abs} = Q_{ext} - Q_{sca} \quad (4)$$

In Eq. 2 and 3, σ corresponds with the cross-section, R with the radius of the spherical particle analysed, Re represents the real part, and x is defined as:

$$x = \frac{2\pi}{\lambda_0} n_m R \tag{5}$$

Where λ_0 is the wavelength in the vacuum of the incident light and n_m is the refractive index of the medium.

The coefficients a_n and b_n of the Eq. 2 and 3 are described in the following equations:

$$a_n = \frac{\psi_n(x)\psi_n'(mx) - m\psi_n(mx)\psi_n'(x)}{\xi_n(x)\psi_n'(mx) - m\psi_n(mx)\xi_n'(x)} \tag{6}$$

$$b_n = \frac{m\psi_n(x)\psi_n'(mx) - \psi_n(mx)\psi_n'(x)}{m\xi_n(x)\psi_n'(mx) - \psi_n(mx)\xi_n'(x)} \tag{7}$$

In Eq. 6 and 7, the parameters $\psi_n(x)$ and $\xi_n(x)$ represent the Riccati-Bessel functions of order *n*, and it is described mathematically by the following expression:

$$\psi_n(x) = \sqrt{\frac{\pi x}{2}} J_{n+\frac{1}{2}}(x) \tag{8}$$

$$\xi_n(x) = \sqrt{\frac{\pi x}{2}} \left[J_{n+\frac{1}{2}}(x) + i\, Y_{n+\frac{1}{2}}(x) \right] \tag{9}$$

where $J_{n+\frac{1}{2}}(x)$ and $Y_{n+\frac{1}{2}}(x)$ are the Bessel functions of first and second order respectively[49].

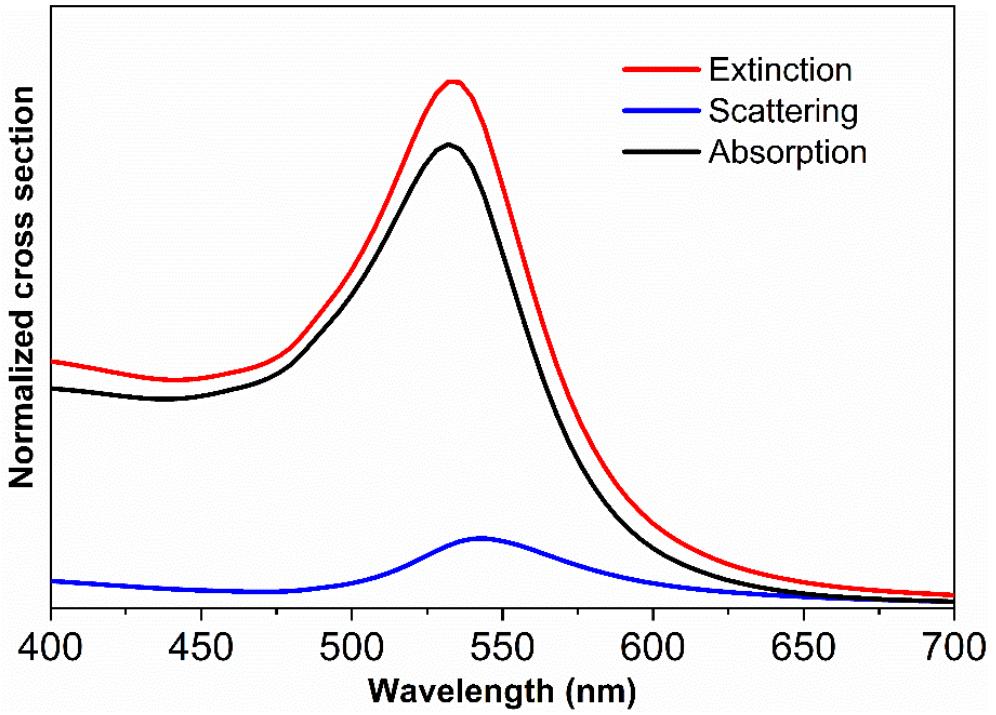

Figure 9. Normalized cross-section of the extinction, scattering, and absorption of one AuNP with a diameter of 50 nm immersed in water (refractive index = 1.33).

Solving Eq. 2 and 3, it is possible to obtain the scattering and absorbance response of spherical nanoparticles. In fact, such equations were solved in MATLAB by ourselves. In Figure 9, the absorbance, extinction, and scattering cross-section of one AuNP immersed in water with a diameter of 50 nm are shown. On the one hand, the dependence of such optical effects on the diameter of the nanoparticle is depicted in Figure 10a. As it can be observed, there is a red shift as the size of the AuNPs increases. Thus, the resonance of AuNPs can change by the modification of the size, which has been used for sensing purposes[50]. On the other hand, the cross-section obtained when the AuNPs are embedded in different refractive indices is shown in Figure 10b. The shift observed due to the changes in the surrounding medium has been highly exploited for sensing applications as well. The dielectric function applied for gold was obtained by the Johnson and Christy work[51].

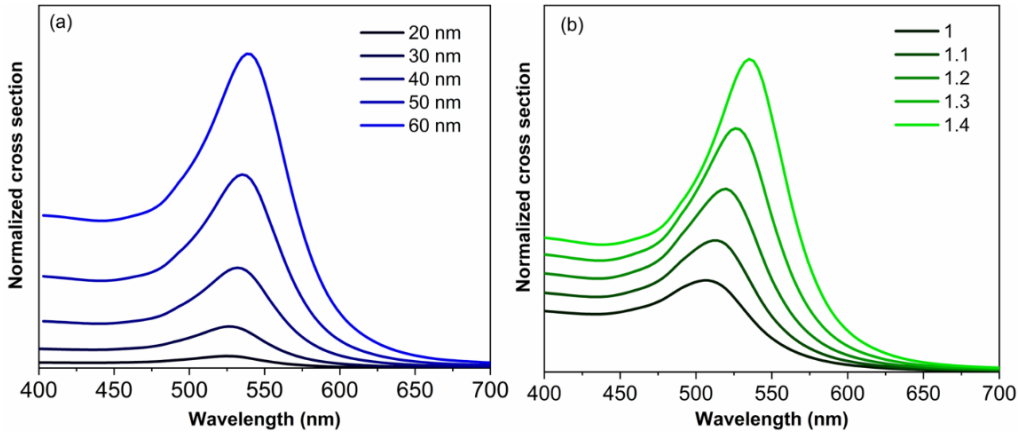

Figure 10. Normalized cross-section of the absorption of one AuNP, (a) depending on the diameter of the nanoparticle, and (b) depending on the refractive index of the surrounding medium.

One of the most relevant features of the LSPR effect is the fact that the electromagnetic field around the metal nanoparticle is very sensitive to changes in the surrounding medium. However, this field decays exponentially as the distance to the nanoparticle increases. To show this behaviour, a simulation of a spherical AuNP with a diameter of 40 nm embedded in water hit by a planar wave is represented in Figure 11. As it can be observed from such figure, the module of the electromagnetic field is very strong near the surface of the nanoparticle. Nevertheless, at further distances, this field decays rapidly.

In order to exploit the sensitivity of the metal nanoparticles to changes in the external medium, they have been used for biochemical sensing in different structures and platforms. Several studies are based on designing different metal nano- structures or particles modifying the shape, to increase the sensitivity. Some examples of such novel particles are cubes, stars, covered spheres by a dielectric like silica to protect the nanoparticle, etc[52-54].

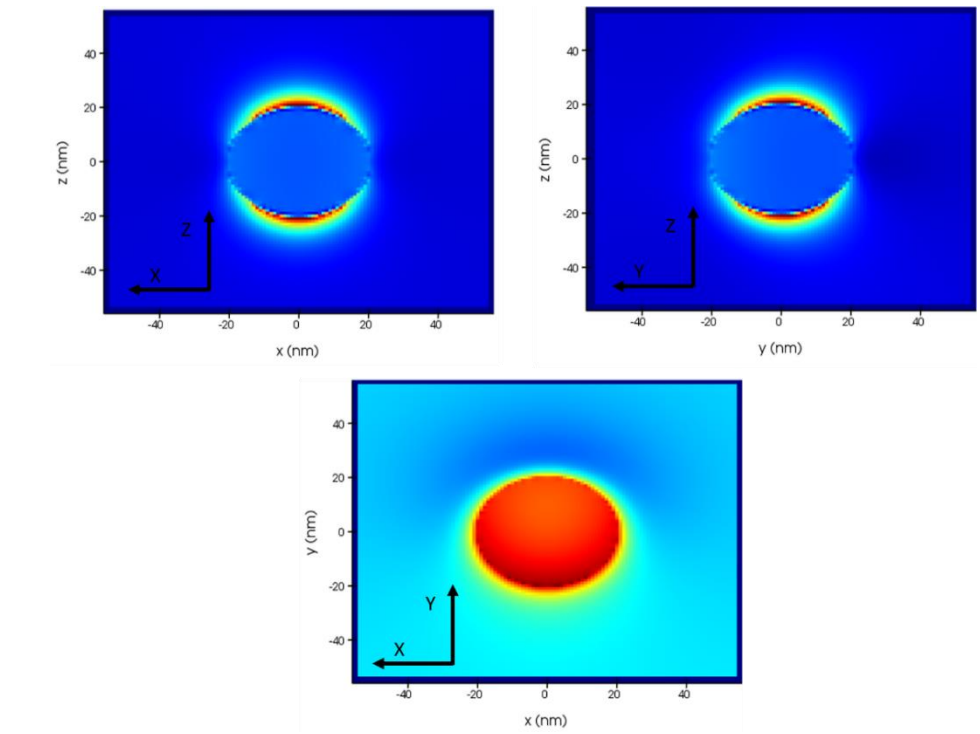

Figure 11. Electromagnetic field of the three planes of one AuNP simulated by Lumerical. The simulation corresponds to AuNP with a diameter of 40 nm immersed in water and excited by a planar wave.

Compared with SPR, the LSPR effect provides more sensitivity near the metal nanoparticle due to the intensity of the electromagnetic field, since it allows a higher interaction AuNP-target. In addition, the LSPR effect amplifies other phenomena, among them the Raman signal. Such effect is called Surface-enhanced Raman Spectroscopy (SERS), which causes an amplification in the Raman signal, and therefore, a substantial increase in the sensitivity[55]. Thus, the LSPR effect has open new approaches for biochemical applications in many different platforms, among them, the optical fiber. In the following sections, we will explain lab-on-fiber technology and the manner that the combination of LSPR and SPR with optical fibers allows developing sensors adding the high sensitivity that both plasmonic effects provide to the advantages of optical fibers.

2.3. Lab-on-fiber technology

The intrinsic properties to conduct the light to remote locations with low losses, the low cost of all the components required to arrange the setup for this technology, the capability to perform *in vivo* measurements, the miniaturized size, and the electromagnetic immunity are only some of the examples among all advantages that optical fibers provide. This is why optical fibers represent a promising technology for biochemical sensing, and, most in particular, for POC applications.

Moreover, the advances in micro- and nano-fabrication of materials able to measure changes in the surrounding medium when there is an external stimulus has made possible a new technology, called lab-on-fiber, based on the combination of optical fibers and such materials[56, 57]. In other words, lab-on-fiber technology is based on the integration of macro- and nano- functionalized materials (the *labs*) on the optical fibers[58]. The aforementioned advantages of optical fibers allows that such probe could be used as plug and play sensors with a high performance[56]. The main goal of this thesis is to address lab-on-fiber technology from a new approach for biochemical applications, but such technology is not only limited to that area, as several sensors for different applications have been developed in the last years, as for example for temperature, gamma radiation, bending, etc[59-62].

Regarding the materials used to manufacture lab-on-fiber sensors, there are several options, as well as polymers, to create resonant cavities, nanowires, microbeams, etc[63-65]. The sensor performed in this thesis is based on the LSPR effect by AuNPs, but we will do an overview of different sensors developed with LSPR and SPR effects on optical fibers. The reason to centre our work on the plasmonic effect relies on the performance, like the sensitivity, that metal structures provide, as we explained in the previous section.

Thus, we can divide lab-on-fiber into three different groups depending on which part of the optical fiber is used[56]:

- **Lab-in-fiber:** this approach is based on embedding the nano-materials inside the optical fiber. The optical probes that best fits are the photonic crystal fibers (PCFs).
- **Lab-around-fiber:** such technology stands out to integrate the materials in the external cylindrical substrate of an optical fiber.
- **Lab-on-tip:** probes of this technology are based on embedding the sensing element in the end face of an optical fiber.

In the following sections, each one of these three approaches shown will be explained in detail, focusing on the main structures and approaches applied in each one. Finally, we will explain our approach, which is included in the lab-on-tip category.

2.3.1. Lab-in-fiber

As we have commented, lab-in-fiber[66] technology includes sensors where the functionalized materials are embedded inside the optical fiber. The most common approach to develop this technology is by using PCFs, although other methods developed, are for example those based on drilling the optical fiber by laser to insert afterwards AuNPs.[67].

PCFs are special fibers developed for the first time by Philip Russell and co-workers[68]. Such fibers are based on drilling air holes around a solid core. By means of this method, the effective refractive index of the cladding changes due to the presence of such holes, that favours the propagation in the core. Another optical fiber-based technique is the denominated hollow core fiber (HCF)[69]. These fibers are based on a core of air and a microstructured cladding. This configuration is based on the propagation of light by the photonic bandgap

effect. An example of the cross-section of both fibers is depicted in Figure 12, manufactured by Eneko Arrospide[21, 70].

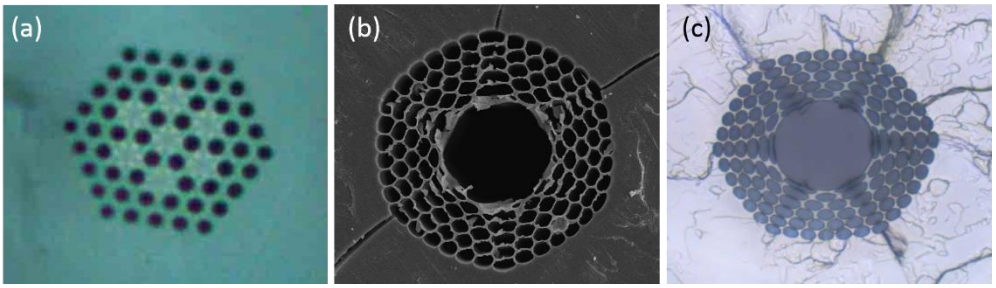

Figure 12. An example of a real microstructured fiber (a) and a hollow core fiber (b) and (c).

The combination of both plasmonic effects, SPR and LSPR, with the Lan-in-fiber technology represents a challenge due to the manufacturing process, in particular, in the integration of metal films inside the air holes. The aim of this approach relies on exciting the SPR wave by the interaction of the light with the metal structure placed inside the PCF. In order to trigger the SPR effect, researchers are focusing on creating tiny metal films around the holes. However, the limitation on the manufacturing process has caused that most of the new developments performed in this field have been based only on a theoretical approach through simulations. Therefore, the impact on the experimental tests is very low[71, 72]. Other approaches based on creating metallic nanowires by a complex fabrication process have been developed in the last decade[73].

Exploiting the LSPR on lab-in-fiber platforms has been more used due to the manufacturing process being less limited compared with the SPR-based one. The majority of the researches are based on inserting bio-functionalized metal nanoparticles inside the holes of the PCFs and HCFs to excite the LSPR effect. In such cases, nanoparticles are dispersed in a liquid media. In fact, this approach has been highly developed for SERS-based applications. The

simplest configuration consists on the filling of cavities in the optical fibers by the solution with the target of interest and metal nanoparticles, obtaining the amplified Raman signal on the corresponding Raman band. An extended review of this method can be found in[58].

2.3.2. Lab-around-fiber

A different approach is based on integrating functional metal layers around the optical fiber. The main idea underneath this technology is to create an interaction between the light and the external cylindrical surface of the optical fiber, where we have placed the functional element, as for example nanoparticles or a metal film. It is important to point out that optical fibers are designed in such a way that the light confined in the core is insensitive to the external medium. However, such idea can be performed by different structures and configurations but we can divide them into two main groups depending on the operating principle[40].

On the one hand, by modifying the structure of the optical fiber and generating an evanescence field that interacts with the surrounding medium. Such optical fiber-based sensors can be developed by removing the cladding of the optical fiber, tapering the fiber, by U-bent configurations, etc. On the other hand, lab-around-fiber-based sensors can be performed by diffraction gratings in the core of the optical fiber. By means of such gratings, there is a coupling between the fundamental mode that propagates in the core and the cladding modes, favouring the interaction of such cladding modes with the nanostructures placed around the optical fiber.

Among the methods aforementioned, the ones based on modifying the structure of the optical fiber were developed to enable the interaction between light and the external medium. Such sensors are based on generating the evanescence field. First, we will show the taper configuration. Tapered fibers consist of

stretched fibers where the size of the optical fiber is reduced to a micro- or nano-scale[74]. Summarized, the manufacturing of these sensors is based on increasing the temperature around the optical fiber by a heated filament or similar, in order for the glass of the fiber to become soft and lengthen the fiber in the propagation axis. Thus, the resulting fiber would have a thinner part with a length over few millimetres, as depicted in a sketch in Figure 13. Reducing the diameter of the optical fiber produces a spreading of the light from the core to the cladding thus making the fiber sensitive to changes of the refractive index in the surrounding medium. In this configuration, the integration of a metal film, such as gold, silver, etc., allows the manufacturing of a biochemical sensor based on the SPR effect easily.

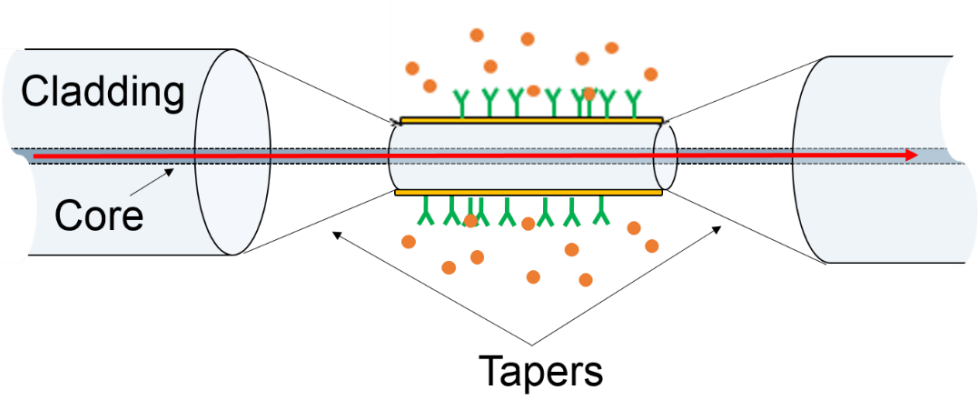

Figure 13. Scheme of a plasmonic optical fiber sensor based on a taper configuration.

Another approach consists on removing the cladding of the optical fiber. An example of this configuration can be observed in Figure 14. By removing the cladding, entirely or in part, the propagation of the light confined in the core depends on the external medium, or, in other words, it is able to measure changes of the external refractive index. Similar to that of the taper-based sensor, this technique allows the use of the LSPR and SPR phenomenon as

functionalized materials for biosensing[75]. Commonly, a chemical etching process is applied to remove the cladding[40].

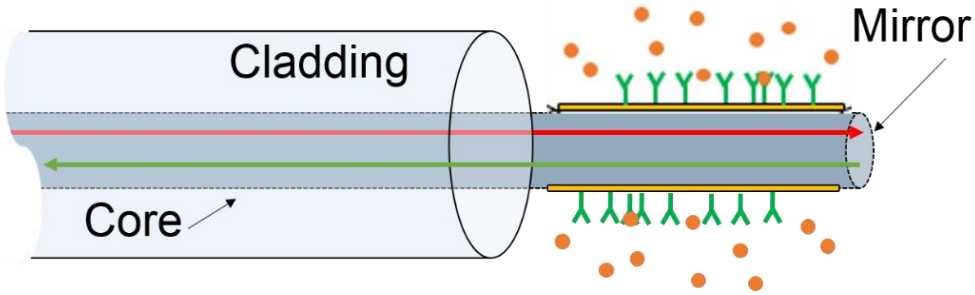

Figure 14. Scheme of a plasmonic optical fiber sensor based on removing the cladding on the tip.

Another group of sensors is called the U-bent configuration, based on bending the fiber in order to create a U-shape form (see Figure 15). This configuration allows exciting the evanescence field due to the bending applied in the fiber[76], makes the propagation more sensitive to refractive index changes in the external medium. Introducing metal nanoparticles or films make this configuration very interesting for SRP and LSPR sensors. The optical fiber used in such configurations are the multimode optical fibers (MMFs), which are fibers that are able to propagate the fundamental mode and higher modes. This effect can be performed by increasing the diameter of the core in the optical fibers. Each mode supported by the MMF has a different propagation constant, in such a way that the angle when the modes arrive to the U-shape is different for each one. Thus, some of these modes propagate after the U-shape, other modes radiate to the surrounding medium, and finally part of such modes excite the evanescence field, and, therefore, the SPR wave, as occurs in the Kretschmann configuration[77].

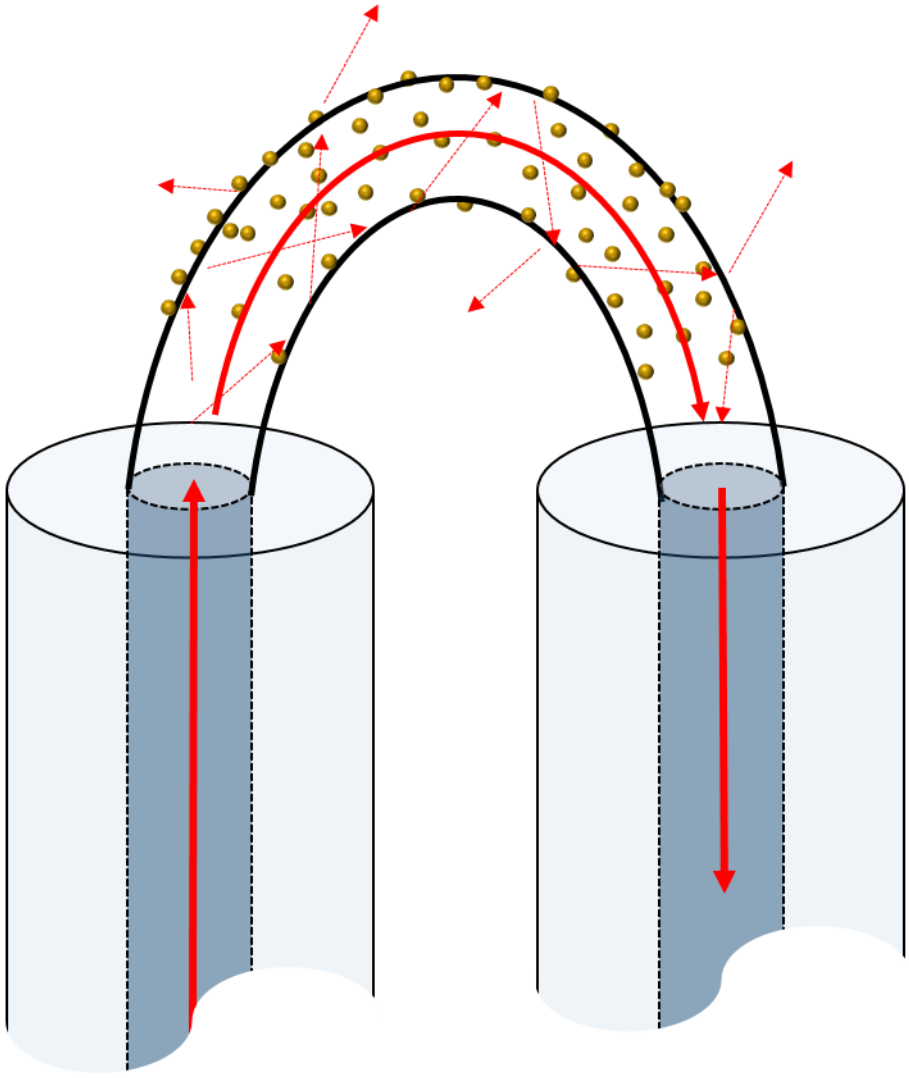

Figure 15. Scheme of a plasmonic optical fiber sensor based on a U-shape configuration. In this case, around the optical fiber, there are AuNPs, and the red pointed lines inside the fiber represent the different rays that appear due to the bending.

The other approach to manufacture lab-around-fiber-based sensors is by diffractive gratings[78]. Such diffractive gratings consist in a periodic modulation of the refractive index of the core creating a periodic structure. This configuration is called Fiber Bragg Gratings (FBGs), and an example is depicted

in Figure 16. However, in FBGs the light is highly confined in the core and it does not interact with the external medium. To that end, FBGs-based sensors modifying the grating structure have been developed to excite cladding modes. Briefly, cladding modes are modes confined in the cladding of an optical fiber, instead of in the core. This electromagnetic solution is based on the fact that the refractive index of the cladding is higher than the refractive index that covers the fiber. Commonly, such modes are undesirable in telecommunications applications, because it results in losses of the light that propagates in the core. Nevertheless, the interaction of these modes with the surrounding medium makes them very sensitive to external changes, which is very useful for sensing, in particular for biochemical applications. This effect can be triggered by the radiation of light confined in the core to the cladding. Among all the gratings configurations, the following are the most remarkable: long period gratings (LPGs) and tilted fiber Bragg gratings (TFBGs). Thus, when optical fibers are covered with metal nanoparticles or metal film it is possible to excite the SPR and LSPR phenomenon by the diffractive gratings-based approach.

In the case of LPGs, these configurations entail a periodic refractive index modulation of several hundreds of microns, higher compared with typical FBGs (see Figure 16a). Normally, the range of such period is between 100 and 700 μm[79]. The period is calculated to satisfy the phase-matching condition between the fundamental mode that propagates in the core and the co-propagating cladding modes. Such calculation can be done by the following expression:

$$\lambda_m = \left(n_{eff}^{core} - n_{eff}^{cladd(m)}\right)\Lambda \tag{9}$$

where λ_m is the resonance wavelength that satisfies the phase-matching condition, n_{eff}^{core} is the effective refractive index of the fundamental mode in the core, $n_{eff}^{cladd(m)}$ is the effective refractive index of the m cladding mode and Λ is the period.

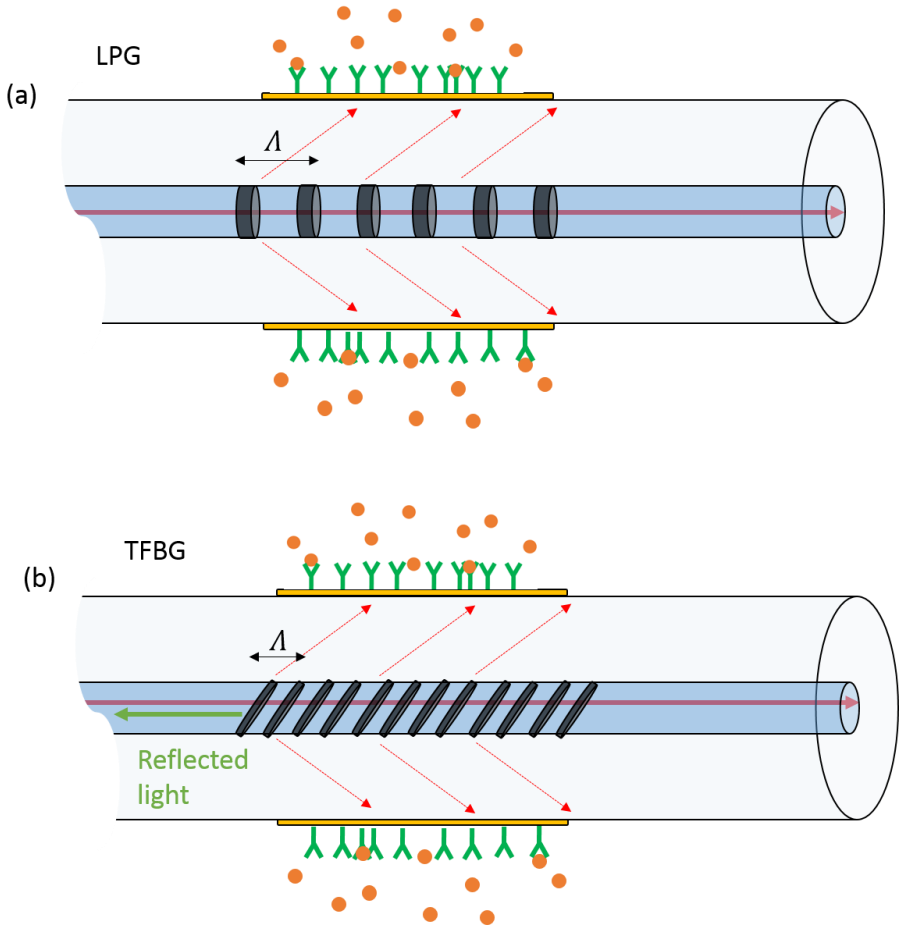

Figure 16. Scheme of optical fiber sensors based on diffractive gratings, (a) LPG-based sensor and (b) TFBG-based sensor.

As we have mentioned, another approach is the TFBGs[80-82]. Such gratings are based on tilting the periodic refractive index modulation by a certain angle (φ) with respect to the propagations axis, as it can be observed in Figure 16b. This structure allows a coupling among the fundamental mode of the fiber and certain cladding modes, depending on the angle. The transmission spectrum consists in the typical Bragg spectrum including many narrow attenuation bands corresponding with the cladding modes. An example of the spectrum in a typical TFBG with an angle of 8º and a period of 514 nm is depicted in Figure 17, where

the two parts are separated. The part of the core mode, which corresponds with the green section in the figure, is sensitive to mechanical forces, as bending, vibration, strain, etc., whereas the part of the cladding modes, the red section in the figure, is sensitive to the external surrounding refractive index, and, therefore, can be used biochemical sensing[83]. The cladding modes that satisfy the phase matching condition can be calculated by the following expression:

$$\lambda_m = \left(n_{eff}^{core} - n_{eff}^{cladd(m)}\right)\frac{\Lambda}{\cos(\varphi)} \tag{10}$$

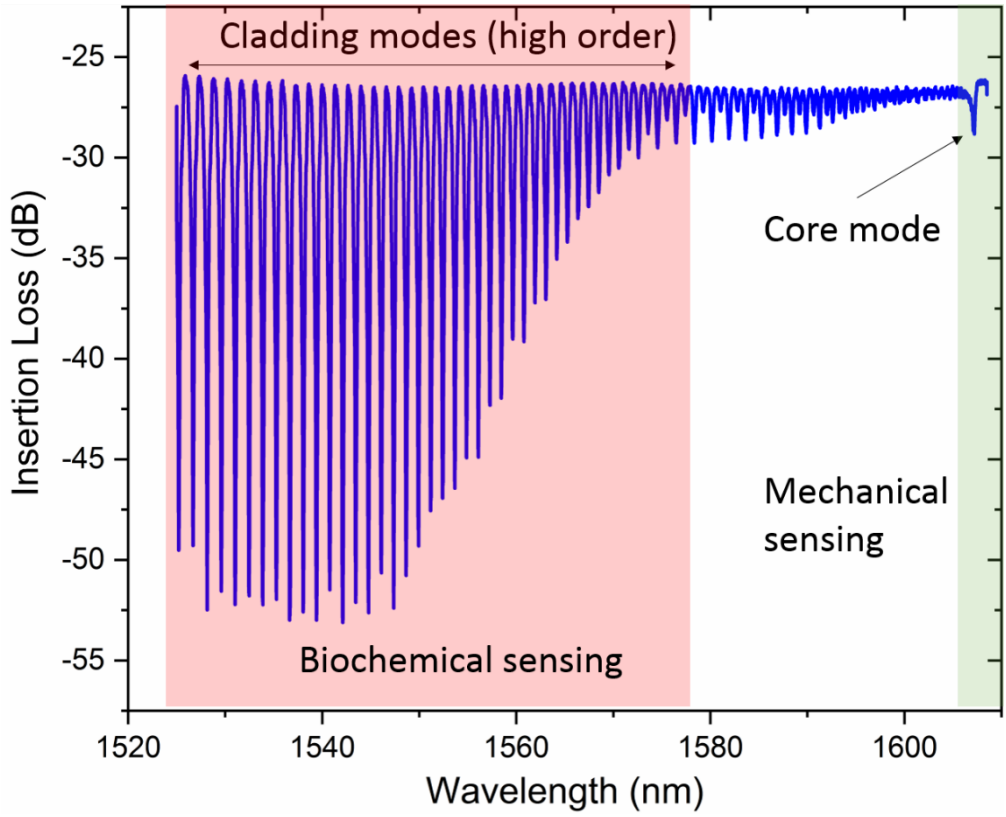

Figure 17. Spectrum in transmission of a TFBG with an angle of 8°. Two different sections can be observed, the green one corresponds with the part of the spectrum sensitive to mechanical forces, whereas the red one corresponds with the part sensitive to the surrounding refractive index.

The main advantage of all the configurations shown in this section is that the integration of sensitive structures around optical fibers, such as films of gold, requires a short time of deposition and provides high sensitivity.

2.3.3. Lab-on-tip

In opposition to the lab-around-fiber technology, sensors based on the integration of functionalized elements in the end face of an optical fiber do not require a special structure or configuration to cause an interaction between the light and the external medium, because such interaction occurs directly on the tip. Thus, the end face of an optical fiber may be an interesting place to integrate sensitive materials to manufacture sensors for remote sensing, in real time, and with high sensitivity[60].

As we have mentioned, in this section we will focus on configurations based on metal nanoparticles or nanostructures placed on the optical fiber end face, with the aim to trigger the LSPR phenomenon. In the majority of cases, the absorption or the scattering of metal nanostructures are recorded through the optical fiber because of the reflection of the light by the mirror formed between the end face of the fiber and the external medium.

In general terms, lab-on-tip-based sensors can be divided into two main groups depending on the manufacturing process: i) fabrication processes based on lithography for metal nanostructures developing on the optical fiber end face. Sensors belonging to this group are conducted by different techniques, which will be explained in the next section; ii) chemical immobilization of metal nanoparticles on the optical fiber facet. The sensor proposed in this thesis is included in the latter fabrication method.

In the following sections, we will explain the most relevant issues of the manufacturing methods according to the two groups mentioned previously.

2.3.3.1. Lab-on-tip by a lithography process

Widely, lithography processes for lab-on-tip are based on developing nanostructures on the optical fiber end face with the aim of exciting the LSPR effect, although there are other approaches focusing on making arrays of holes in a metal film on the tip of an optical fiber. Such holes cause the same physical effect compared with the one obtained by nanostructures. The main advantages of all the lithography-based processes are the high accuracy and the reproducibility, or, in other words, a nanoscale control, due to the technological advance of the equipment employed in this method. However, the main limitations that this fabrication approach provides is the high cost of the equipment required and the complexity of the manufacturing process compared with the chemical immobilization.

Among all the methods based on lithography, it is possible to distinguish those which are based on creating the nanostructures directly on the optical fiber facet, and those that are based on transferring such structures to the tip after developing it.

Manufacturing plasmonic structures on the optical fiber tip has been addressed by different methods, such as those based on femtosecond lasers or on interference lithography. However, in this section, we will focus on the two most common methods, the focus ion beam (FIB) milling and electron-beam lithography (EBL).

Regarding the FIB-based fabrication process, a scheme is depicted in Figure 18. This method relies on adding a metal layer on the optical fiber end face, such as gold, and then, to create the nanostructures directly on the surface, such as disks, cubes, etc., removing the gold directly[84-86]. One of the main limitations of FIB milling is the time-consumption required and the limited area that can be covered in one fabrication step. Other approaches based on FIB

milling have been conducted adding a new step, including a high refractive index layer over the metallic layer in order to create more complex and sensitive nanostructures[87].

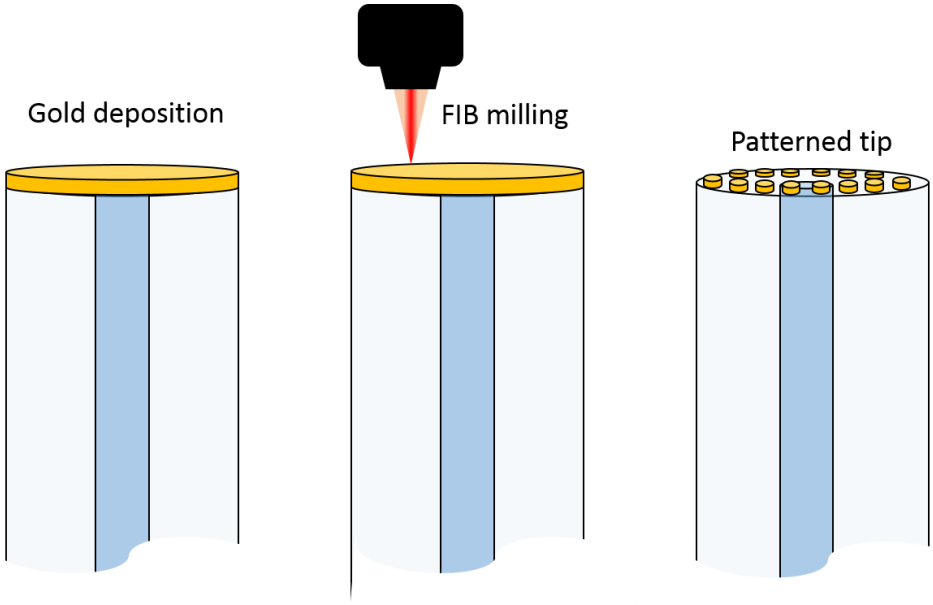

Figure 18. Scheme of the FIB milling fabrication process. First, a film of gold is deposited, and then, a milling process is carried out on the Au overlay.

The other attempt for manufacturing plasmonic structures directly is the EBL technique[88], which is a similar method compared with the FIB milling one. EBL takes advantage of materials electron beam resist. Usually, in this method, a conductive layer, such as chrome (Cr)[89], is attached to the optical fiber end face first. After which the electron beam-resistant material is attached over the previous layer, which is modified according to the nanostructure designed previously. Finally, the electron beam is injected to the optical fiber facet, and only the gold under the last material added remains on the tip[90, 91], thus a plasmonic nanostructure can be developed (see Figure 19). By this method, structures composed of metal and dielectric materials have been designed as well[60].

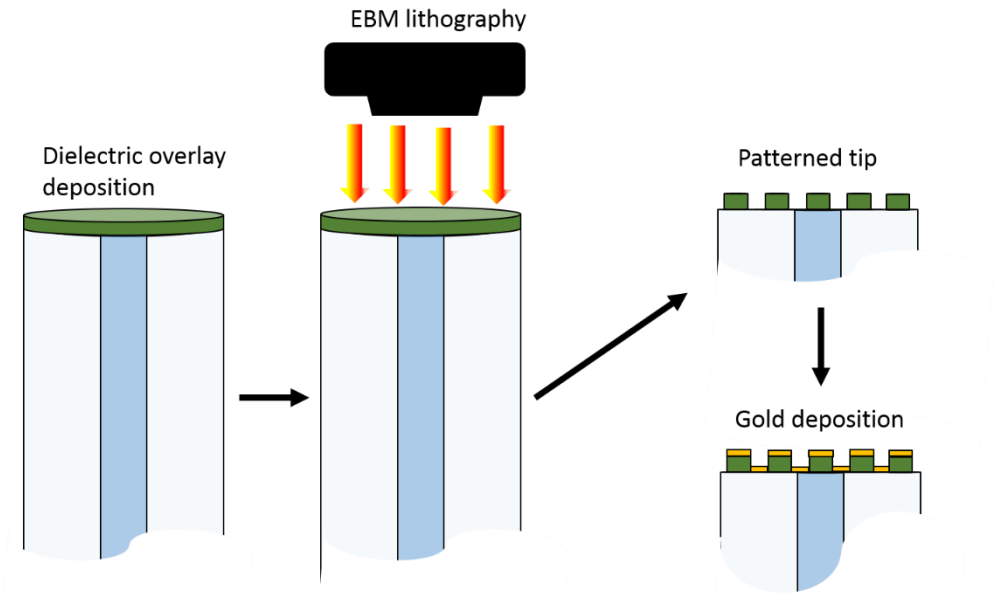

Figure 19. Facet of an optical fiber during the EBL fabrication process. First, a dielectric overlay is deposited, then, a pattern on the tip is created by the EBL process, and finally, the gold is attached.

In order to avoid the limitations and complexity that entails working directly on the optical fiber end face, new manufacturing methods have been developed in the last decade based on developing plasmonic structures first out of the optical fiber, usually by FIB milling or EBL, and, subsequently, transferring it to the tip. However, the transfer of the nanostructures to the optical fiber end face represents a fragile step that can modify the performance of the sensor.

As is discussed in[58], there are two main techniques performed to transfer the plasmonic pattern. The first is based on releasing the structure in a typical planar substrate, and then, transfer it to the optical fiber end face, which can be carried out by different procedures, such as increasing the temperature to melt and splice them. Commonly, the aforementioned techniques require an extra step because it is necessary to manufacture a new pattern before each transfer[92]. However, new researches are trying to avoid this additional step by the use of templates[93].

The other method is based on transferring the plasmonic structure to the optical fiber facet by direct contact. In other words, an adhesive is used for the transfer. Generally, an epoxy resin can be used as an adhesive[94], but by using such adhesives we may affect the repeatability in the manufacturing process, obtaining a low reproducibility. The transfer method of direct contact has been used to develop sensors based on resonance nanoapertures and nanostructures[95].

To reduce the total cost of the manufacturing methods explained in this section, new approaches have been developed with the aim of modifying the transfer step. Thus, new transfer techniques based on plasma etching and polystyrene nanospheres are being investigated[96-98]. However, the transfer step is still necessary, and the cost is not reduced enough compared with the chemical immobilization-based approach.

2.3.3.2. Lab-on-tip by a chemical immobilization

Contrary to the manufacturing methods explained in the previous section based on lithography, attaching metal nanoparticles on the tip of an optical fiber by a chemical immobilization allows a faster and cheaper method for developing sensors for lab-on-tip technology. By this method, which has been named self-assembly as well[58], the cost of the manufacturing can be reduced drastically, as only the price of the optical setup to the reagents and the metal nanoparticles has to be added. In addition, another relevant advantage of this method is the simplicity to conduct it effectively, which opens the possibility to manufacture several sensors at the same time, and thus, to manufacture them on a large scale. Figure 20 shows a scheme of typical sensors developed by this method, and, in Figure 21, a scanning electronic microscopy (SEM) image of an optical fiber facet, where the AuNPs attached on the surface can be observed.

Figure 20. Sketch of typical lab-on-tip-based sensor based on a chemical immobilization of AuNPs.

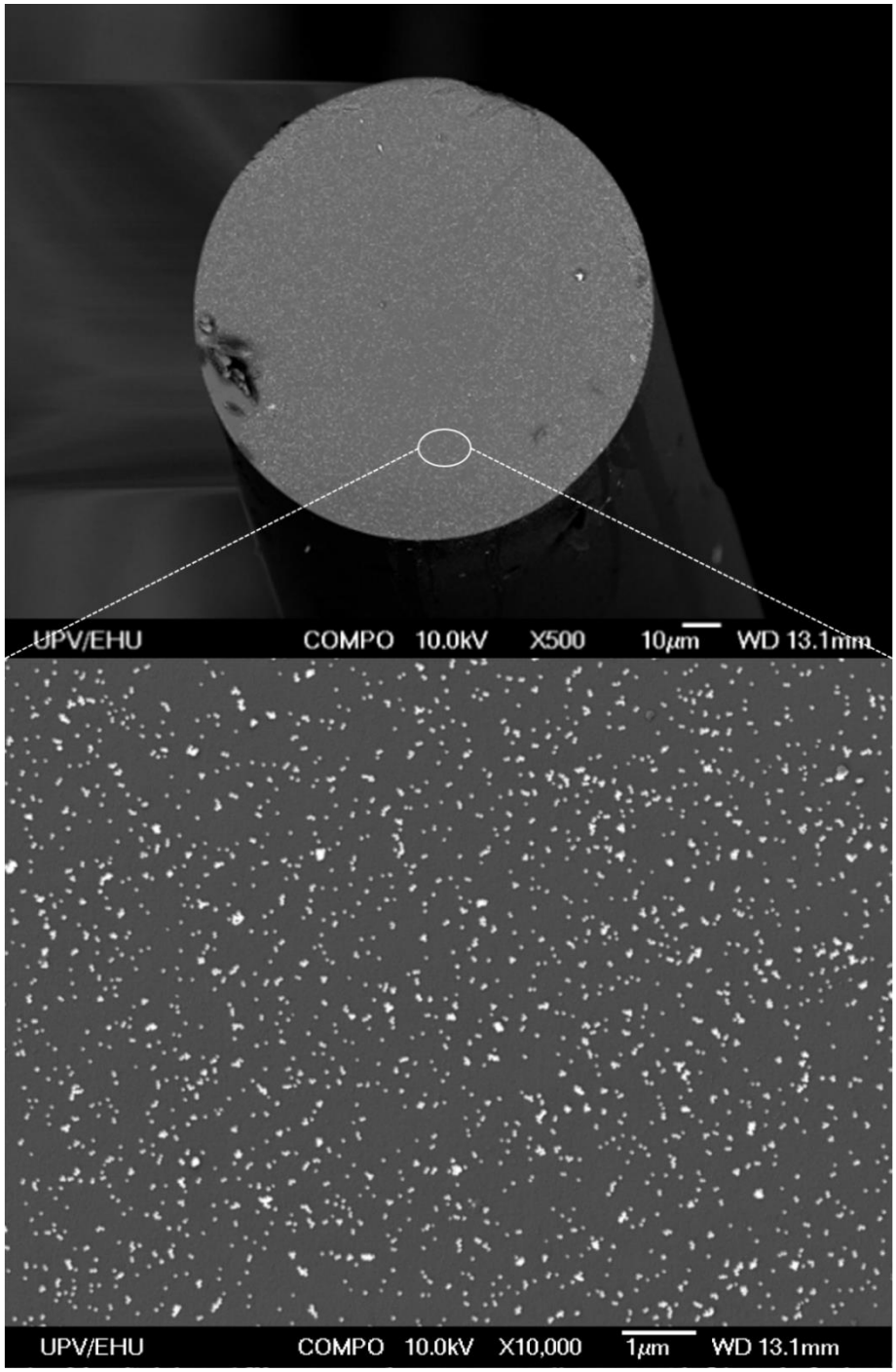

Figure 21. SEM images of a multimode optical fiber facet after the AuNPs immobilization.

The first approach of this method for optical fibers was developed by K. Mitsui and co-workers[99]. In such work, the researchers immobilized AuNPs in the optical fiber facet and proved the sensitivity changing the refractive index of the surrounding medium. In addition, they conducted measurements to detect avidin, which is a protein majorly used as proof of concept in biosensing. After this research, many sensors have been developed by the chemical immobilization of metal nanoparticles. We will now explain briefly the most interesting researches, in our opinion, based on this technique.

In the last decade, several sensors based on this manufacturing technique for different applications have been published. For instance, S. Lee *et al.* developed a sensor by this method with a multimode fiber (MMF) that was used for the detection of a prostate specific antigen (PSA)[100], with a LoD of 124 fg/ml.

To study the impact on the sensitivity of both the size of AuNPs and the density on the optical fiber surface, theoretical and experimental research was carried out as well[101]. The conclusion was that as the size of AuNPs and the density of them increases, the resonance intensity, or in other words, the LSPR intensity effect, increases. However, although an increase in the sensitivity was obtained with a low density and smaller AuNPs, such increase was too weak. Therefore, it can be concluded a raise in intensity does not imply higher sensitivity.

A dengue immunoassay was designed by this method as well. In this case, the sensor was used for the detection of the dengue infection when it is in the critical step of the disease. This sensor was developed by the immobilization of the dengue anti-NS1 antibody on the AuNPs, in such a way that the sensor is able to detect different concentrations of NSI monitoring the shift in the LSPR spectrum, with a LoD around 1.5 nM[102].

Another approach was based on taking advantage of the LSPR signal and the SERS effect as an additional detection tool[103]. With the immobilization of AuPs

on the end face of an optical fiber and by the combination of the LSPR and SERS effect, E. Norov *et al.*[104] were able to detect the molecule of 4-aminothiphenol in real time by changes in the LSPR and Raman spectrum.

A very interesting research based on attaching AuNPs and AgNPs was developed by T. Monro *et al*[105]*.* In this work, they proved the possibility to immobilize two different metal nanoparticles at the same time obtaining the LSPR signal from both. This approach opens the possibility to measure different samples at the same time, as the resonance band of the two metal nanoparticles is localized at two different wavelengths. In the case of the cited research, the resonance bands of the nanoparticles is around 550 nm and 430 nm for gold and silver respectively. In addition, they were able to detect two different gastric cancer biomarkers, antipoliprotein E (apoE) and Cluster (CLU) by this assay.

Recently, to increase the sensitivity of these optical probes, a new line of development based on including ZnO (zinc oxide) nanowires on the optical fiber facet has been published[106]. The main motivation of this technique is to improve the sensitivity by the use of ZnO nanowires and take advantage of decorating them with AuNPs, in such a way that nanoparticles are placed in a three-dimensional (3D) form, thus extending the interaction area.

Integrating optical fibers LSPR-based sensors in a microfluidic channel has provided significant progress in biochemical sensors as well. Such channels allow the miniaturization of the sensors to obtain a compact device, reducing considerably the cost because it allows working with low doses of the liquid that is intended to analyse. Moreover, microfluidic channels are excellent for multiplexing purposes as they are easy to rescale and they provide the opportunity to integrate different analysis systems in the same circuit[100, 107]. For instance, sensors of PSA have been developed by the combination of lab-on-tip technology and microfluidic channels. However, it is important to point out that the use of microfluidic channels is independent to the technology applied.

Several sensors based on lab-around-fiber technology have been applied and used in microfluidic channels as well.

Recently, our group has worked on a new detection approach based on AuNPs immobilized chemically in a MMF end face. Such an approach is the nanospectroscopy, and it is based on used the AuNPs as light sources whose intensity changes by the presence of samples with the resonance band in the same wavelength range that the AuNPs. Thus, an improvement in the sensitivity and in the selectivity can be achieved. Through this concept, we were able to detect Cu^{2+} and Cyt c [108, 109]. We will explain more in detail this nanospectroscopic approach in the following section.

Despite the advantages that the chemical immobilization method provides, the main limitation compared with the lithography method relies on the fact that the deposition of the metal nanoparticles is a random process. Such randomness has a significant impact, as it implies, in the majority of cases, a poor reproducibility in the manufacturing process. In addition, such intrinsic random behaviour can trigger many nanoparticles to become attached among them, creating accumulations of nanoparticles. This fact is called “aggregation of nanoparticles”, and it causes a shift in the LSPR spectrum. In the present thesis, to address the reproducibility problem, we have characterized deeply the immobilization process of AuNPs on the optical fiber facet. Thus, our aim is to understand the immobilization process and its impact on the manufacturing process and, thus, increase the reproducibility. Our study is based on a spectral characterization, where the LSPR spectrum is recorded in real time as the AuNPs attach on the surface, and on image analysis by SEM. Such research will be further addressed in Chapter 3.

2.4. Nanospectroscopy

Spectroscopy is a technique based on obtaining the electromagnetic radiation or absorption of a sample by the interaction of the light with such sample. To conduct this measurement, it is necessary to have a light source, a sample, and a detector. The light launched by the source interacts with the sample. By this interaction part of the light ray is reflected or absorbed by the sample, and in other cases, the sample may radiate to other wavelengths due to this interaction. Finally, the light that arrives at the detector has to be analysed and interpreted to understand the interaction between the sample and the light ray. The aforementioned scheme explained corresponds to the simplest version of spectroscopy (see Figure 22).

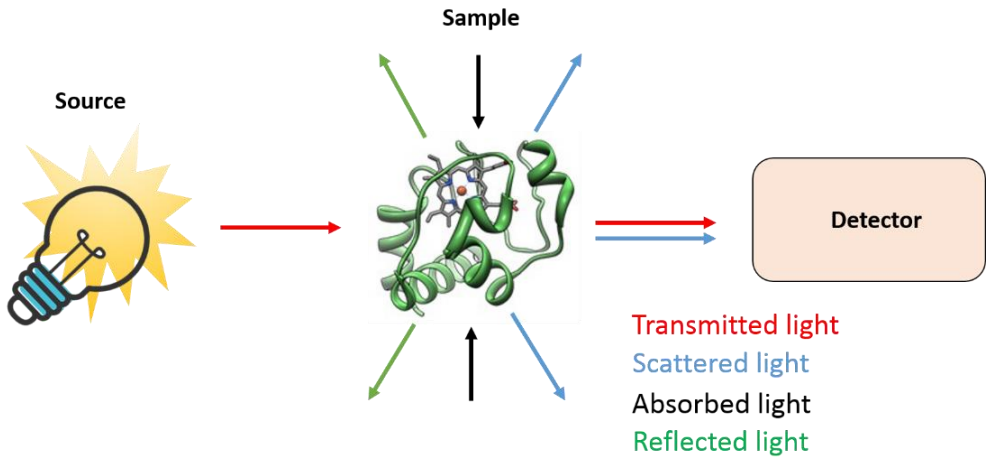

Figure 22. Scheme of the operating principle of spectroscopy in the simplest form.

Therefore, a nanoscale version of this technique is called nanospectroscopy. In such case, the source has a nanometric size and the interaction with the sample occurs on such scale. Thus, AuNPs would act as nanosources, because we obtain the information of the sample under study by changes in the absorption or scattering band of the AuNPs. Figure 23 shows a scheme of this idea.

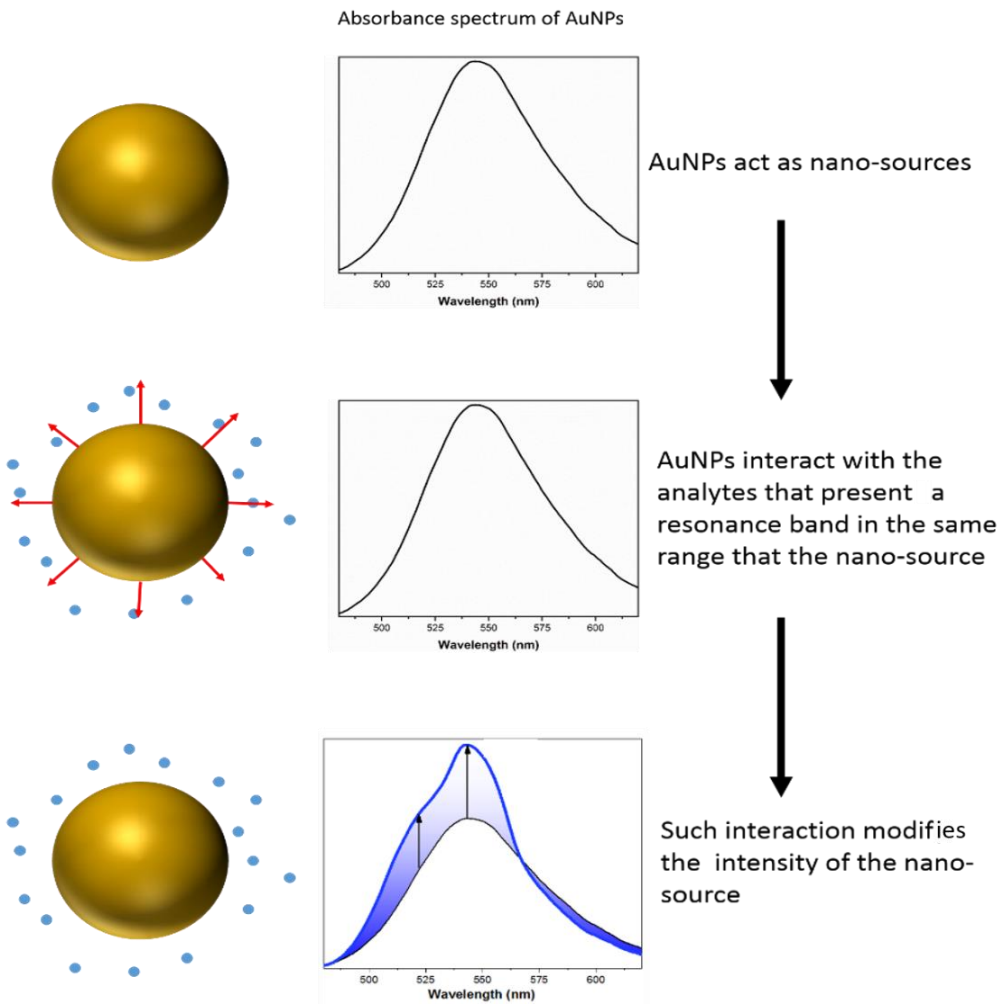

Figure 23. Scheme of the nanospectroscopic approach studied in this thesis.

An example of nanospectroscopy is the plasmon resonance energy transfer (PRET). PRET was studied for the first time by Luke P. Lee and co-workers[110], and it is based on the energy transfer between a plasmonic donor and an adjacent resonance receptor, similar to FRET, but with a metal nanoparticle as a donor. This effect only occurs when there is a match between the AuNP resonance frequency and the resonance frequency of the element under testing. One of the most relevant advantages of this nanospectroscopic effect

is the selectivity that it provides, as a variation in the AuNPs spectrum only occurs when the aforementioned matching between the resonance bands exists. Thus, if we want to detect a certain sample that is mixed, for example, in a liquid with other different samples, we are able to excite a specific electromagnetic band that corresponds with the one that characterizes our sample of interest. Thanks to the properties of metal nanoparticles, selecting the convenient band does not represent a problem because, as we have shown previously, it is possible to change the wavelength resonance by modifying the metal, shape, or size.

Several studies have been developed by exploiting this nanospectroscopic effect with a variety of applications, such as proteins (like Cyt c), hydrogen peroxide, fluoride and copper ions in water, and 2,4,6-trinitrotoluene (TNT)[110-115]. Further applications include the study of the adhesion kinetics of biomolecules and enzymes, observing quenches or dips in the spectrum of the nanoparticle. Sensors based on PRET provide high selectivity and sensitivity, however, this phenomenon has not been used as much as it would be expected, due to the fact that it is very difficult exploit it with traditional setups. Usually, the setup used to trigger this effect is the dark-field microscopy. Such microscopy method is based on exciting the LSPR effect of the metal nanoparticles by the evanescence field, in such a way that the light used to excite the LSPR effect does not arrive to the viewer. Therefore, only the light that scatters the nanoparticles is observed. The operating principle of this technique is depicted in Figure 24. The main limitation of these setups is that they are not useful for measurements out of the laboratory and, therefore, for POC applications are not applicable.

For this reason, the novelty that we introduce in this thesis is the combination of the nanospectroscopy with the lab-on-fiber technology, to obtain very sensitive and selective sensors. It is important to emphasize that our strategy is

to monitor changes in the AuNPs spectrum intensity, instead of the majority of sensors that are based on monitoring a shift in the spectrum caused by changes in the surrounding refractive index. Monitoring the shift may produce a lack of selectivity because a shift can be triggered due to changes in the external conditions, such as temperature or humidity, and thus resulting in a false positive.

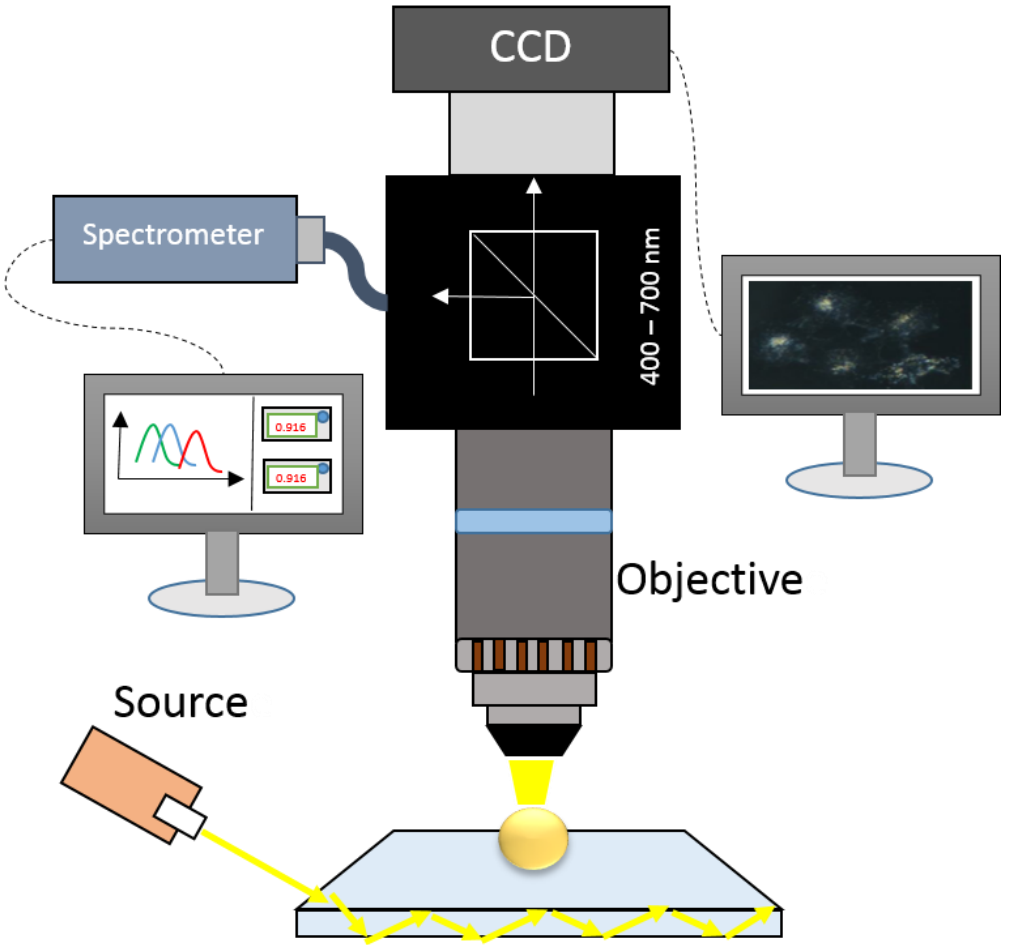

Figure 24. Scheme of a typical dark-field microscope, which consist of a source that excites the AuNPs by the evanescence field, an objective, that capture the scattered light from AuNPs, a splitter to divide the light to obtain the image and the spectrum from the focal point by a charge-coupled device (CCD) and a spectrometer, respectively.

In this thesis, we apply this strategy of detection in optical fibers with a chemical and biological application, Cu^{2+} and Cyt c, which will be explained in detail in Chapters 4 and 5 respectively.

References of Chapter 2

1. Clark Jr., L. C.; Lyons, C. Electrode systems for continuous monitoring in cardiovascular surgery. *Annals of the New York academy of sciences* **1962,** *102* (1), 29-45.
2. Shrivastava, A.; Gupta, V. Methods for the determination of limit of detection and limit of quantitation of the analytical methods. *Chronicles of Young Scientists* **2011,** *2*, 21.
3. Mohanty, S. P.; Kougianos, E. Biosensors: a tutorial review. *IEEE Potentials* **2006,** *25* (2), 35-40.
4. Gutiérrez, F. J. S. Development and fabrication of optical biosensors based on biophotonic sensing cells (BICELLs). Universidad Politécnica de Madrid, 2015.
5. Biosensors Market Size, S. T. A. R. B. A. M., Agriculture, Bioreactor) By Technology (Thermal, Electrochemical, Optical), By End Use, By Region, And Segment Forecasts, 2020 - 2027.
6. Mehrotra, P. Biosensors and their applications – A review. *Journal of Oral Biology and Craniofacial Research* **2016,** *6* (2), 153-159.
7. Syahir, A.; Usui, K.; Tomizaki, K.-y.; Kajikawa, K.; Mihara, H. Label and Label-Free Detection Techniques for Protein Microarrays. *Microarrays* **2015,** *4* (2), 228-244.
8. Ghosh, K.; Sarkar, T.; Majumdar, A.; Mandal, S. K.; Khuda-Bukhsh, A. R. Rhodamine-labelled simple architectures for fluorometric and colorimetric sensing of Hg2+ and Pb2+ ions in semi-aqueous and aqueous environments. *Analytical Methods* **2014,** *6* (8), 2648-2654.
9. Kim, H. N.; Ren, W. X.; Kim, J. S.; Yoon, J. Fluorescent and colorimetric sensors for detection of lead, cadmium, and mercury ions. *Chemical Society Reviews* **2012,** *41* (8), 3210-3244.
10. Medintz, I. L.; Hildebrandt, N. FRET-Förster resonance energy transfer: from theory to applications. *John Wiley & Sons* **2013**.
11. Selvin, P. R. Fluorescence resonance energy transfer. *Methods in Enzymology* **1995**, 246, 300-334.
12. Cardoso Dos Santos, M.; Algar, W. R.; Medintz, I. L.; Hildebrandt, N. Quantum dots for Förster Resonance Energy Transfer (FRET). *TrAC Trends in Analytical Chemistry* **2020,** *125*, 115819.
13. Bhatnagar, D.; Kumar, V.; Kumar, A.; Kaur, I. Graphene quantum dots FRET based sensor for early detection of heart attack in human. *Biosensors and Bioelectronics* **2016,** *79*, 495-499.
14. MacBeath, G.; Schreiber, S. L. Printing Proteins as Microarrays for High-Throughput Function Determination. *Science* **2000,** *289* (5485), 1760-1763.
15. Zhu, H.; Bilgin, M.; Bangham, R.; Hall, D.; Casamayor, A.; Bertone, P.; Lan, N.; Jansen, R.; Bidlingmaier, S.; Houfek, T.; Mitchell, T.; Miller, P.;

Dean, R. A.; Gerstein, M.; Snyder, M. Global Analysis of Protein Activities Using Proteome Chips. *Science* **2001,** *293* (5537), 2101-2105.
16. Michaud, G. A.; Salcius, M.; Zhou, F.; Bangham, R.; Bonin, J.; Guo, H.; Snyder, M.; Predki, P. F.; Schweitzer, B. I. Analyzing antibody specificity with whole proteome microarrays. *Nature Biotechnology* **2003,** *21* (12), 1509-1512.
17. de Castro, A. C. H.; Alves, L. M.; Siquieroli, A. C. S.; Madurro, J. M.; Brito-Madurro, A. G. Label-free electrochemical immunosensor for detection of oncomarker CA125 in serum. *Microchemical Journal* **2020,** *155*, 104746.
18. Andrade, J. E. d.; Machado, R.; Macêdo, M. A.; Cunha, F. G. C. J. P. AFM and XRD characterization of silver nanoparticles films deposited on the surface of DGEBA epoxy resin by ion sputtering. **2013,** *23* (1), 19-23.
19. Hu, Y.; Xing, H.; Li, G.; Wu, M. Magnetic Imprinted Polymer-Based Quartz Crystal Microbalance Sensor for Sensitive Label-Free Detection of Methylene Blue in Groundwater. *Sensors* **2020,** *20* (19), 5506.
20. Tateno, H.; Uchiyama, N.; Kuno, A.; Togayachi, A.; Sato, T.; Narimatsu, H.; Hirabayashi, J. A novel strategy for mammalian cell surface glycome profiling using lectin microarray. *Glycobiology* **2007,** *17* (10), 1138-1146.
21. Azkune, M.; Frosch, T.; Arrospide, E.; Aldabaldetreku, G.; Bikandi, I.; Zubia, J.; Popp, J.; Frosch, T. Liquid-Core Microstructured Polymer Optical Fiber as Fiber-Enhanced Raman Spectroscopy Probe for Glucose Sensing. *Journal of Lightwave Technology* **2019,** *37* (13), 2981-2988.
22. Negahdary, M. Aptamers in nanostructure-based electrochemical biosensors for cardiac biomarkers and cancer biomarkers: A review. *Biosensors and Bioelectronics* **2020,** *152*, 112018.
23. Khanmohammadi, A.; Aghaie, A.; Vahedi, E.; Qazvini, A.; Ghanei, M.; Afkhami, A.; Hajian, A.; Bagheri, H. Electrochemical biosensors for the detection of lung cancer biomarkers: A review. *Talanta* **2020,** *206*, 120251.
24. Putzbach, W.; Ronkainen, N. J. Immobilization Techniques in the Fabrication of Nanomaterial-Based Electrochemical Biosensors: A Review. *Sensors* **2013,** *13* (4), 4811-4840.
25. Arlett, J. L.; Myers, E. B.; Roukes, M. L. Comparative advantages of mechanical biosensors. *Nature Nanotechnology* **2011,** *6* (4), 203-215.
26. Nabaei, V.; Chandrawati, R.; Heidari, H. Magnetic biosensors: Modelling and simulation. *Biosensors and Bioelectronics* **2018,** *103*, 69-86.
27. Chen, Y.; Liu, J.; Yang, Z.; Wilkinson, J. S.; Zhou, X. Optical biosensors based on refractometric sensing schemes: A review. *Biosensors and Bioelectronics* **2019,** *144*, 111693.
28. Lopez, G. A.; Estevez, M.-C.; Soler, M.; Lechuga, L. M. Recent advances in nanoplasmonic biosensors: applications and lab-on-a-chip integration. *Nanophotonics* **2017,** *6* (1), 123-136.
29. Wangüemert-Pérez, J. G.; Hadij-ElHouati, A.; Sánchez-Postigo, A.; Leuermann, J.; Xu, D.-X.; Cheben, P.; Ortega-Moñux, A.; Halir, R.;

Molina-Fernández, Í. Subwavelength structures for silicon photonics biosensing. *Optics & Laser Technology* **2019,** *109*, 437-448.
30. Gauglitz, G. Point-of-Care Platforms. *Annual review of analytical chemistry* **2014,** *7* (1), 297-315.
31. Molina-Fernández, Í.; Leuermann, J.; Ortega-Moñux, A.; Wangüemert-Pérez, J. G.; Halir, R. Fundamental limit of detection of photonic biosensors with coherent phase read-out. *Opt. Express* **2019,** *27* (9), 12616-12629.
32. Bastos, A. R.; Vicente, C. M. S.; Oliveira-Silva, R.; Silva, N. J. O.; Tacão, M.; Costa, J. P. d.; Lima, M.; André, P. S.; Ferreira, R. A. S. Integrated Optical Mach-Zehnder Interferometer Based on Organic-Inorganic Hybrids for Photonics-on-a-Chip Biosensing Applications. *Sensors* **2018,** *18* (3), 840.
33. Chang, C.-W.; Xu, X.; Chakravarty, S.; Huang, H.-C.; Tu, L.-W.; Chen, Q. Y.; Dalir, H.; Krainak, M. A.; Chen, R. T. Pedestal subwavelength grating metamaterial waveguide ring resonator for ultra-sensitive label-free biosensing. *Biosensors and Bioelectronics* **2019,** *141*, 111396.
34. Hänsel, A.; Heck, M. J. R. Opportunities for photonic integrated circuits in optical gas sensors. *Journal of Physics: Photonics* **2020,** *2* (1), 012002.
35. Huang, Y.; Tian, Z.; Sun, L.-P.; Sun, D.; Li, J.; Ran, Y.; Guan, B.-O. High-sensitivity DNA biosensor based on optical fiber taper interferometer coated with conjugated polymer tentacle. *Opt. Express* **2015,** *23* (21), 26962-26968.
36. Arrizabalaga, O.; Velasco, J.; Zubia, J.; Sáez de Ocáriz, I.; Villatoro, J. Miniature interferometric humidity sensor based on an off-center polymer cap onto optical fiber facet. *Sensors and Actuators B: Chemical* **2019,** *297*, 126700.
37. Loyez, M.; Hassan, E. M.; Lobry, M.; Liu, F.; Caucheteur, C.; Wattiez, R.; DeRosa, M. C.; Willmore, W. G.; Albert, J. Rapid Detection of Circulating Breast Cancer Cells Using a Multiresonant Optical Fiber Aptasensor with Plasmonic Amplification. *ACS Sensors* **2020,** *5* (2), 454-463.
38. Li, M.; Cushing, S. K.; Wu, N. Plasmon-enhanced optical sensors: a review. *Analyst* **2015,** *140* (2), 386-406.
39. Homola, J. Surface Plasmon Resonance Sensors for Detection of Chemical and Biological Species. *Chemical Reviews* **2008,** *108* (2), 462-493.
40. Caucheteur, C.; Guo, T.; Albert, J. Review of plasmonic fiber optic biochemical sensors: improving the limit of detection. *Analytical and Bioanalytical Chemistry* **2015,** *407* (14), 3883-3897.
41. Raether, H. Surface plasmons on smooth surfaces. In *Surface plasmons on smooth and rough surfaces and on gratings*, Springer: 1988; pp 4-39.
42. Takagi, K.; Sasaki, H.; Seki, A.; Watanabe, K. Surface plasmon resonances of a curved hetero-core optical fiber sensor. *Sensors and Actuators A: Physical* **2010,** *161* (1), 1-5.

43. Huang, X.; El-Sayed, M. A. Gold nanoparticles: Optical properties and implementations in cancer diagnosis and photothermal therapy. *Journal of Advanced Research* **2010,** *1* (1), 13-28.
44. Sepúlveda, B.; Angelomé, P. C.; Lechuga, L. M.; Liz-Marzán, L. M. LSPR-based nanobiosensors. *Nano Today* **2009,** *4* (3), 244-251.
45. Haes, A. J.; Van Duyne, R. P. A unified view of propagating and localized surface plasmon resonance biosensors. *Analytical and Bioanalytical Chemistry* **2004,** *379* (7), 920-930.
46. Horvath, H. Gustav Mie and the scattering and absorption of light by particles: Historic developments and basics. *Journal of Quantitative Spectroscopy and Radiative Transfer* **2009,** *110* (11), 787-799.
47. Mie, G. J. A. d. p. Beiträge zur Optik trüber Medien, speziell kolloidaler Metallösungen. *Annalen der physik* **1908,** *330* (3), 377-445.
48. Bohren, C. F.; Huffman, D. R. Absorption and scattering of light by small particles. *John Wiley & Sons* **2008**.
49. Duque, J. S.; Blandón, J. S.; Riascos, H. Localized Plasmon resonance in metal nanoparticles using Mie theory. *Journal of Physics: Conference Series* **2017,** *850*, 012017.
50. Saa, L.; Coronado-Puchau, M.; Pavlov, V.; Liz-Marzán, L. M. Enzymatic etching of gold nanorods by horseradish peroxidase and application to blood glucose detection. *Nanoscale* **2014,** *6* (13), 7405-7409.
51. Johnson, P. B.; Christy, R. W. Optical Constants of the Noble Metals. *Physical Review B* **1972,** *6* (12), 4370-4379.
52. Ong, Q. K.; Reguera, J.; Silva, P. J.; Moglianetti, M.; Harkness, K.; Longobardi, M.; Mali, K. S.; Renner, C.; De Feyter, S.; Stellacci, F. High-Resolution Scanning Tunneling Microscopy Characterization of Mixed Monolayer Protected Gold Nanoparticles. *ACS Nano* **2013,** *7* (10), 8529-8539.
53. Senthil Kumar, P.; Pastoriza-Santos, I.; Rodríguez-González, B.; Javier García de Abajo, F.; Liz-Marzán, L. M. High-yield synthesis and optical response of gold nanostars. *Nanotechnology* **2007,** *19* (1), 015606.
54. Chin, C. D.-W.; Akbarian-Tefaghi, S.; Reconco-Ramirez, J.; Wiley, J. B. J. M. C. Rapid microwave synthesis and optical activity of highly crystalline platinum nanocubes. *MRS Communications* **2018,** *8* (1), 71-78.
55. Halvorson, R. A.; Vikesland, P. J. Surface-Enhanced Raman Spectroscopy (SERS) for Environmental Analyses. *Environmental Science & Technology* **2010,** *44* (20), 7749-7755.
56. Pisco, M.; Cusano, A. J. S. Lab-on-fiber technology: a roadmap toward multifunctional plug and play platforms. **2020,** *20* (17), 4705.
57. Cusano, A.; Consales, M.; Crescitelli, A.; Ricciardi, A. Lab-on-fiber technology. *Springer* **2015**.
58. Vaiano, P.; Carotenuto, B.; Pisco, M.; Ricciardi, A.; Quero, G.; Consales, M.; Crescitelli, A.; Esposito, E.; Cusano, A. Lab on Fiber Technology for

biological sensing applications. *Lasers & Photonics reviews* **2016,** *10* (6), 922-961.
59. Ricciardi, A.; Crescitelli, A.; Vaiano, P.; Quero, G.; Consales, M.; Pisco, M.; Esposito, E.; Cusano, A. Lab-on-fiber technology: a new vision for chemical and biological sensing. *Analyst* **2015,** *140* (24), 8068-8079.
60. Consales, M.; Ricciardi, A.; Crescitelli, A.; Esposito, E.; Cutolo, A.; Cusano, A. Lab-on-Fiber Technology: Toward Multifunctional Optical Nanoprobes. *ACS Nano* **2012,** *6* (4), 3163-3170.
61. Giaquinto, M.; Aliberti, A.; Micco, A.; Gambino, F.; Ruvo, M.; Ricciardi, A.; Cusano, A. Cavity-Enhanced Lab-on-Fiber Technology: Toward Advanced Biosensors and Nano-Opto-Mechanical Active Devices. *ACS Photonics* **2019,** *6* (12), 3271-3280.
62. Calero, V.; Suarez, M. A.; Salut, R.; Baida, F.; Caspar, A.; Behague, F.; Courjal, N.; Galtier, L.; Gillette, L.; Duvillaret, L.; Gaborit, G.; Bernal, M. P. An ultra wideband-high spatial resolution-compact electric field sensor based on Lab-on-Fiber technology. *Scientific Reports* **2019,** *9* (1), 8058.
63. Arrizabalaga, O.; Zubia, J.; Villatoro, J. Microrefractometer Based on Off-Center Polymer Caps Bonded Onto Optical Fiber Tips. *Journal of Lightwave Technology* **2018,** *36* (17), 3573-3579.
64. Yao, M.; Ouyang, X.; Wu, J.; Zhang, A. P.; Tam, H.-Y.; Wai, P. K. A. Optical Fiber-Tip Sensors Based on In-Situ μ-Printed Polymer Suspended-Microbeams. *Sensors* **2018,** *18* (6), 1825.
65. Giaquinto, M.; Micco, A.; Aliberti, A.; Bobeico, E.; La Ferrara, V.; Ruvo, M.; Ricciardi, A.; Cusano, A. Optimization Strategies for Responsivity Control of Microgel Assisted Lab-On-Fiber Optrodes. *Sensors* **2018,** *18* (4), 1119.
66. Pissadakis, S. Lab-in-a-fiber sensors: A review. *Microelectronic Engineering* **2019,** *217*, 111105.
67. Liu, G.; Zhang, K.; Nadort, A.; Hutchinson, M. R.; Goldys, E. M. Sensitive Cytokine Assay Based on Optical Fiber Allowing Localized and Spatially Resolved Detection of Interleukin-6. *ACS Sensors* **2017,** *2* (2), 218-226.
68. Birks, T. A.; Knight, J. C.; Russell, P. S. J. Endlessly single-mode photonic crystal fiber. *Optics Letters.* **1997,** *22* (13), 961-963.
69. Cregan, R. F.; Mangan, B. J.; Knight, J. C.; Birks, T. A.; Russell, P. S. J.; Roberts, P. J.; Allan, D. C. Single-Mode Photonic Band Gap Guidance of Light in Air. *Science* **1999,** *285* (5433), 1537-1539.
70. Arrospide, E.; Durana, G.; Azkune, M.; Aldabaldetreku, G.; Bikandi, I.; Ruiz-Rubio, L.; Zubia, J. Polymers beyond standard optical fibres–fabrication of microstructured polymer optical fibres. *Polymers* **2018,** *67* (9), 1155-1163.
71. Wang, J.; Liu, C.; Wang, F.; Su, W.; Yang, L.; Lv, J.; Fu, G.; Li, X.; Liu, Q.; Sun, T.; Chu, P. K. Surface plasmon resonance sensor based on coupling effects of dual photonic crystal fibers for low refractive indexes detection. *Results in Physics* **2020,** *18*, 103240.

72. Qu, Y.; Yuan, J.; Zhou, X.; Li, F.; Yan, B.; Wu, Q.; Wang, K.; Sang, X.; Long, K.; Yu, C. Mid-infrared silicon photonic crystal fiber polarization filter based on surface plasmon resonance effect. *Optics Communications* **2020,** *463*, 125387.
73. Lee, H. W.; Schmidt, M. A.; Russell, R. F.; Joly, N. Y.; Tyagi, H. K.; Uebel, P.; Russell, P. Pressure-assisted melt-filling and optical characterization of Au nano-wires in microstructured fibers. *Opt. Express* **2011,** *19* (13), 12180-12189.
74. Ding, Z.; Lang, T.; Wang, Y.; Zhao, C. Surface Plasmon Resonance Refractive Index Sensor Based on Tapered Coreless Optical Fiber Structure. *Journal of Lightwave Technology* **2017,** *35* (21), 4734-4739.
75. Loyez, M.; Lobry, M.; Hassan, E. M.; DeRosa, M. C.; Caucheteur, C.; Wattiez, R. HER2 breast cancer biomarker detection using a sandwich optical fiber assay. *Talanta* **2021,** *221*, 121452.
76. Azkune, M.; Ruiz-Rubio, L.; Aldabaldetreku, G.; Arrospide, E.; Pérez-Álvarez, L.; Bikandi, I.; Zubia, J.; Vilas-Vilela, J. L. U-Shaped and Surface Functionalized Polymer Optical Fiber Probe for Glucose Detection. *Sensors* **2018,** *18* (1), 34.
77. Zhang, C.; Li, Z.; Jiang, S. Z.; Li, C. H.; Xu, S. C.; Yu, J.; Li, Z.; Wang, M. H.; Liu, A. H.; Man, B. Y. U-bent fiber optic SPR sensor based on graphene/AgNPs. *Sensors and Actuators B: Chemical* **2017,** *251*, 127-133.
78. Chiavaioli, F.; Baldini, F.; Tombelli, S.; Trono, C.; Giannetti, A. Biosensing with optical fiber gratings. *Nanophotonics* **2017,** *6* (4), 663-679.
79. Schuster, T.; Herschel, R.; Neumann, N.; Schaffer, C. G. Miniaturized Long-Period Fiber Grating Assisted Surface Plasmon Resonance Sensor. *Journal of Lightwave Technology* **2012,** *30* (8), 1003-1008.
80. Loyez, M.; Albert, J.; Caucheteur, C.; Wattiez, R. Cytokeratins Biosensing Using Tilted Fiber Gratings. **2018,** *8* (3), 74.
81. Márquez-Cruz, V.; Albert, J. High Resolution NIR TFBG-Assisted Biochemical Sensors. *Journal of Lightwave Technology* **2015,** *33* (16), 3363-3373.
82. Caucheteur, C.; Guo, T.; Liu, F.; Guan, B.-O.; Albert, J. Ultrasensitive plasmonic sensing in air using optical fibre spectral combs. *Nature Communications* **2016,** *7* (1), 13371.
83. Guo, T.; Liu, F.; Guan, B.-O.; Albert, J. [INVITED] Tilted fiber grating mechanical and biochemical sensors. *Optics & Laser Technology* **2016,** *78*, 19-33.
84. Kim, H.-M.; Uh, M.; Jeong, D. H.; Lee, H.-Y.; Park, J.-H.; Lee, S.-K. Localized surface plasmon resonance biosensor using nanopatterned gold particles on the surface of an optical fiber. *Sensors and Actuators B: Chemical* **2019,** *280*, 183-191.
85. Dhawan, A.; Muth, J. F.; Leonard, D. N.; Gerhold, M. D.; Gleeson, J.; Vo-Dinh, T.; Russell, P. Focused ion beam fabrication of metallic nanostructures on end faces of optical fibers for chemical sensing

applications. *Journal of Vacuum Science & Technology B* **2008,** *26* (6), 2168-2173.
86. Nguyen, H.; Sidiroglou, F.; Collins, S. F.; Davis, T. J.; Roberts, A.; Baxter, G. W. A localized surface plasmon resonance-based optical fiber sensor with sub-wavelength apertures. *Applied Physics Letters* **2013,** *103* (19), 193116.
87. Micco, A.; Ricciardi, A.; Pisco, M.; La Ferrara, V.; Cusano, A. Optical fiber tip templating using direct focused ion beam milling. *Scientific Reports* **2015,** *5* (1), 15935.
88. Chen, Y. Nanofabrication by electron beam lithography and its applications: A review. *Microelectronic Engineering* **2015,** *135*, 57-72.
89. Lin, Y.; Zou, Y.; Mo, Y.; Guo, J.; Lindquist, R. G. E-Beam Patterned Gold Nanodot Arrays on Optical Fiber Tips for Localized Surface Plasmon Resonance Biochemical Sensing. *Sensors* **2010,** *10* (10), 9397-9406.
90. Lin, Y.; Zou, Y.; Lindquist, R. G. A reflection-based localized surface plasmon resonance fiber-optic probe for biochemical sensing. *Biomed. Opt. Express* **2011,** *2* (3), 478-484.
91. Sanders, M.; Lin, Y.; Wei, J.; Bono, T.; Lindquist, R. G. An enhanced LSPR fiber-optic nanoprobe for ultrasensitive detection of protein biomarkers. *Biosensors and Bioelectronics* **2014,** *61*, 95-101.
92. Smythe, E. J.; Dickey, M. D.; Whitesides, G. M.; Capasso, F. A Technique to Transfer Metallic Nanoscale Patterns to Small and Non-Planar Surfaces. *ACS Nano* **2009,** *3* (1), 59-65.
93. Jia, P.; Yang, Z.; Yang, J.; Ebendorff-Heidepriem, H. Quasiperiodic Nanohole Arrays on Optical Fibers as Plasmonic Sensors: Fabrication and Sensitivity Determination. *ACS Sensors* **2016,** *1* (8), 1078-1083.
94. Siegfried, T.; Ekinci, Y.; Martin, O. J. F.; Sigg, H. Engineering Metal Adhesion Layers That Do Not Deteriorate Plasmon Resonances. *ACS Nano* **2013,** *7* (3), 2751-2757.
95. Jia, P.; Yang, J. A plasmonic optical fiber patterned by template transfer as a high-performance flexible nanoprobe for real-time biosensing. *Nanoscale* **2014,** *6* (15), 8836-8843.
96. Liang, Y.; Yu, Z.; Li, L.; Xu, T. A self-assembled plasmonic optical fiber nanoprobe for label-free biosensing. *Scientific Reports* **2019,** *9* (1), 7379.
97. Polley, N.; Basak, S.; Hass, R.; Pacholski, C. Fiber optic plasmonic sensors: Providing sensitive biosensor platforms with minimal lab equipment. *Biosensors and Bioelectronics* **2019,** *132*, 368-374.
98. Pisco, M.; Galeotti, F.; Quero, G.; Grisci, G.; Micco, A.; Mercaldo, L. V.; Veneri, P. D.; Cutolo, A.; Cusano, A. Nanosphere lithography for optical fiber tip nanoprobes. *Light: Science & Applications* **2017,** *6* (5), e16229-e16229.
99. Mitsui, K.; Handa, Y.; Kajikawa, K. Optical fiber affinity biosensor based on localized surface plasmon resonance. *Applied Physics Letters* **2004,** *85* (18), 4231-4233.

100. Kim, H.-M.; Park, J.-H.; Jeong, D. H.; Lee, H.-Y.; Lee, S.-K. Real-time detection of prostate-specific antigens using a highly reliable fiber-optic localized surface plasmon resonance sensor combined with micro fluidic channel. *Sensors and Actuators B: Chemical* **2018,** *273*, 891-898.
101. Jeong, H.-H.; Erdene, N.; Park, J.-H.; Jeong, D.-H.; Lee, S.-K. Analysis of Fiber-Optic Localized Surface Plasmon Resonance Sensor by Controlling Formation of Gold Nanoparticles and its Bio-Application. *Journal of Nanoscience and Nanotechnology* **2012,** *12* (10), 7815-7821.
102. Camara, A. R.; Gouvêa, P. M. P.; Dias, A. C. M. S.; Braga, A. M. B.; Dutra, R. F.; de Araujo, R. E.; Carvalho, I. C. S. Dengue immunoassay with an LSPR fiber optic sensor. *Opt. Express* **2013,** 21 (22), 27023-27031.
103. Shi, C.; Yan, H.; Gu, C.; Ghosh, D.; Seballos, L.; Chen, S.; Zhang, J. Z.; Chen, B. A double substrate “sandwich” structure for fiber surface enhanced Raman scattering detection. *Applied Physics Letters* **2008,** *92* (10), 103107.
104. Norov, E.; Jeong, H.-H.; Park, J.-H.; Lee, S.-K.; Jeong, D. H. J. R. C. i. P. Fiber-Optic Sensor Simultaneously Detecting Localized Surface Plasmon Resonance and Surface-Enhanced Raman Scattering. *Rapid Communication in Photoscience* **2013,** *2* (2), 46-51.
105. Sciacca, B.; Monro, T. M. Dip Biosensor Based on Localized Surface Plasmon Resonance at the Tip of an Optical Fiber. *Langmuir* **2014,** *30* (3), 946-954.
106. Kim, H.-M.; Park, J.-H.; Lee, S.-K. Fiber optic sensor based on ZnO nanowires decorated by Au nanoparticles for improved plasmonic biosensor. *Scientific Reports* **2019,** *9* (1), 15605.
107. Uh, M.; Kim, J.-S.; Park, J.-H.; Jeong, D. H.; Lee, H.-Y.; Lee, S.-M.; Lee, S.-K. Fabrication of Localized Surface Plasmon Resonance Sensor Based on Optical Fiber and Micro Fluidic Channel. *Journal of Nanoscience and Nanotechnology* **2017,** *17* (2), 1083-1091.
108. Ortega-Gomez, A.; Barroso, J.; Calatayud-Sánchez, A.; Zubia, J.; Benito-Lopez, F.; Basabe-Desmonts, L.; Villatoro, J. Cytochrome c detection by plasmonic nanospectroscopy on optical fiber facets. *Sensors and Actuators B: Chemical* **2021,** *330*, 129358.
109. Barroso, J.; Ortega-Gomez, A.; Calatayud-Sanchez, A.; Zubia, J.; Benito-Lopez, F.; Villatoro, J.; Basabe-Desmonts, L. Selective Ultrasensitive Optical Fiber Nanosensors Based on Plasmon Resonance Energy Transfer. *ACS Sensors* **2020,** *5* (7), 2018-2024.
110. Liu, G. L.; Long, Y.-T.; Choi, Y.; Kang, T.; Lee, L. P. Quantized plasmon quenching dips nanospectroscopy via plasmon resonance energy transfer. *Nature Methods* **2007,** *4* (12), 1015-1017.
111. Kim, Y.; Park, J. Y.; Kim, H. Y.; Lee, M.; Yi, J.; Choi, I. A single nanoparticle-based sensor for hydrogen peroxide (H2O2) via cytochrome

c-mediated plasmon resonance energy transfer. *Chemical Communications* **2015,** *51* (84), 15370-15373.
112. Choi, Y.; Park, Y.; Kang, T.; Lee, L. P. Selective and sensitive detection of metal ions by plasmonic resonance energy transfer-based nanospectroscopy. *Nature Nanotechnology* **2009,** *4* (11), 742-746.
113. Qu, W.-G.; Deng, B.; Zhong, S.-L.; Shi, H.-Y.; Wang, S.-S.; Xu, A.-W. Plasmonic resonance energy transfer-based nanospectroscopy for sensitive and selective detection of 2,4,6-trinitrotoluene (TNT). *Chemical Communications* **2011,** *47* (4), 1237-1239.
114. Li, S.-S.; Kong, Q.-Y.; Zhang, M.; Yang, F.; Kang, B.; Xu, J.-J.; Chen, H.-Y. Plasmon-Resonance-Energy-Transfer-Based Spectroscopy on Single Nanoparticles: Biomolecular Recognition and Enzyme Kinetics. *Analytical Chemistry* **2018,** *90* (6), 3833-3841.
115. Xin, H.; Sim, W. J.; Namgung, B.; Choi, Y.; Li, B.; Lee, L. P. Quantum biological tunnel junction for electron transfer imaging in live cells. *Nature Communications* **2019,** *10* (1), 3245.

3. Fiber probe manufacturing

As we explained in Chapter 2, lab-on-fiber represents a promising technology for biochemical sensing[1]. The combination of optical fibers and the plasmonic effect in different schemes provides highly performance adding the advantages of optical fibers. As we previously explained, the approach of this thesis is based on the excitation of AuNPs immobilized onto an optical fiber tip for biochemical sensing. In this chapter, we will explain the fabrication process of our lab-on-fiber-based probe, and in the following chapters, we will show the different applications based on the nanospectroscopic approach.

First, we will explain the operating principle and the immobilization protocol of the AuNPs, and then, the characterization of such process will be shown. At this point, two different characterization have been carried out: i) spectral characterization, to study the variation of the LSPR signal of AuNPs in real time during the immobilization process; and ii) SEM characterization, where many fibers were characterized by image analysis to understand the relation between the number of AuNPs and the LSPR intensity of the spectrum. In addition, SEM images provide us much information about the aggregation of AuNPs and its impact on the probe response. The main goal of both characterizations is to control the immobilization of AuNPs, in order to increase the reproducibility ratio. Finally, the effect in the immobilization process of the temperature, the size of the fiber's core, and the concentration of AuNPs was studied by spectral characterization, and the results of such experiments will be shown. The setup used in this chapter to record the LSPR spectrum of AuNPs is shown in Appendix 1.

3.1. Operating principle

The working principle of the optical probe developed in this thesis is based on the excitation of the LSPR effect. In our case, the AuNPs are attached on the optical fiber end face chemically. Therefore, the sensitivity part of the fiber is the tip of the fiber. A scheme of the probe is depicted in Figure 25.

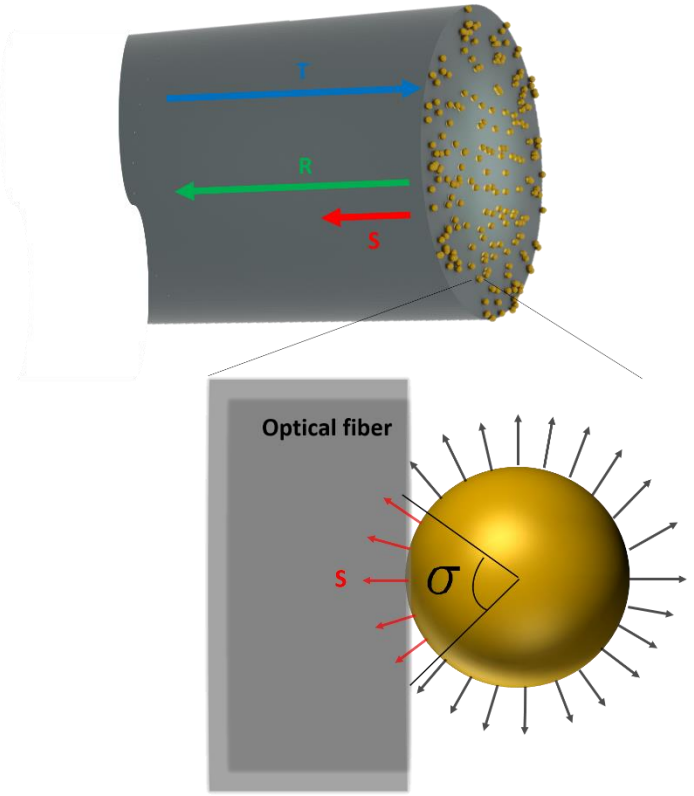

Figure 25. Scheme of AuNPs immobilized onto the optical fiber end face. The blue, green and red rays represent the transmission light, the reflected one by the end face, and the scattering from the AuNPs when are excited by the transmission light, respectively.

The light propagates through the optical fiber, and when it arrives to the end face, one part is reflected and the other is transmitted to the outside. In this

manner, the end face acts as a low reflectivity mirror. However, the presence of nanoparticles causes an interaction light-AuNPs that excites the electrons of the AuNPs, setting them in an oscillatory movement, which generates two fundamental phenomena: scattering and absorption[2-4]. In Figure 26, the electromagnetic field generated around one AuNP with a diameter of 40 nm caused by the LSPR effect is shown. The simulations were done by Lumerical. This effect is very strong; however, as it can be observed in such figure, that the electromagnetic field decays exponentially. This phenomenon was further explained in Chapter 2, section 2.2.2.

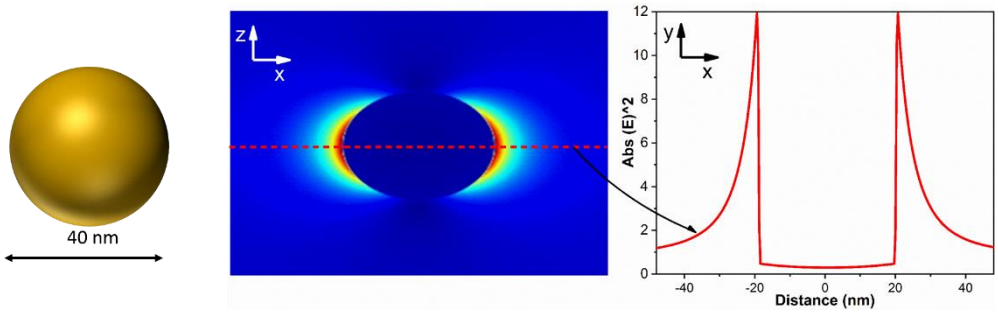

Figure 26. Electromagnetic distribution of one AuNPs at 550 nm when it is excited by a planar wave.

In Figure 25, we show all the contributions of AuNPs in the optical fiber. The most relevant contributions are the scattered light from AuNPs, and the reflected light due to the Fresnel reflection. Thus, the total light that arrives to our spectrometer can be expressed as:

$$I = R + S \tag{11}$$

Where R is the reflected light, green ray in Figure 25, and S is the scattered light from nanoparticles, red ray in Figure 25.

The reflected light is the combination of a fraction of the transmitted light and the light absorbed by the AuNPs. Note that the excitation wavelength of AuNPs

has to match with the wavelength of the transmission light to trigger the LSPR effect. Thus, the reflected light can be expressed as:

$$R = (T * \rho) - A \tag{12}$$

where T represents the transmission light, A the absorbed one by the AuNPs, and ρ the Fresnel coefficient, that can be described as $(n_c - n_o)^2/(n_c + n_o)^2$, being n_c and n_o the refractive index of the core and the outside medium respectively.

Regarding the scattered light, if we assume that the AuNPs scatter the light in all directions in a uniform manner, not all the light radiated from AuNPs is able to propagate in the optical fiber. On the one hand, because the half of the scattering goes to the outside, and on the other hand, because only the rays with an angle lower than the numerical aperture (NA) can be coupled to the fiber (see Figure 25) backward. Thus, the part of the scattered light from the AuNPs that propagates in the fiber can be simplify as:

$$S = S_{scatt-total} * \frac{2*\sin^{-1}\left(\frac{\sqrt{n_{core}-n_{cladd}}}{n_0}\right)}{360^\circ} \tag{13}$$

where $S_{scatt-total}$ referees to all the scattered light from the AuNPs, n_{core} and n_{cladd} are the refractive index of the core and cladding respectively, and n_0 the refractive index where the fiber is immersed (the refractive index surrounding medium).

Finally, the light that arrives at the spectrometer, if we do not take into account the losses, can be expressed according to the following equation:

$$I = T * \frac{(n_{core}-n_o)^2}{(n_{core}+n_o)^2} - A + S_{scatt-total} * \left(\frac{2*sin^{-1}\left(\frac{\sqrt{n_{core}-n_{cladd}}}{n_0}\right)}{360^\circ}\right) \tag{14}$$

Note that, normally, in this thesis, the spectra of AuNPs recorded in this chapter were obtained when the fiber is immersed into an aqueous solution. Therefore, we can approximate that $n_o = 1{,}33$, $n_{core} = 1{,}459$ and $n_{cladd} = 1{,}443$, evaluated at 550 nm. Thus, the Eq. 14 could be expressed as:

$$I = 0.0021 * T - A + 0.03 * S_{scatt-total} \quad (15)$$

As it can be observed in Eq. 15, the contribution of the absorbed light may be higher than the one of the scattered light. For this reason, in our experiments, we observe an absorbance behaviour, as we will see in the following sections. However, it is important to point out that the signal recorded is a contribution of both optical phenomenon, absorbance and scattering.

3.2. AuNPs immobilization process

In this section, the manufacturing process of the optical fiber-based probe is shown. As we mentioned, this method is based on the chemical immobilization of AuNPs, which is a very simple method previously reported[5-7].

First, we have to prepare the optical fiber, removing the polymer coating, cleaning and cleaving it, where the tip of the fiber looks as shown in Figure 27. Then, it is mandatory to remove all the dirt localized on the tip of the fiber, and this was performed by the piranha solution, which is an acid that removes the organic waste. The piranha solution consists in a 3:1 mixture of sulfuric acid (H_2SO_4) and hydrogen peroxide (H_2O_2). Due to the irritating gas that the solution releases, this step was done in a gas chamber for 30 minutes. Once the fiber was cleaned, the end face was modified with 3-aminoproyltriethoxysilane (APTES) by incubation in 1mM APTES isopropanol for 2 hours and subsequently rinsed out with a solution of isopropanol-water (1:1). At this point, the optical fiber is ready for the immobilization of AuNPs. The last step is to immerse the fiber in the AuNPs solution. The chosen diameter of the AuNPs

was 40 nm, due to the wavelength excitation matches with the light source used in all our experiments (see Appendix 1). The time of this last step is one of the most relevant factors in the manufacturing process, as it has a strong impact on the intensity and the excitation wavelength of the LSPR spectrum.

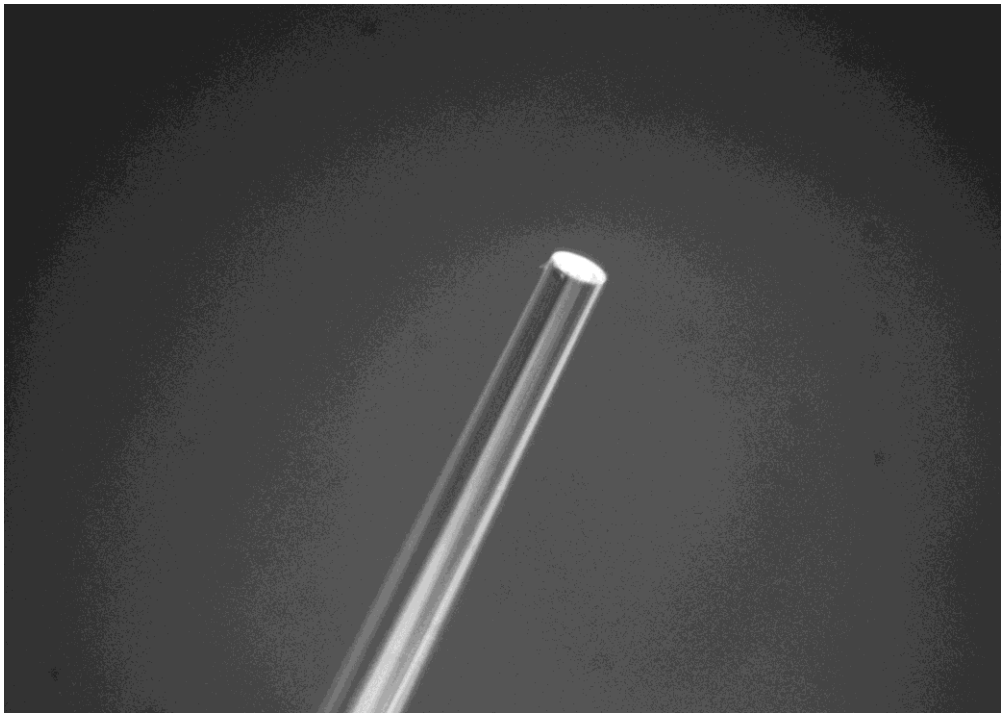

Figure 27. Photograph of the optical fiber after cleaning and cleaving.

This immobilization process is summarized in Figure 28. On the top of the figure, the recorded spectrum in each step is shown. Note that the spectra were obtained when the fiber was immersed in water. As it can be observed, the piranha solution and the tip modification by APTES does not have any impact on the spectrum, as it was expected. Only when the AuNPs are immobilized, the spectrum changes, and an absorption localized around 550 nm appears, which is the wavelength expected for the AuNPs@40 used. In the middle of the figure, a scheme of the fiber after each process is shown, and finally, photographs in the bottom which correspond with each step. The APTES is very

sensitive to the light. Which makes its polymerize, hindering the AuNPs immobilization. For this reason, the bottle with the APTES solution has to be covered (see Figure 28).

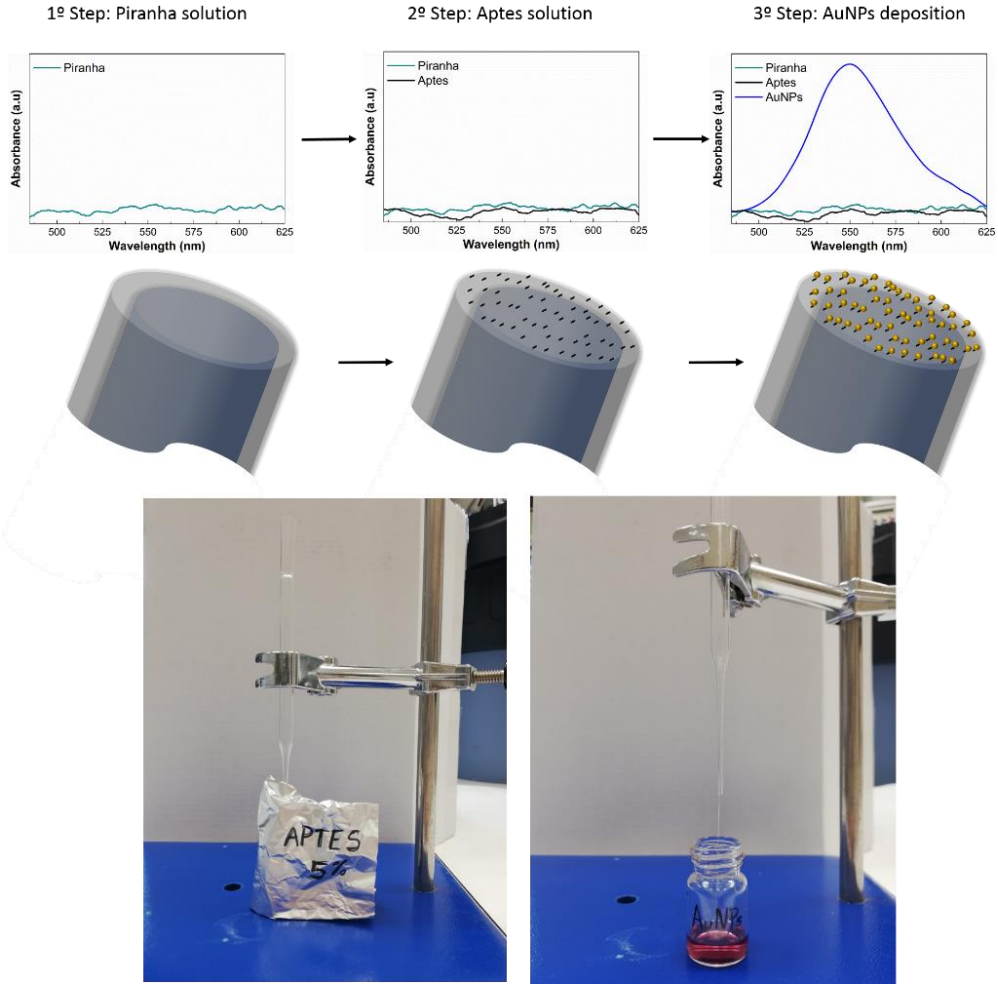

Figure 28. At the top, the recorded spectrum in each of the main steps of the immobilization protocol. In the middle, a graphical scheme of the fiber end face, and in the bottom photograph obtained in the process.

A deep study of the stability of the AuNPs immobilization was not performed, but the spectrum of the same optical probe once the immobilization was done

and after 4 months is shown in Figure 29, indicating that the coverage of the optical fiber with AuNPs is stable.

The last step of the immobilization protocol shown above, which corresponds with the AuNPs attachment, is the most significant and critical on to obtain the LSPR signal. This is due to the chemical immobilization being a random process and the obtained intensity has a strong dependence on the number of AuNPs immobilized, the aggregation of such AuNPs between them, etc. To obtain control about the immobilization process, we will do a characterization by the spectrum and by image analysis in the following sections.

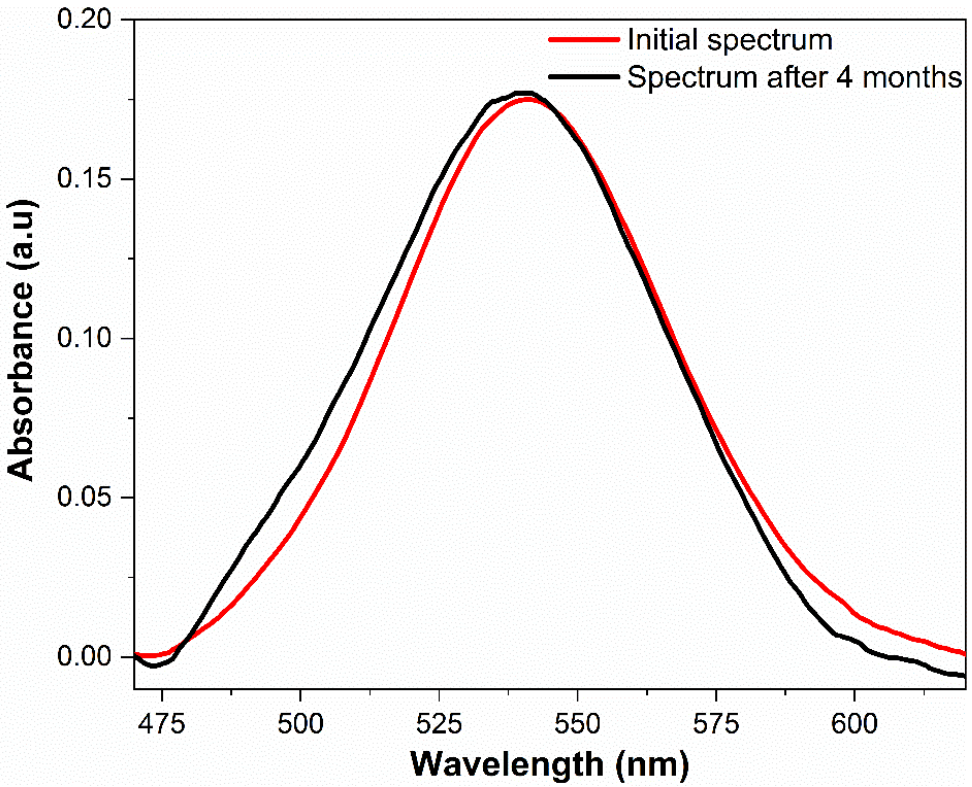

Figure 29. The red line corresponds to the spectrum that was obtained after the AuNPs immobilization and the black line corresponds with the same probe but 4 months after.

3.3. Characterization of the AuNPs immobilization

3.3.1. Spectral characterization

The evolution of the absorbance spectrum of AuNPs can be monitored in real time due to the optical fibers capabilities, which allow us to control the AuNPs deposition and its impact on the spectrum in real time. To that end, we monitored in real time the AuNPs immobilization under normal laboratory conditions (25 ^{0}C), stock concentration of AuNPs (optical density or OD 1) and using a fiber with a core of 105 µm. The evolution of the absorbance intensity with the time, the recorded spectra, and the shift observed are depicted in Figure 30.

The spectra shown in Figure 30 were obtained while the optical fiber was immersed in the AuNP solution. As it can be observed, there are three different tendencies on the AuNPs immobilization. The first one, represented by red, is observed at shorter times, and it has a linear behaviour. It is expected that the number of AuNPs attached to the optical fiber surface increases with time, and, therefore, that the absorbance intensity increases as well. We assume that the obtained LSPR signal corresponds to the contribution of each AuNP. However, this linear behaviour stops at a certain time, and the absorbance intensity achieves a plateau, which is represented in Figure 30 by the black colour. In other words, the absorbance intensity has a limit due to the covered surface by AuNPs (see Figure 30). At this point, AuNPs are not in a single form mostly and the resonance wavelength shifts, as it can be observed in Figure 30, due to the increasing number of aggregated AuNPs. Nevertheless, this plateau is not constant over time; on the contrary, what is observed is a third behaviour (see Figure 30, blue colour), where the intensity decreases. The absorbance

intensity drops because the aggregation of AuNPs increases and there is a higher coverage of the optical fiber end face, which works as a reflective layer.

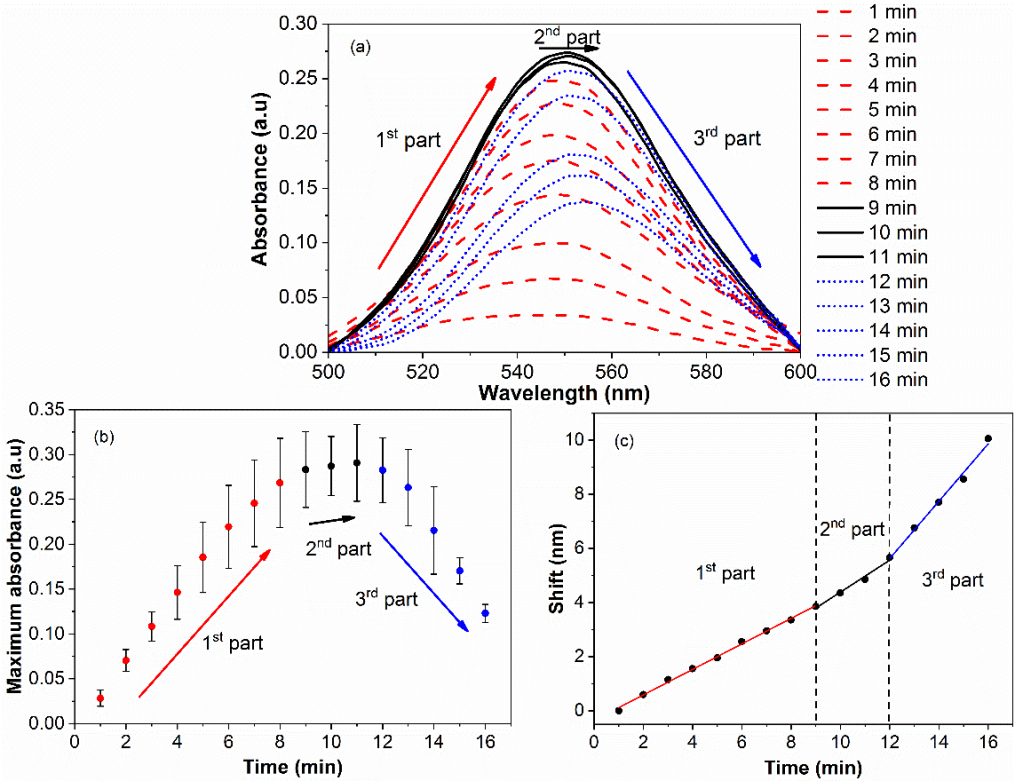

Figure 30. Spectral characterization of the AuNPs immobilization process. The time corresponds with the immersion of the optical fiber tip in the AuNPs solution. The graph (a) corresponds with the spectral variation, while in (b) and (c) the temporal evolution of the maximum absorbance and shift is shown respectively.

Thanks to the capabilities of optical fibers, it is possible to monitor in real time changes on the facet and characterize the LSPR phenomenon by the spectrum, as it is shown in Figure 30. In fact, we prove that different behaviours appear that depend on the immobilization time. Such tendencies can be explained by the following two main factors: i) The number of AuNPs attached onto the optical surface; and ii) the distribution of such AuNPs. Regarding the last one, it is known that the aggregation of two or more nanoparticles provokes a shift in the

resonance wavelength and a broadening in the spectrum[8]. As the immobilization method is a chemical one, the deposition is a random process, which allows the aggregation of AuNPs, that, with time, causes the creation of a reflective layer, observed first in a red shift and then in the decreasing of absorbance intensity. In other words, the LSPR effect is lost because AuNPs are nor single, but they are aggregated forming a reflective layer. Thus, to prove this hypothesis, it is mandatory to carry out a surface image characterization, which has been done by SEM imaging and image analysis.

3.3.2. Scanning electronic microscopy characterization

To conduct the SEM characterization, the next experiment was done: 21 optical fibers were prepared and modified by APTES as it was explained in the previous section. Subsequently, the optical fibers were immersed in the AuNPs solution. The conditions of the laboratory were at room temperature, the AuNPs solution was in the stock concentration, and the optical fiber used was the one with a diameter of core of 105 µm. As it was explained, the LSPR signal changes with time, and, therefore, seven different time points were studied. In other words, the fibers were immersed during 4, 6, 8, 10, 12, 14 and 16 minutes, and three replicas of each one of these times were manufactured. Thus, our intention was to observe the AuNPs distribution at different points that corresponds with the three different behaviours.

Once the optical probes were fabricated, they were covered by sputtering coating of chromium, and three images of three different spatial points of each optical fiber was obtained. Each SEM image has a surface of 100 μm^2. In Figure 31, the SEM images are shown, with the three replicas of each time. It is easy to observe that with time, the number of AuNPs at the end face of the optical fiber increases.

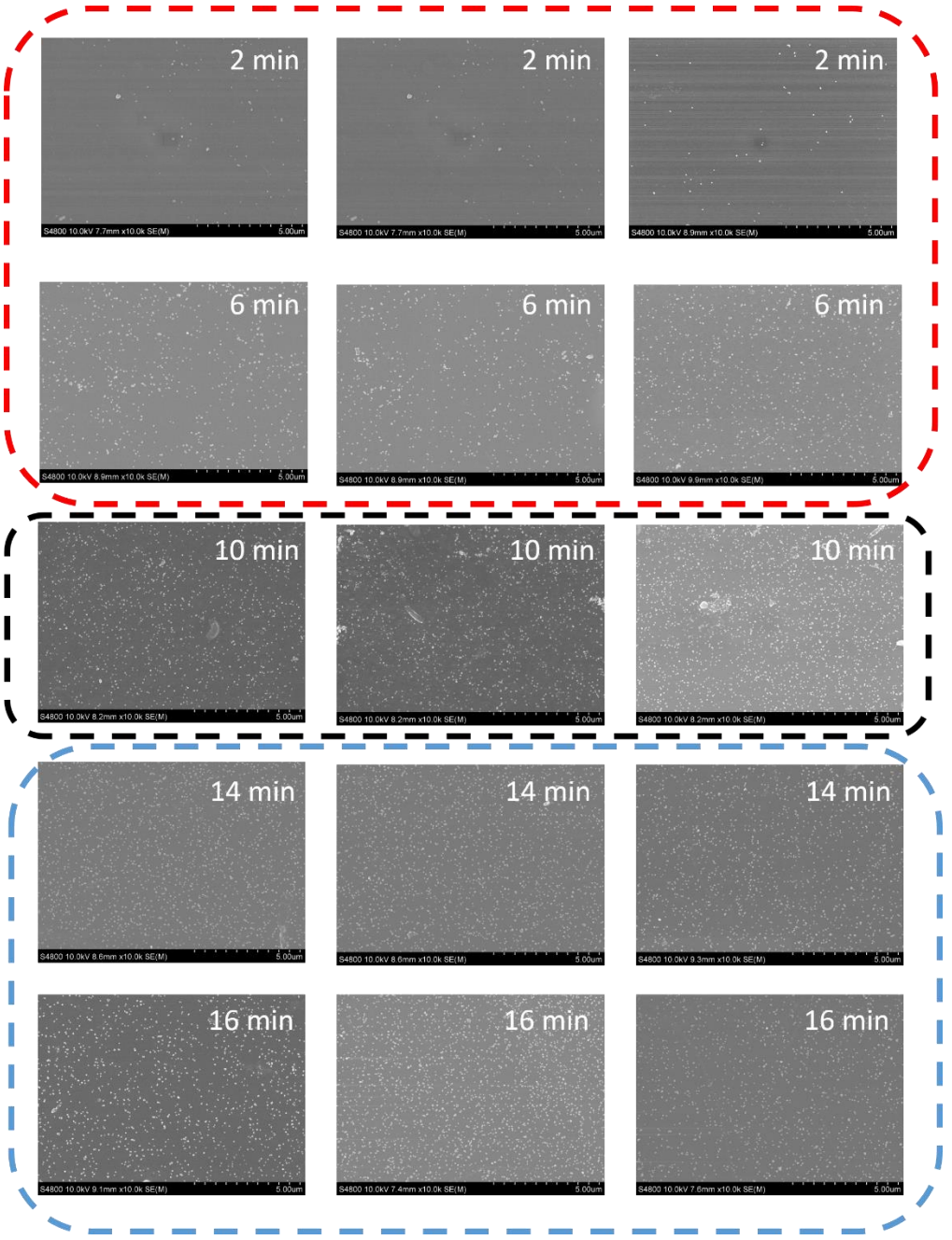

Figure 31. SEM images of the optical fiber end face for different times. Three different optical fibers are shown for each time. The colour of the dashed lines corresponds with the tendency, the red the first part of the temporal evolution, and the black and blue corresponds with second and third tendency respectively.

The calculations of the surface coated with AuNPs in different times are shown in Table 1. It is necessary to point out that each time was calculated taken into account that the part of the surface where the AuNP-light interaction occurs is in the core.

As it can be observed in Table 1, the percentage of covered increases with time, which is in agreement with Figure 31. This phenomenon, the increasing of AuNPs attached onto the fiber end face with time, explains the first tendency exposed in Figure 30 (spectral characterization). However, in order to understand the other two behaviours it is mandatory to know the distribution of such nanoparticles with time, which lets us know the proportions of different aggregation configurations, namely: single, double, triple, quadruple and five or more joined AuNPs.

Table 1. Percentage of the optical end face covered surface by AuNPs at different times with three different fibers of each one.

Time (min)	**4**	**6**	**8**	**10**	**12**	**14**	**16**
Sample 1	1.92%	2.59%	4.08%	7.24%	8.35%	11.92%	11.65%
Sample 2	1.66%	2.34%	4.28%	6.26%	9.24%	11.09%	12.53%
Sample 3	1.31%	2.71%	4.77%	8.01%	10.43%	10.94%	14.03%

To that end, an image analysis was done, and the number of the different aggregation configurations was calculated. Such analysis is depicted in Figure 32, with SEM images at the scale of 5 μm for the immersion times studied and their respective nanoparticles distributions.

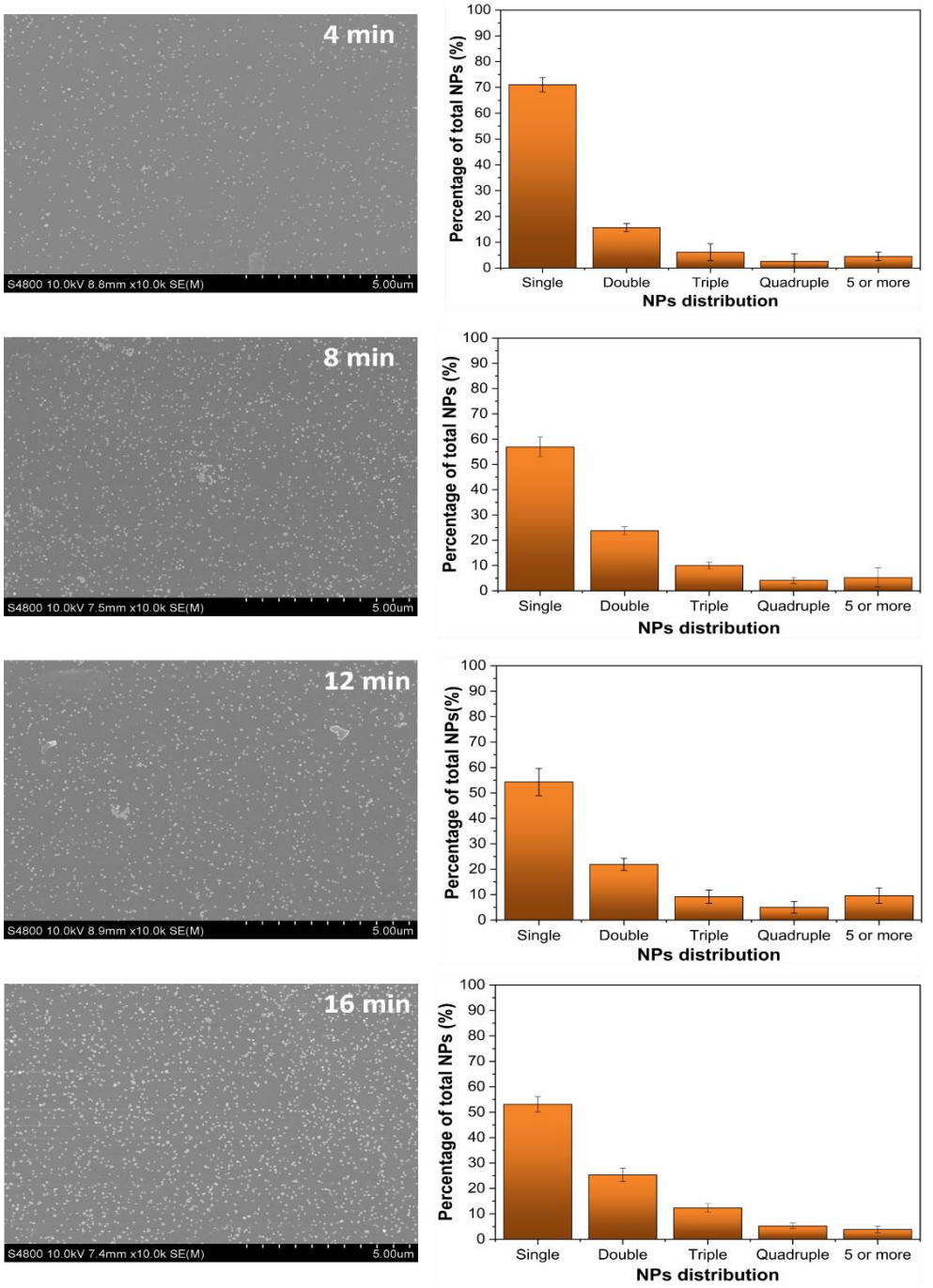

Figure 32. SEM images of the fiber end-face for different immersion times and their respective AuNPs distribution. The percentage of the nanoparticles regarding the level of aggregation is shown. Errors bars correspond with the standard error of 3 probes.

Figure 33 represents the distribution vs time. The graph allows knowing the distribution of the AuNPs in each tendency part previously observed. As it can be observed, the number of single nanoparticles decreases with time, while the double, triple, quadruple and five or more aggregated nanoparticles configurations increases. Thus, the red shift shown in Figure 30 may be explained by the increasing of the aggregations, as the contribution of them at higher wavelengths of resonance causes a red shift. In addition, the aggregation of the AuNPs affects in the creation of a refractive layer, as we explained before, and as we prove in Figure 32, 33 and Table 1.

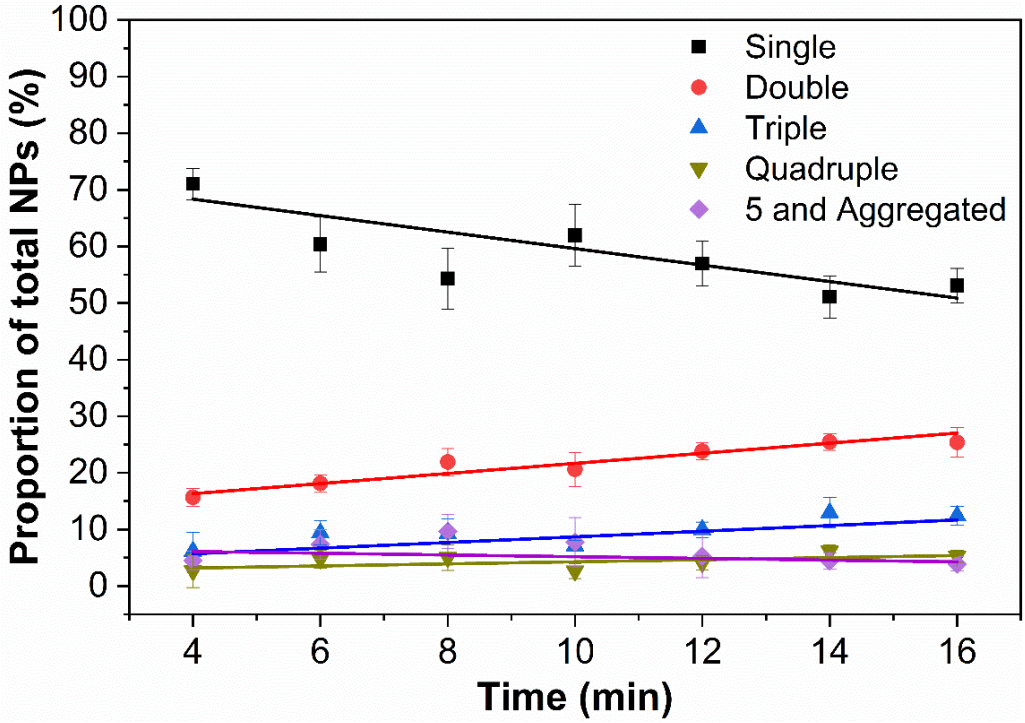

Figure 33. Distribution of the AuNPs against their respective immersion time. Errors bars correspond with the standard error of 3 probes.

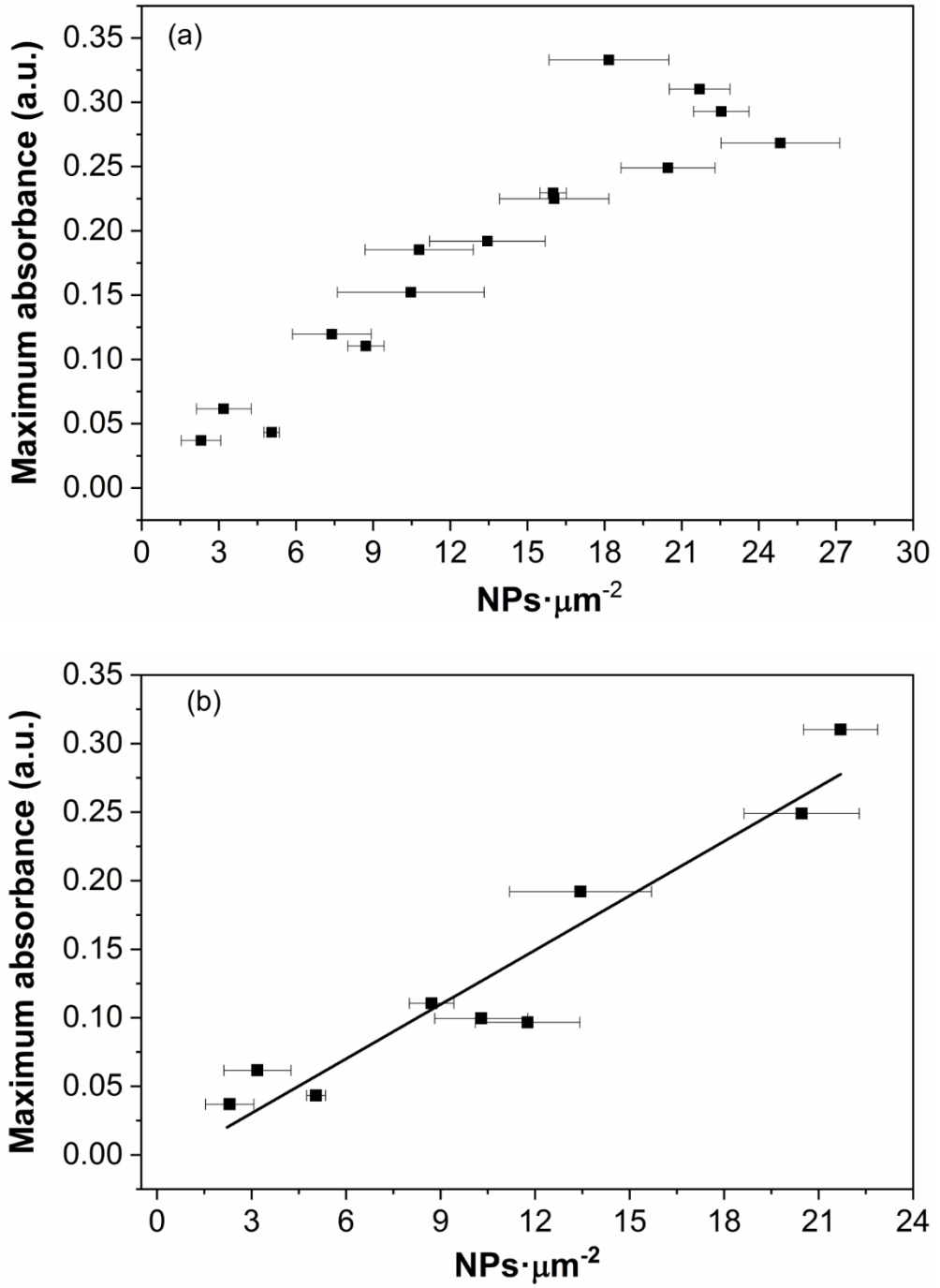

Figure 34. Maximum absorbance spectra against with the total nanoparticles optical fiber end-face (a) for all the immersion times and (b) for the first 10 minutes (R^2 = 0.93), which corresponds with the linear tendency.

The temporal evolution of the absorbance signal at times below 10 min is linear, as we shown in Figure 34. This can be related to the increasing number of total nanoparticles, as we mentioned. The plateau, around 10 minutes, is achieved when the number of single AuNPs is 2,2670 ∓ 410, and the covered surface is 7.36 %. In Figure 34, the intensity of the obtained spectrum is related to the number of nanoparticles per area immobilized on the optical fiber end face. As we can observe, there is a linear relation when the number of AuNPs is low, but as it increases, this linearity is lost, as it is observed in Figure 34a. This tendency is noticed when all the data points are plotted, nevertheless, when only the points that correspond with the linear tendency of Figure 30 are indicated, the linearity is achieved (see Figure 34b). This is a very interesting result because it suggests that in the first moments of the fiber incubation on AuNPs solution, we are able to know the minimum quantity of AuNPs that can be detected. From the straight line depicted in Figure 34b, we can determine that the limit of detection (LoD) is 7,500 nanoparticles approximately, which corresponds with a volume of 12 nL taking into account the concentration of our AuNPs (3.6E+10 nanoparticles/mL).

From the results obtained in the characterization process, it is possible to conclude that there is a relation between the number of AuNPs and the LSPR amplitude observed, in the way as the number of AuNPs increases, the amplitude increases as well. This relation is linear with the amplitude and with time as well, as we have demonstrated in Figures 30 and 34. However, this phenomenon is lost at a certain time, when the number of AuNPs keeps increasing but the amplitude of the LSPR spectrum achieves a plateau. Thus, the previous explanation about why the amplitude increased is not valid after this time. For this reason, we took into account the aggregation of these AuNPs, and we have shown in Figure 33 that the percentage of aggregated nanoparticles increased at the same time the percentage of single AuNPs decreased. This provokes, first, a stagnation in the LSPR amplitude, and, then,

a decreasing and a red shift, given that the aggregations trigger a red shift in the wavelength resonance. Finally, the clustering of AuNPs causes a reflective layer of gold.

3.4. Reproducibility

A reproducibility study of the immobilization process was performed as well. To this end, a batch of 20 optical fibers were prepared first and then immersed in the AuNPs solution at the same time. After 10 minutes, the immobilization process was stopped and the probes were subsequently immersed in miliQ water. We chose this time because, as we proved in the characterization section, it is the limit we found for the linear tendency, just before the saturation point. This experiment was done with a 105 μm fiber's core and with a stock AuNPs concentration.

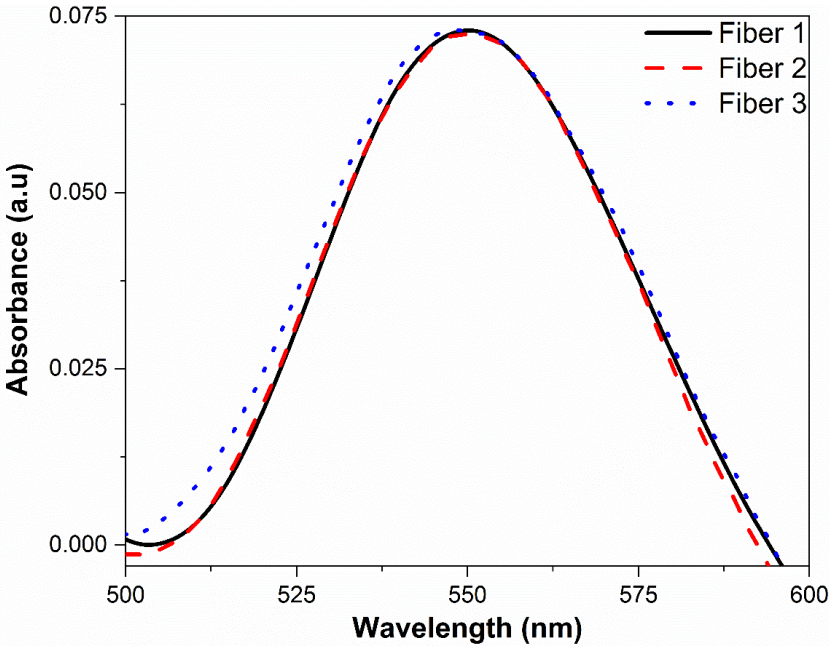

Figure 35. Absorbance spectra of three different optical fibers after the AuNPs immobilization.

With the purpose of studying the reproducibility, all spectra were characterized considering the standard deviation (STD) of x (wavelength peak) and y (absorbance intensity) axis. It was found to be 0.3 % for the wavelength peak position and 9 % for the absorbance intensity. Thus, the reproducibility obtained in this batch was of 88 %, which represents the percentage of optical fibers that fits in the STD range detailed previously. Figure 35 shows three spectra of the aforementioned manufactured 20 optical fibers.

3.5. Impact of fiber core diameter, temperature and AuNPs concentration

Many factors may affect the AuNPs immobilization on the optical facet. Once the characterization was conducted and it has provided us the information about the immobilization process, such as the relation between the aggregation and the LSPR spectrum, the LoD of AuNPs of our fiber-based system, etc., our main objective is to study the impact of different parameters on the AuNPs immobilization. We have focused on three parameters:

i) the diameter of the core, with three different fibers,
ii) the temperature at which the AuNPs immobilization is done, and
iii) the concentration of the AuNPs solution, from the stock one to lower concentrations.

All these experiments were analysed by the spectral characterization. In other words, as we have made a relation between the distribution and number of AuNPs with the temporal evolution of the spectrum, our purpose is to study the impact on such temporal evolution.

In order to study the impact of the diameter of the fiber's core in the LSPR spectrum, we used three different optical fibers. One MMF with a diameter of 105 µm, which is the fiber used in the characterization exposed previously, another MMF but with a smaller diameter, of 50 µm, and finally, a SMF with 2.5 µm of diameter. The specifications of the fibers and the couplers used for each one are included in Appendix 1. All of these fibers work in the visible range. As we explained before, the place where the interaction light-AuNPs occurs is in the core of the optical fiber, and for this reason the diameter of such core is underlined, not the diameter of all the fiber.

The temporal evolution of the three fibers is shown in Figure 36. The immobilization was performed at room temperature and with a stock solution of AuNPs, with the remaining conditions unaltered in all three fibers. Thus, the speed of the AuNPs immobilization is identical for all the cases. However, the temporal evolution is different depending on the core of the fiber, as we can see in Figure 36. In fact, the experiment shows that as the surface is smaller, a faster saturation and a lower amplitude is achieved. The faster saturation can be explained because of as the diameter decreases, less time is required to obtain certain covered surface levels. This links with the behaviour shown in the previous section, as the covered surface and the AuNPs distribution have an impact in the time required for the saturation. In this manner, it seems reasonable that by reducing the core's diameter, the plateau was achieved earlier. The lower achieved levels of amplitude as the core is smaller can be explained as follows: by reducing the surface, the number of AuNPs that contributes to the total absorbance is reduced as well.

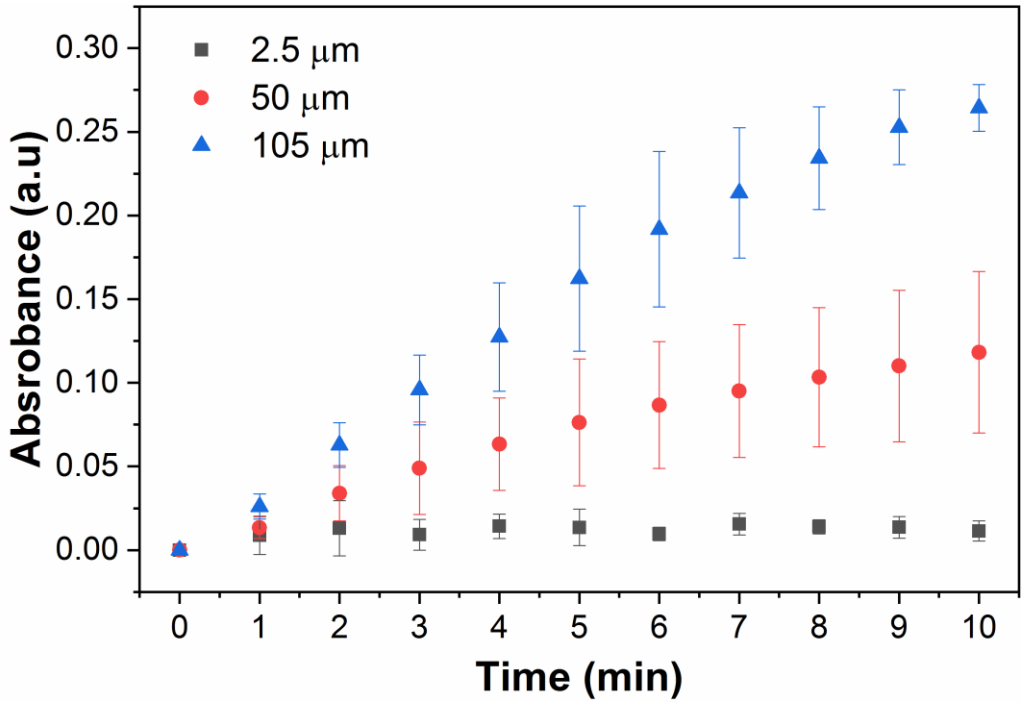

Figure 36. Maximum absorbance intensity values for optical fibers with different core diameters (105, 50 or 2.5 µm) onto which AuNPs were chemically immobilized for different times (from 1 to 10 min).

The effect of the concentration of AuNPs is depicted in Figure 37. This experiment was performed at room temperature and with the MMF of 105 µm. To do that, three concentrations were used: a stock one, one diluted to half, and finally, one diluted to a quarter of concentration. Such dilutions were carried out with miliQ water. As it can be observed, as the concentration decreases, the temporal evolution changes. The expected result was that, as the AuNPs concentration decreases, it would take longer to achieve the same level of covered surface than with higher concentrations. Lower concentration means that the saturation is achieved slowly, that is the behaviour shown in Figure 37.

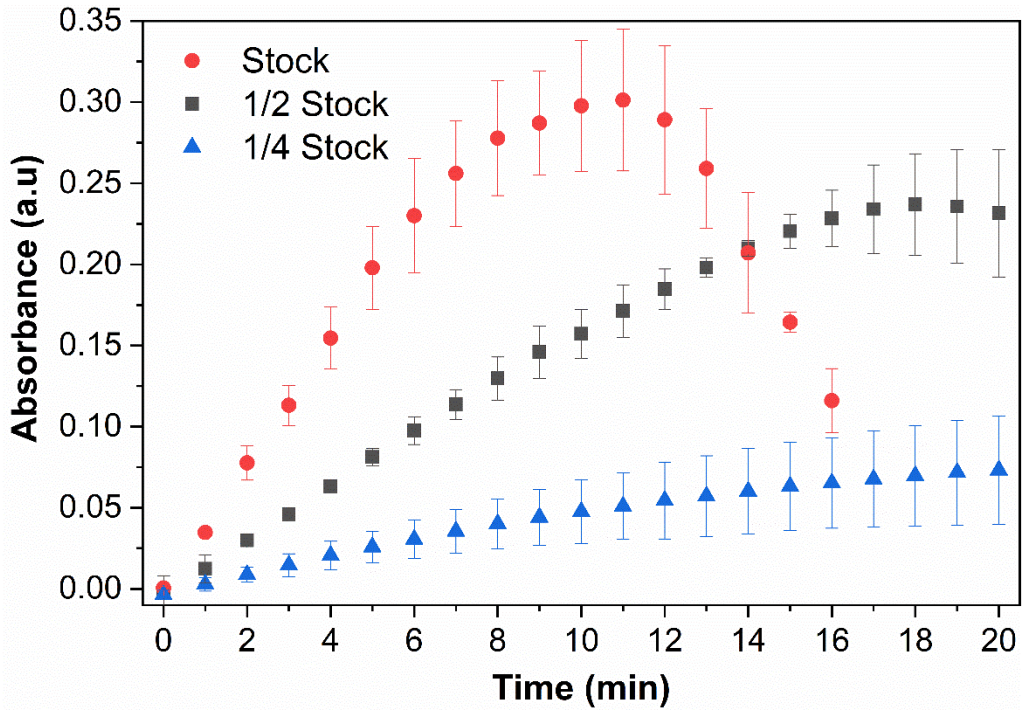

Figure 37.Maximum absorbance intensities achieved at control parameters (room temperature and fiber core diameter 105 µm) with different AuNPs concentrations at certain times of immersion (from 1 to 20 min).

To evaluate the impact of the temperature in the AuNPs immobilization, experiments at three temperatures were performed. For this purpose, the immobilization process was carried out in an oven, where the temperature can be controlled. First, the AuNPs solution was introduced in the oven for 20 minutes, and then the probe modified by APTES was immersed in the solution. The three temperatures applied were 5, 25, and 50 ºC. It is relevant to point out that the limit of higher temperature is given by the APTES link, as it can be broken at 100 ºC approximately (data given by the company). All of these experiments were conducted with the stock concentration and with the MMF of 105 µm of core, and the results are depicted in Figure 38. The main feature observed in the experiments was that, as the temperature increases, the saturation is achieved faster. The temperature is a crucial parameter in chemical

reactions, as it has an impact on the speed of such reactions. As the temperature increases, the agitation of AuNPs may increase as well, and therefore, the immobilization process is faster. Thus, the plateau may be achieved in less time by increasing the temperature.

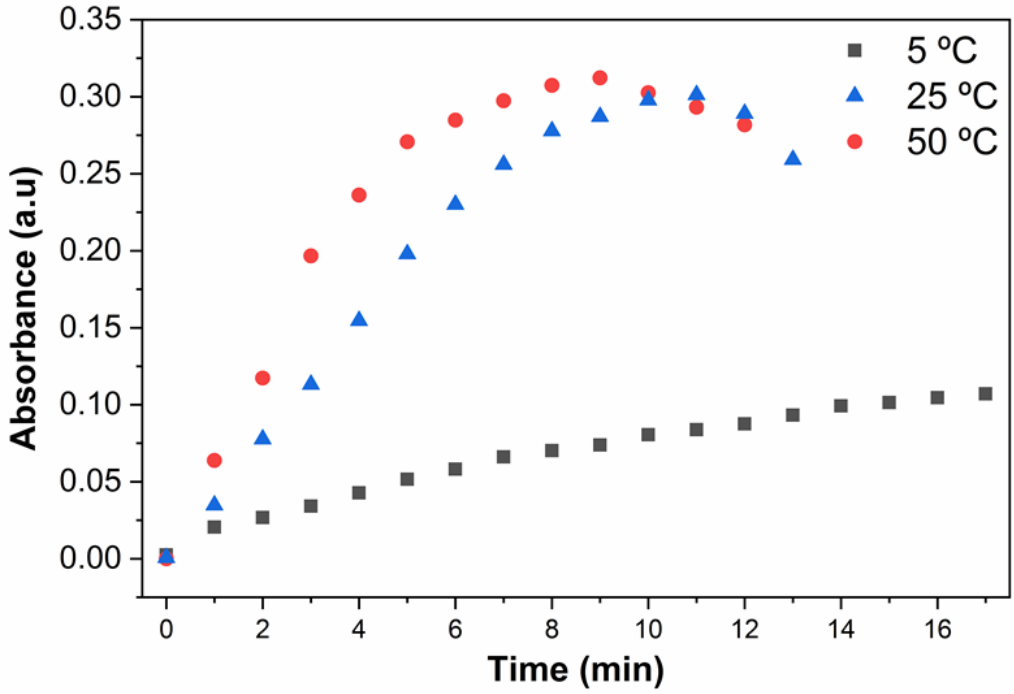

Figure 38. Maximum absorbance values for 105MMFs at different temperatures (5, 25, and 50 ºC).

3.6. Summary

As we explained before, the lab-on-fiber technology shown in this thesis is based on the chemical immobilization of AuNPs on the end face of an optical fiber. Such probe will be used for biochemical sensing by a nanospectroscopic approach, but first, in this chapter, we have introduced the operating principle of the probe and the fabrication process. We have characterized the AuNPs immobilization by two different manners, by the spectrum and by an image

analysis. From such characterization, we observed a temporal evolution in the spectrum with three different behaviours, due to the number of AuNPs on the surface and the distribution of AuNPs, which can be in a single form, or aggregated between them. As each nanoparticle contributes to the LSPR effect, the increase of AuNPs implies an increase in the amplitude of the LSPR spectrum as well, which would explain the linear tendency at shorter times. However, this amplitude achieves a plateau, and then starts decreasing and shifts to the red. As we have explained by image analysis, this is due to the number of aggregates being higher and the number of single nanoparticles being lower with time, creating a reflective layer, and, thus, the LSPR effect is lost. This is a very interesting study saying that it if we want to use the LSPR effect, we have to be in the linear zone. Finally, we have shown the effect of the temperature, the AuNPs concentration, and the optical fiber in the probe fabrication. We concluded that a higher intensity in the spectrum is obtained increasing the core's diameter, although the plateau appears late, and that a faster saturation is achieved increasing the temperature and the AuNPs concentration. Such conclusion is useful to optimize the fabrication process of these probes.

References of Chapter 3

1. Pisco, M.; Cusano, A. J. S. Lab-on-fiber technology: a roadmap toward multifunctional plug and play platforms. *Sensors* **2020,** *20* (17), 4705.
2. Horvath, H. Gustav Mie and the scattering and absorption of light by particles: Historic developments and basics. *Journal of Quantitative Spectroscopy and Radiative Transfer* **2009,** *110* (11), 787-799.
3. Mie, G. Beiträge zur Optik trüber Medien, speziell kolloidaler Metallösungen. *Annalen der physik* **1908,** *330* (3), 377-445.
4. Bohren, C. F.; Huffman, D. R. Absorption and scattering of light by small particles. *John Wiley & Sons*: **2008**.
5. Ortega-Gomez, A.; Barroso, J.; Calatayud-Sánchez, A.; Zubia, J.; Benito-Lopez, F.; Basabe-Desmonts, L.; Villatoro, J. Cytochrome c detection by plasmonic nanospectroscopy on optical fiber facets. *Sensors and Actuators B: Chemical* **2021,** *330*, 129358.
6. Barroso, J.; Ortega-Gomez, A.; Calatayud-Sanchez, A.; Zubia, J.; Benito-Lopez, F.; Villatoro, J.; Basabe-Desmonts, L. Selective Ultrasensitive Optical Fiber Nanosensors Based on Plasmon Resonance Energy Transfer. *ACS Sensors* **2020,** *5* (7), 2018-2024.
7. Ortega-Gomez, A.; Barroso, J.; Calatayud-Sanchez, A.; Benito-Lopez, F.; Zubia, J.; Basabe-Desmonts, L.; Villatoro, J. In *Fiber optic biosensor by plasmon resonance energy transfer*, OSA Advanced Photonics Congress (AP) 2020 (IPR, NP, NOMA, Networks, PVLED, PSC, SPPCom, SOF), Washington, DC, 2020/07/13; Caspani, L. T.-P. A. L. F.; Yang, B., Eds. Optical Society of America: Washington, DC, 2020; p SoM2H.6.
8. Sepúlveda, B.; Angelomé, P. C.; Lechuga, L. M.; Liz-Marzán, L. M. LSPR-based nanobiosensors. *Nano Today* **2009,** *4* (3), 244-251.

4. Chemical sensing application: copper ions (II) detection

The work shown in this thesis is based on optical fiber sensors based on a nanospectroscopic approach, which means that the detection method is by changes in the AuNPs intensity because such nanoparticles resonance band overlaps with the absorption band of the analyte, and not by changes in the refractive index of the surrounding medium.

This chapter is related to the implementation of the optical probe shown in the previous chapter for chemical applications, most specifically, for Cu^{2+} detection. The main results of this work were published in[2], were a LoD measured of 1 pM was achieved, 1000 times more sensitive compared with other works based on nanospectroscopic effects but in microscopy-based platforms[4].

First, we will explain the main motivations for Cu^{2+} detection. Then, the preparation of the probe to make the sensor specific to Cu^{2+} will be shown. The main results of the experiments will be discussed, such as the Cu^{2+} measurements, the study of the selectivity, etc. Finally, the results will be compared with the state of the art. The information about the setup used for the measurements carried out in this chapter is shown in Appendix 1.

4.1. Motivation: the risks of copper ions

Heavy metals are metals with a density five times that of water, and they are very toxic to humans, animals, plants, and environment[6]. The gradual accumulation in the organism may cause many diseases depending on the

heavy metal, such as kidney diseases, lung disorders, etc. Nickel (Ni), Mercury (Hg), Chromium (Cr), Lead (Pb) and Copper (Cu) are the main heavy metals, among others. Human activity has provoked a rise in the concentration of such heavy metals in the environment, mainly by pollutions generated in the industry, agriculture, mining, and the use of petroleum fuels. For this reason, these metals are a major problem in cities with an uncontrollable expansion of the industry.

Heavy metals dumping by contaminants causes damage to the biosphere, but are very harmful to humans as well, due to its ingestion. Humans can ingest heavy metals directly, by drinking water and breathing air, and indirectly, by animals or plants that have accumulated such metals in their bodies through the environment[6].

However, the ingestion by drinking water represents one of the potential hazards, due to the pipeline corrosion in houses where there are still pipelines of copper, the high concentration in the aquatic system, like lakes, rivers, and seas, originated by the industry, etc. Therefore, our research focuses on the detection of Cu^{2+} in water, and we explain the principal detriment effects of it.

Copper is one of the essential transition metals in human bodies, along with zinc and iron[9, 10]. In fact, the presence of copper in humans is absolutely necessary for the correct human development, as it plays a crucial role in many physiological roles[9, 13], but the ingestion of high levels of Cu^{2+} can be harmful.

As the World Health Organization (WHO) indicates[15], to intake low doses of Cu^{2+}, that means from a concentration of 60 μML^{-1} approximately, may cause headache, nausea, etc. An increase in the doses of Cu^{2+} can produce many problems in our biological system, such as gastrointestinal bleeding or hematuria. Indeed, a high ingest of such metal ions, around 4.4-440 mML^{-1} can be lethal (see Figure 39). However, not only the concentration of Cu^{2+} ingested

is a relevant factor, the exposure time to these ions is a key factor in order to evaluate the risks on the health. In this manner, taking minor doses of Cu^{2+} but over a long period can be dangerous for humans as well. In addition, multiple research papers connect an excess of Cu^{2+} to neurodegenerative diseases, such as Menkes and Wilson disease[10], Alzheimer's disease, prion disease[6], and liver damage in infants.

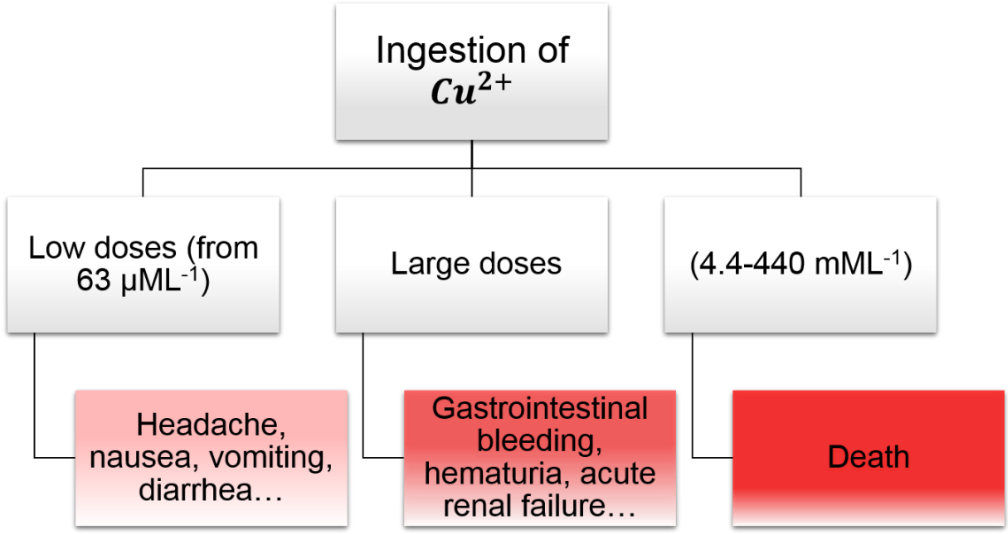

Figure 39. Scheme of the effect for the ingestion of Cu2+ in water depending on the doses.

Therefore, there is a real interest in monitoring and detecting Cu^{2+} due to its toxicity and the potential damage to humans. The standard techniques used to measure Cu^{2+} in water are the atomic absorption spectrometry and inductively coupled plasma mass spectroscopy. Nevertheless, both techniques have a limit of detection around the micromolar range, which implies a limitation. Moreover, they are very expensive techniques that can operate only in laboratories, which means that are not useful for outside measurements. Thus, developing specific sensors that can detect lower concentrations of Cu^{2+} is a crucial challenge.

To that end, optical fibers represent a promising technology for this purpose, due to their passiveness, causing a null impact on the environment. The sensor developed in the thesis may cover the necessities for the detection of Cu^{2+}. On the one hand, because of the possibility to make remote measurements, which is very interesting for the real world environments, such as lakes or rivers, and, on the other hand, for real time use of optical fibers, to monitor the tap water in pollution sources, such as in industrialized settings.

In the following sections, we will discuss the fabrication process of the sensor and the results obtained, as the limit of detection and the selectivity.

4.2. Probe preparation

As we have explained before, nanospectroscopy means that the interaction between material and light occurs at the nanometric scale, where AuNPs act as a source of energy. Some nanospectroscopic effects like PRET are based on the transfer of energy from such AuNPs to the target molecules of which it can be detected. However, this transfer only occurs under specific conditions, as the resonance frequencies of the absorbance spectrum of both AuNPs and molecules have to match. Therefore, to trigger the PRET phenomenon, AuNPs and the specific target (Cu^{2+} in the case of this chapter) have to be close enough between them[4]. The transfer of energy results in a variation in the intensity of the AuNPs spectrum, which can be quantified in order to estimate the concentration of Cu^{2+} (see Figure 40).

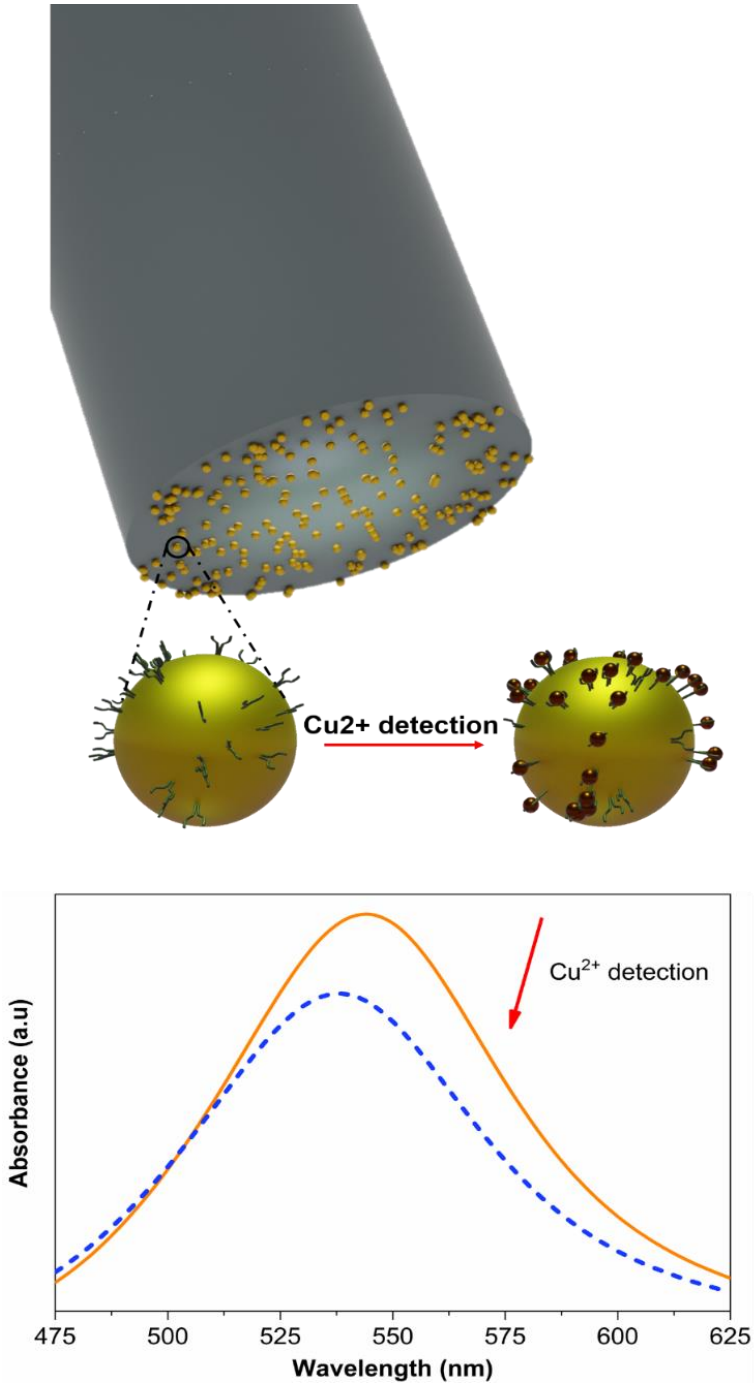

Figure 40. Graphical abstract of the nanospectroscopic effect on a MMF facet. The graph shows the change in the spectrum when the $Cu^{2+}$are detected.

In order to make our lab-on-fiber-based probe sensitive only to Cu^{2+}, AuNPs have to be functionalized by a highly selective metal ligand complexation. For this purpose, the optical fiber coated with AuNPs was immersed in 1 mM APTES solution for 90 min. Then was washed with a solution of isopropanol-water (1:1) and immersed in a 0.1 M hydrochloric acid (HCl) solution for hydrolysis of the methoxy groups of APTES for 1h. Finally, the MMF probe was immersed into 1mM *N*-[3-(trimethoxysilyl)propyl] ethylediamine (TMSen) solution for 2 h. The photographs of the setup used to perform this step are depicted in Figure 41. Thus, it is possible to form Cu^{2+} specific ligands on the surface of the AuNPs. See in Figure 42 the chemical scheme of the sensor.

The use of this ligand has a double intention:

i) to collocate AuNPs and Cu^{2+} close between them to enable the nanospectroscopic effect, and
ii) to match the resonance frequency.

With respect to the second point, it is interesting to mention that when Cu^{2+} are dissolved in water, the absorbance spectrum of such ions is founded in the blue-purple wavelength range, not in the green one. However, by the formation of metal ligand complexation for Cu^{2+} detection on the surface of AuNPs, the absorption spectrum is predominant in the green wavelength range (see Figure 43), which is the resonance frequency of the AuNPs that we use, with a radius of 40 nm (see Chapter 2).

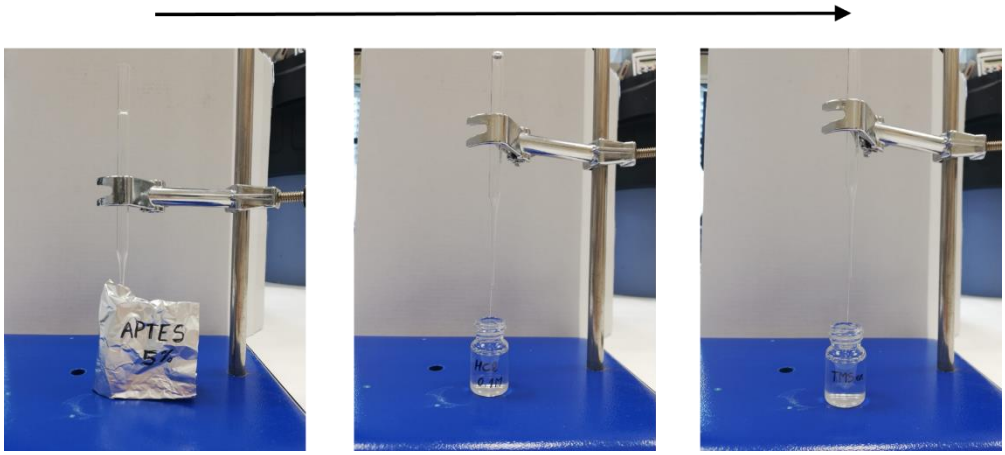

Figure 41. Photographs of the steps involved in the functionalization process. Chronologically, from left to right.

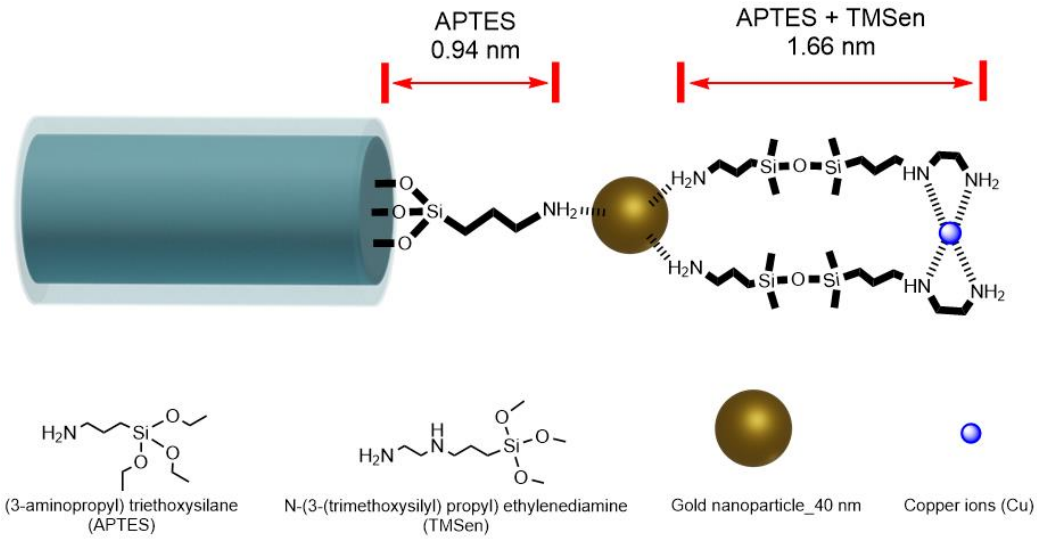

Figure 42. Chemical structure obtained when AuNPs are functionalized by TMSen.

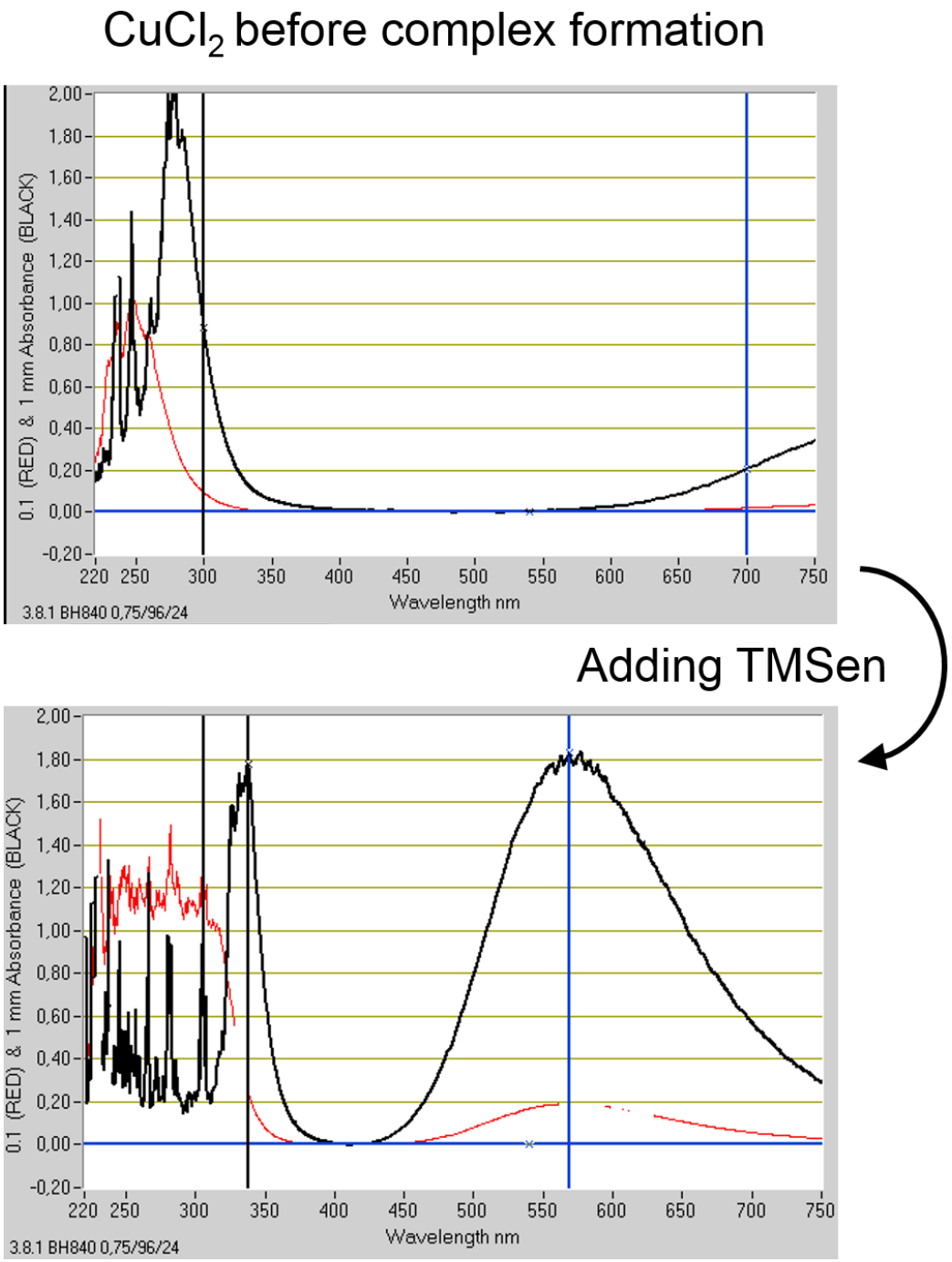

Figure 43. Absorbance spectrum of the Cu2+ solution before complex formation and after adding TMSen.

The functionalization of the AuNPs for Cu^{2+} detection does not induce big changes in the absorbance spectrum of the MMF coated with AuNPs, as it can be observed in Figure 44, where both spectra are similar. However, a small shift in the wavelength peak can be appreciated, which can be explained due to the high sensitivity of AuNPs, since adding ligands on the surface of such nanoparticles provokes a small change in the refractive index of the surrounding medium.

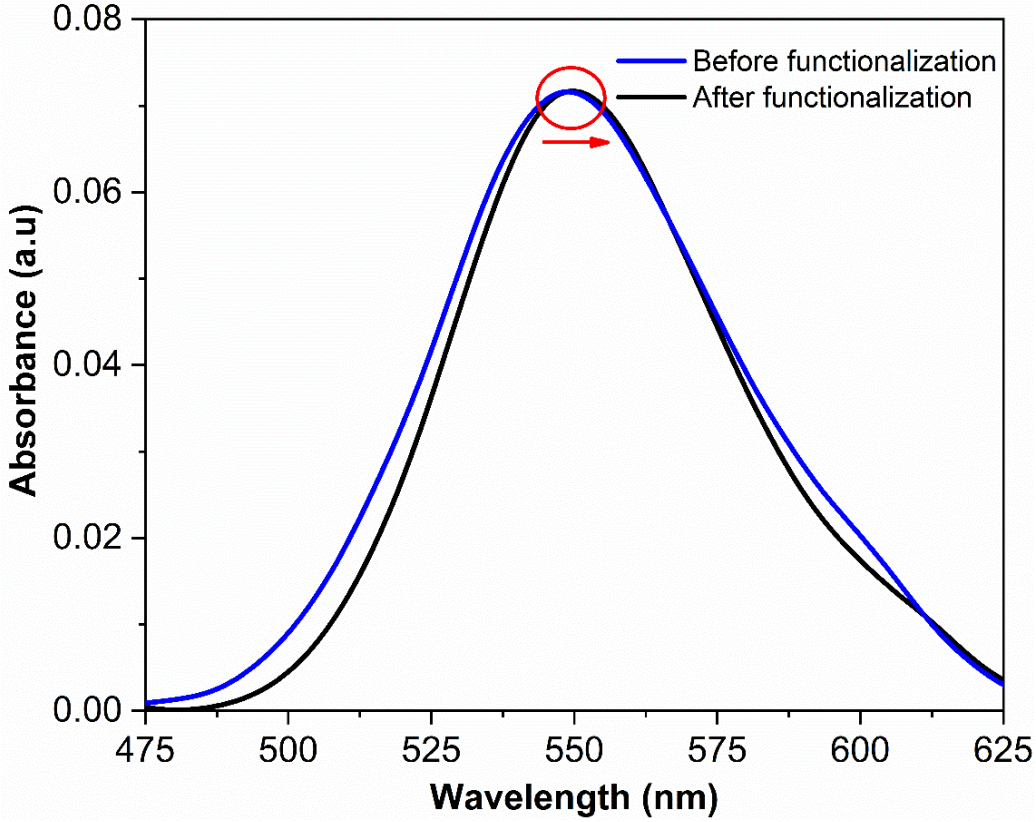

Figure 44. .Absorbance spectra before (blue line) and after (black line) the functionalization process for Cu2+ detection.

To confirm the complexation of Cu^{2+} by MMF probes, further characterization based on X-ray photoelectron spectroscopy (XPS) was performed, but due to the miniaturized size of the MMF, it was not possible to use the fiber in the XPS

setup. As the intention was to corroborate that the complexation of Cu^{2+} by TMSen was correct, the characterization was conducted with a slide made of glass.

To maintain the conditions as similar as possible, slides were modified chemically with the same protocol explained in Chapter 3, and then, the modified glass slides were incubated in a miliQ water solution of Cu^{2+} with a concentration of 10^{-4} M during 5 minutes, and subsequently washed with isopropanol:water 1:1, dried and measured.

The results of the XPS characterization are summarized in Table 2. Two different slides were measured, which corresponds with two different steps in the entire process. The first slide corresponds to the AuNPs immobilization step, and the second slide to the TMSen functionalization and immersion in the Cu^{2+} solution. Figure 45 corresponds with the spectrum before and after such immersion, where the presence of Cu is clearly observed.

Table 2. Elements detected by XPS.

Samples	**Elements detected**
AuNPs immobilized	C, O, Si, **Au**, Na, N, Ca
AuNPs after Cu^{2+} incubation	C, O, Si, **Au**, Sn, Na, N, Ca, **Cu**, Cl

Regarding Table 2, the presence of Cl in the second slide can be explained because the aqueous solution of Cu^{2+} was obtained from the $CuCl_2$ salt (see a saturated sample of such salt in Figure 46). In this manner, it is proven that by the protocol used in this section, our sensor is able to catch, and therefore, create a complex Cu^{2+} ligand. More information about the XPS measurements is explained in Appendix 2.

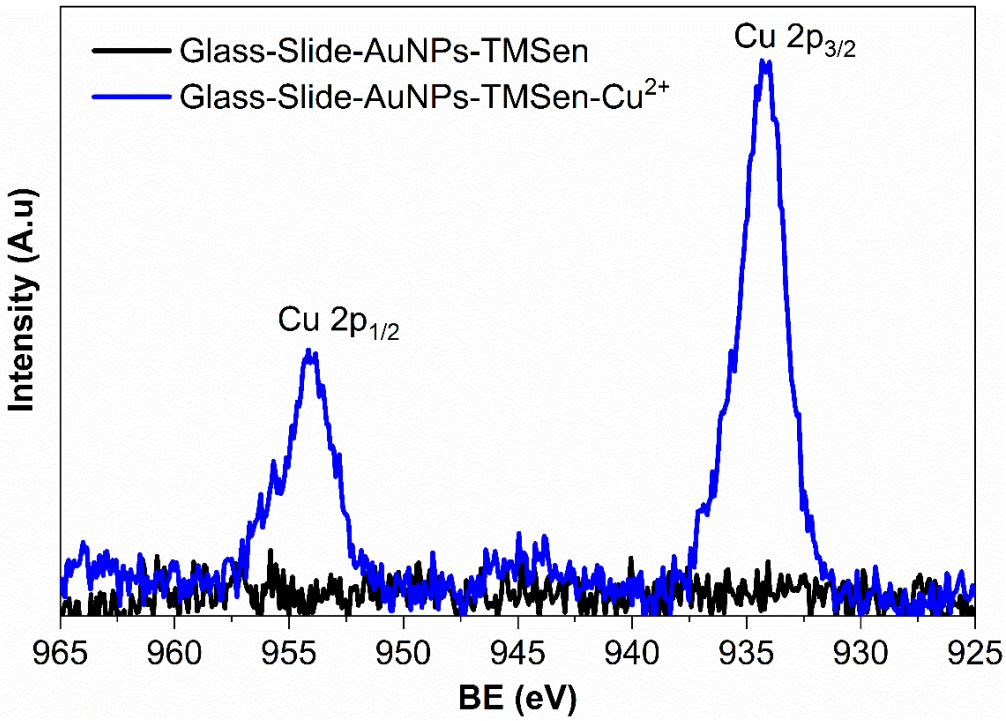

Figure 45. XPS spectra were obtained when the sample was functionalized, which corresponds with the black line, and when then the sample was immersed in a Cu2+ solution, which corresponds with the blue line.

Figure 46. Sample of a CuCl2 with a concentration of 0.4 M.

4.3. Results and discussion

In order to demonstrate the performance of the fiber sensor, it was immersed into an aqueous solution with different concentrations of Cu^{2+}. To prepare the solutions, the salt $CuCL_2$ was dissolved in miliQ water with a concentration of 0.02 M. From this solution, the other concentrations were prepared to maintain constant the final volume that was 300 µL. The sensor was immersed in such concentrations from the lower to the higher one, where the range used was from 10^{-12} to 10^{-4} M, in steps of 10^{-2}M. The spectrum was recorded after 5 minutes for each point. Figure 47 shows the normalized absorbance spectra for each concentration with respect to the obtained spectrum when the sensor was immersed in pure water, which means, 0 M concentration of Cu^{2+}. As it can be observed, as the concentration of Cu^{2+} increases, the intensity of the LSPR peak decreases. The calibration of the sensor corresponds with the blue line in Figure 48, where each point of the calibration curve was calculated as follows:

$$A = 1 - \frac{A_r}{A_0} \tag{16}$$

where A_r and A_0 correspond with the absorbance intensity of each concentration and 0 M concentration (what it means, no Cu2+), respectively. The assay showed a linear response from 10^{-12} up to 10^{-4} M. The LoD of Cu^{2+} measured was 1 pM, while the LoD that corresponds with the signal-to-noise ratio of 3 (S/N = 3) was found to be equal to 242 fM. The averaged relative standard deviation (RSD) obtained using at least three independent fiber probes was 4 %.

To confirm that the results depicted in Figure 47 were obtained due to the nanospectroscopic effect, the experiments described above were repeated but with AuNPs-coated MMF facets that were not modified with TMSen.

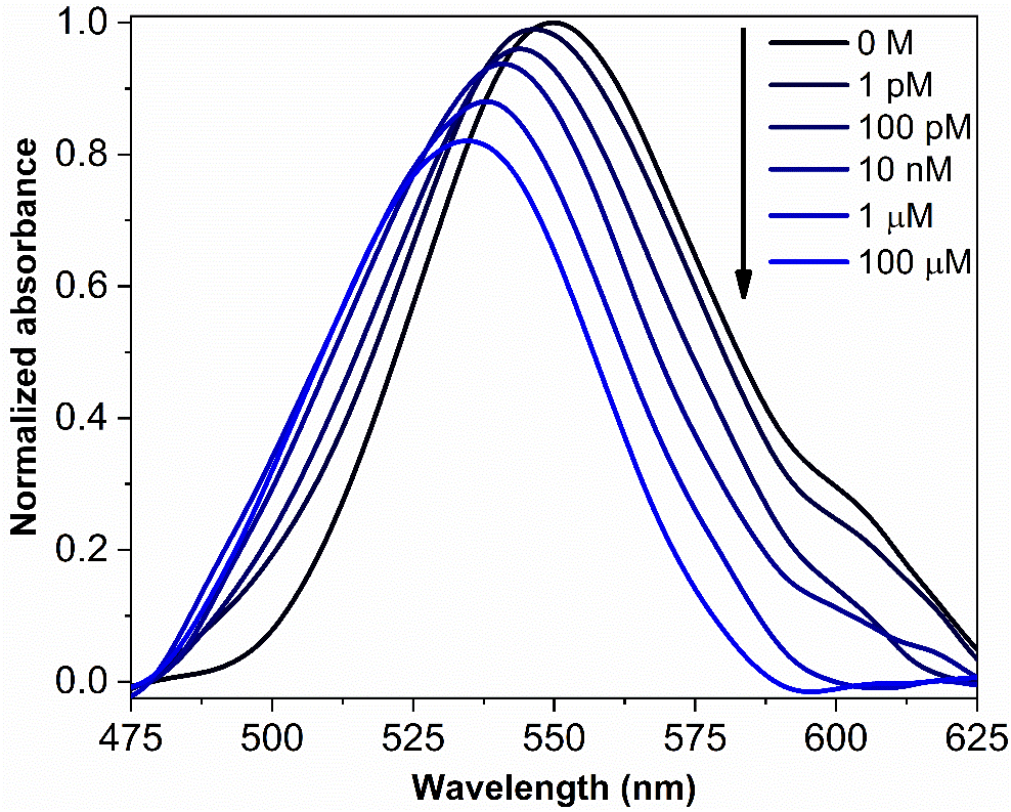

Figure 47. Absorption spectra in different solutions increasing the concentration of Cu2+. Each spectrum has been normalized with respect to the spectrum in water, that means, 0 M.

Under this condition, no complexation and, therefore, no transfer of energy is triggered. Such results correspond with the dashed red line in Figure 48. As it can be observed, no significant changes in the absorbance were observed when AuNPs were not functionalized. Thus, we prove that this change is due to the nanospectroscopic phenomenon. The LSPR spectrum of AuNPs matches with the optical absorption of the copper complex. This situation allows that when such nanoparticles are excited with the white light that propagates through the MMF, exists an exchange of energy between AuNPs and Cu^{2+}.

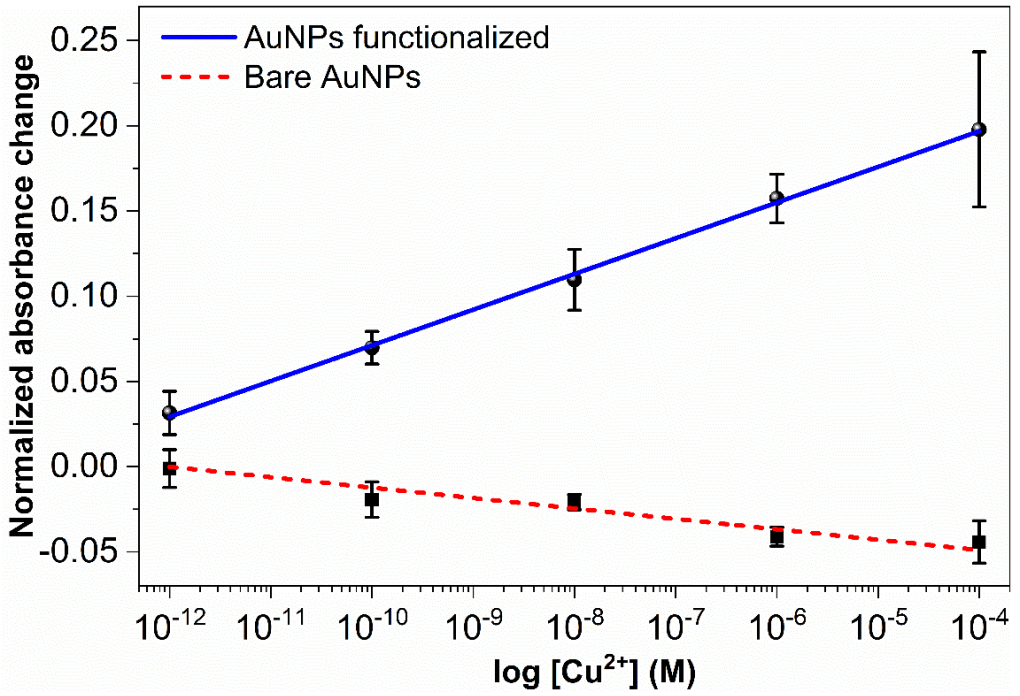

Figure 48. Calibration plot of the experimental data. The blue solid line corresponds with the fitting of the sensor, and the red dashed line corresponds with the fitting of the non-functionalize probe. Errors bars correspond with the standard error of 3 tests.

Under such conditions, AuNPs act as a light source that changes in the presence of the ions, which may be explained by the transfer of energy that results in a change of such light source, which means, a variation in the intensity of the spectrum. This is exactly what we observe in our experiments (Figure 47), but, in addition, we demonstrate it with the experiments carried out when AuNPs does not catch the Cu^{2+} (Figure 48), where both AuNPs and ions are not close enough between them, and, therefore, there is no transfer of energy. Thus, nanospectroscopy permits a detection by the intensity variation, and this differs from the classical methods of detection, usually based on monitoring the wavelength shift. Nanospectroscopy allows avoiding errors in the measurements for changes in the temperature or humidity, as these effects generally cause a shift that has to be calibrated previously.

4.4. Selectivity experiments

We conducted additional experiments to analyse the selectivity of the proposed sensor. The response of our sensor when measuring different heavy metal ions (Co^{2+}, Pb^{2+}, Ni^{2+}) and other ions (Na^{+}) that usually accompany Cu^{2+} in water were studied. All components were measured in the same concentration ranges according to the calibration curve for Cu^{2+} (see Figure 48). It is worth highlighting that the readout signals remain almost without significant fluctuations upon the addition of different ions, as it is depicted in Figure 49, compared with the response obtained in the Cu^{2+} measurements.

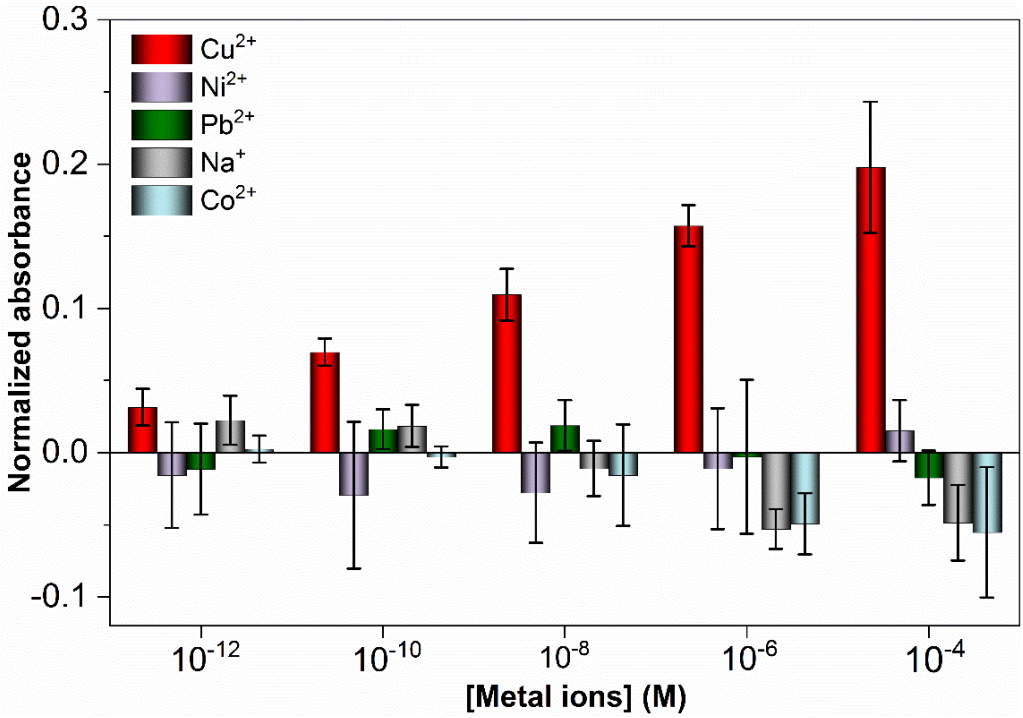

Figure 49. Bars diagram of the effect on the absorbance spectrum height of Cu2+, Ni2+, Pb2+, Na2+, and Co2+. Errors bars correspond with the standard error of 3 tests.

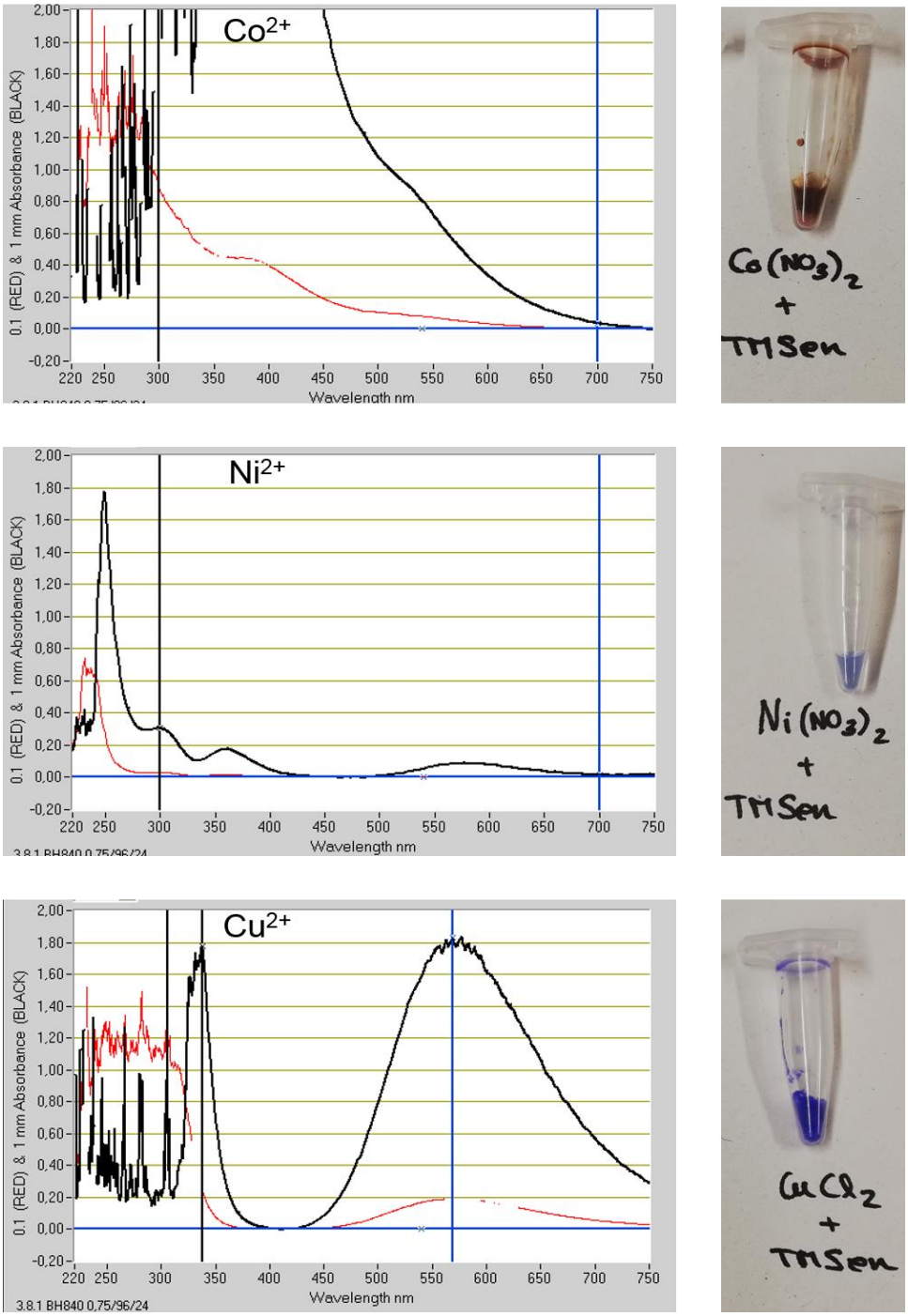

Figure 50. Absorbance spectra of Co2+, Ni+, and Cu2+ after the functionalization by TMSen.

As it was expected, the absence of metal-complex for different cations provoked that the resonance energy transfer was not satisfied. Nevertheless, free ethylenediamine (that is a part of the TMSen) can form complexes with other metals and transition metals, and, therefore, a similar response could be expected for Co^{2+} and Ni^{2+}, which absorption band match with the LSPR spectrum of AuNPs as well. However, the higher affinity of Cu^{2+} and its higher intensity of the absorption band compared with the other complexes causes the selectivity shown in Figure 49. In order to prove it, the absorption band of Cu^{2+}, Ni^{2+} and Co^{2+} complexes with a concentration of 0.05 M are shown in Figure 50, where it can be observed how the Cu^{2+} predominated in the wavelength absorbance band of interest.

Thus, a highly selective detection caused by the nanospectroscopic effect and Cu^{2+} complex formation was demonstrated. In addition, these results are in good agreement with those reported by Lee *et al* [4].

4.5. Repeatability of measurements

A study of the repeatability of the measurements was carried out. The aim was to know the possibility to re-use a probe after the measurements. Thus, the first goal was to study the capability to remove the Cu^{2+} from the AuNPs surface. To that end, a competitive binding test was done using ethylenediaminetetraacetic acid (EDTA), which is a chelating agent with a high affinity for Cu^{2+}. First, a fiber probe was immersed in a solution of Cu^{2+} with a concentration of 1 µM for 5 minutes, and then it was incubated into 0.1 M EDTA solution during 5 minutes. Finally, it was rinsed with miliQ water. The spectra of the three steps were recorded and it is shown in Figure 51. As it can be observed, the final spectrum is similar with respect to the one recorded before the measurement of Cu^{2+}. Thus, it is demonstrated the usefulness of EDTA to remove such ions.

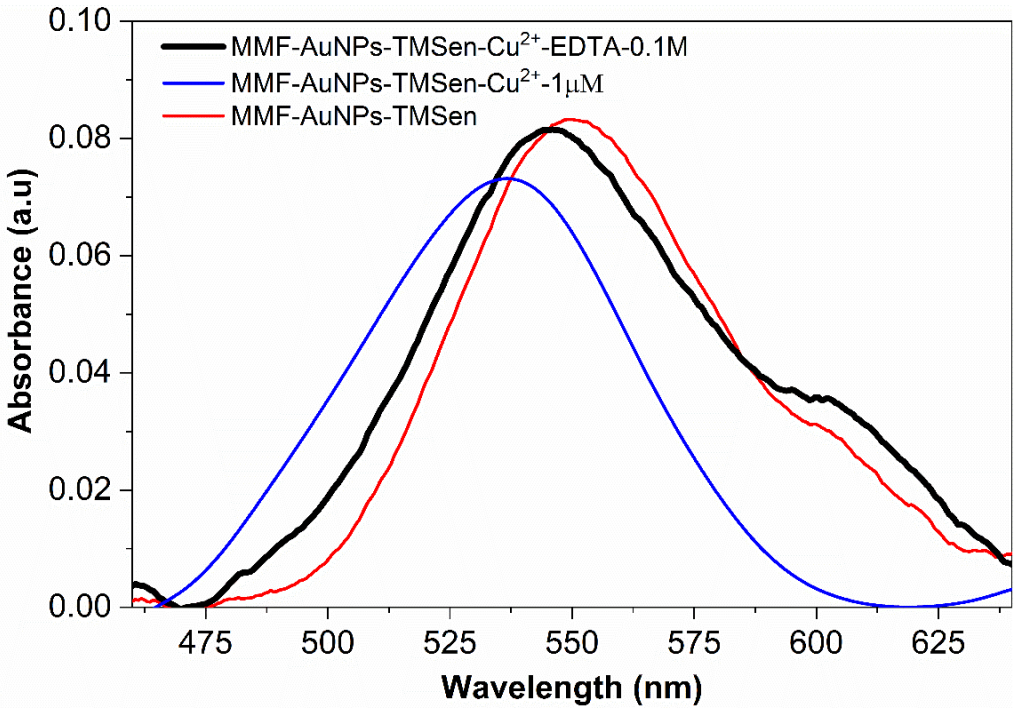

Figure 51. Spectra obtained in the EDT process. The red spectrum corresponds with the probe functionalized immersed in water, which was subsequently immersed in a Cu^{2+} solution with a concentration of 1 µM (blue spectrum). Finally, the black spectrum corresponds with the immersion of such probe in an EDTA solution.

Once the capability to remove Cu^{2+} was demonstrated, we did an experiment to study the repeatability in the measurements with the same probe. The calibration of such experiment is shown in Figure 52. As it can be observed, the first measurements of different concentrations of ions agree with the results obtained previously shown in Figure 48. However, when the signal is recovered by EDTA process, the following measurements do not match with the expected results. According to Figure 52, we can say that the repeatability in the measurements with the same probe is poor, which is one of the limitations that the sensor shown in this chapter presents.

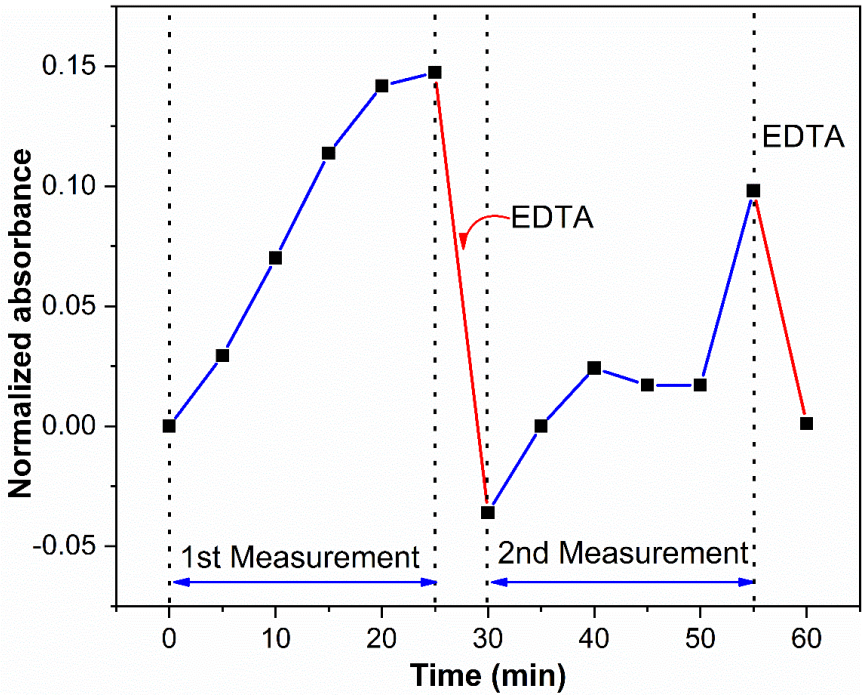

Figure 52. Repeatability study of the fiber sensor for Cu^{2+} detection.

4.6. Performance of copper ions (II) sensors

In this section, the performance of different Cu^{2+} sensors published recently will be compared with the one shown in this chapter. A summary of such works is shown in Table 3. The main features in which we have focused on are the LoD, the range measurement and the method used. As it can be observed, the lab-on-fiber-based sensor developed along this thesis offers a very LoD in a huge range, 1000 times if it is compared with sensors based on PRET but in microscopic platforms[4].

Table 3. Comparison of detection performance of different methods for Cu^{2+} detection.

Technology	**Year**	**Working range**	**Limit of detection**	**Reference**
Fluorescence	2018	1-10 µM	270 nM	[1]
DNAzyme and fluorescence	2020	10 nM-20 µM	2 nM	[3]
Ag/Au nanocluster	2019	20-600 nM	5 nM	[5]
Quantum dots	2019	0.50-2.25 µM	0.36 µM	[7]
Quantum dots	2020	40-600 nM	35 nM	[8]
Electrochemical	2019	1-50 µM	1 µM	[11]
Electrochemical	2019	10 nM-100 µM	35 nM	[12]
Photoelectrochemical	2021	1 nM-10 µM	0.4 nM	[14]
Colorimetry	2020	5-40 µM	1.57 µM	[16]
Colorimetry	2019	20-200 nM	20 nM	[17]
SERS	2019	0.1 nM-1 µM	10 pM	[18]
SERS	2020	1 pM-100 µM	0.1 pM	[19]
PRET-Dark field	2009	1 nM-1 mM	1 nM	[4]
Lab-on-fiber	**2020**	**1 pM-1 µM**	**1 pM**	**[2]**

Other works show a high performance regarding the LoD as well, as, for instance, the ones based on SERS effect[18, 19]. However, the equipment required is not able to measure out of the laboratory and the cost of Raman spectroscopy compared with optical fibers is higher, but in any case, it represents a promising technology for Cu^{2+} detection. Therefore, monitoring in real time is a crucial limitation for interesting applications, as was explained in section 4.1. This drawback is overcome by the use of optical fibers due to its advantages. Nevertheless, the repeatability in measurements of the sensor is very poor, which is a disadvantage compared with the other technologies. Finally, if we consider the price of each technology, our sensor takes advantage with respect to the others, because of the low cost of optical fibers decreases the total price considerably. In fact, all the equipment used in this work (see Appendix 1) costs 2500 euros approximately.

4.7. Summary

To sum up, in this chapter the detection of Cu^{2+} by our lab-on-fiber-based sensor has been shown. The overlapping of the AuNPs spectrum and the complexes Cu^{2+} is the key to develop sensors based on the nanospectroscopic approach, and for this reason, we have proven this factor first. In fact, when the ions are not complexed, the sensor does not notice a change in the intensity of the AuNPs spectrum, but when such complexation is triggered, the sensor is able to detect Cu^{2+} with a LoD measured of 1 pM or 242 fM under the signal-to-noise ratio of 3 (S/N = 3) criteria. Thus, it is proven that the nanospectroscopic approach combined with the lab-on-fiber technology provides high sensitivity, compared with other technologies.

In addition, measurements with other ions were performed in the same range of concentrations, but a high selectivity was demonstrated, being this performance one of the advantages that the nanospectroscopy provides.

However, reproducibility is one of the drawbacks of this sensor, as in the second batch of measurements, the same calibration was not obtained. This problem needs to be solved to use the sensor in real conditions.

References of Chapter 4

1. Han, J.; Tang, X.; Wang, Y.; Liu, R.; Wang, L.; Ni, L. A quinoline-based fluorescence “on-off-on” probe for relay identification of Cu2+ and Cd2+ ions. *Spectrochimica Acta Part A: Molecular and Biomolecular Spectroscopy* **2018,** *205*, 597-602.
2. Barroso, J.; Ortega-Gomez, A.; Calatayud-Sanchez, A.; Zubia, J.; Benito-Lopez, F.; Villatoro, J.; Basabe-Desmonts, L. Selective Ultrasensitive Optical Fiber Nanosensors Based on Plasmon Resonance Energy Transfer. *ACS Sensors* **2020**.
3. Wu, W.; Yu, C.; Chen, J.; Yang, Q. Fluorometric detection of copper ions using click chemistry and the target-induced conjunction of split DNAzyme fragments. *International Journal of Environmental Analytical Chemistry* **2020,** *100* (3), 324-332.
4. Choi, Y.; Park, Y.; Kang, T.; Lee, L. P. Selective and sensitive detection of metal ions by plasmonic resonance energy transfer-based nanospectroscopy. *Nature Nanotechnology* **2009,** *4* (11), 742-746.
5. Babaee, E.; Barati, A.; Gholivand, M. B.; Taherpour, A.; Zolfaghar, N.; Shamsipur, M. Determination of Hg2+ and Cu2+ ions by dual-emissive Ag/Au nanocluster/carbon dots nanohybrids: Switching the selectivity by pH adjustment. *Journal of Hazardous Materials* **2019,** *367*, 437-446.
6. Sardar, K.; Ali, S.; Hameed, S.; Afzal, S.; Fatima, S.; Shakoor, M. B.; Bharwana, S. A.; Tauqeer, H. Heavy metals contamination and what are the impacts on living organisms. *Greener Journal of Environmental management and public safety* **2013,** *2* (4), 172-179.
7. Ngamdee, K.; Chaiendoo, K.; Saiyasombat, C.; Busayaporn, W.; Ittisanronnachai, S.; Promarak, V.; Ngeontae, W. Highly selective circular dichroism sensor based on d-penicillamine/cysteamine‑cadmium sulfide quantum dots for copper (II) ion detection. *Spectrochimica Acta Part A: Molecular and Biomolecular Spectroscopy* **2019,** *211*, 313-321.
8. Xie, Y. F.; Jiang, Y. J.; Zou, H. Y.; Wang, J.; Huang, C. Z. Discrimination of copper and silver ions based on the label-free quantum dots. *Talanta* **2020,** *220*, 121430.
9. Wu, S.-P.; Huang, R.-Y.; Du, K.-J. J. D. T. Colorimetric sensing of Cu (II) by 2-methyl-3-[(pyridin-2-ylmethyl)-amino]-1, 4-naphthoquinone: Cu (II) induced deprotonation of NH responsible for color changes. *Dalton Transactions* **2009,** (24), 4735-4740.
10. Ma, Y.-R.; Niu, H.-Y.; Cai, Y.-Q. J. C. C. Colorimetric detection of copper ions in tap water during the synthesis of silver/dopamine nanoparticles. *Chemical Communications* **2011,** *47* (47), 12643-12645.
11. Frag, E. Y.; Abdel Hameed, R. M. Preparation, characterization and electrochemical application of CuNiO nanoparticles supported on graphite

for potentiometric determination of copper ions in spiked water samples. *Microchemical Journal* **2019,** *144*, 110-116.
12. Atapour, M.; Amoabediny, G.; Ahmadzadeh-Raji, M. J. R. Integrated optical and electrochemical detection of Cu 2+ ions in water using a sandwich amino acid–gold nanoparticle-based nano-biosensor consisting of a transparent-conductive platform. *RSC advances* **2019,** *9* (16), 8882-8893.
13. Yuan, Z.; Cai, N.; Du, Y.; He, Y.; Yeung, E. S. Sensitive and Selective Detection of Copper Ions with Highly Stable Polyethyleneimine-Protected Silver Nanoclusters. *Analytical Chemistry* **2014,** *86* (1), 419-426.
14. Li, J.; Mo, F.; Guo, L.; Huang, J.; Lu, Z.; Xu, Q.; Li, H. Ligand reduction and cation exchange on nanostructures for an elegant design of copper ions photoelectrochemical sensing. *Sensors and Actuators B: Chemical* **2021,** *328*, 129032.
15. Loyez, M.; Ribaut, C.; Caucheteur, C.; Wattiez, R. Functionalized gold electroless-plated optical fiber gratings for reliable surface biosensing. *Sensors and Actuators B: Chemical* **2019,** *280*, 54-61.
16. Kim, A.; Chae, J. B.; Rha, C. J.; Kim, C. A colorimetric chemosensor for selective detection of copper ions. **2020,** *136* (6), 459-467.
17. Liu, S.; Li, X. Colorimetric detection of copper ions using gold nanorods in aquatic environment. *Materials Science and Engineering: B* **2019,** *240*, 49-54.
18. Liu, Y.; Wu, Y.; Guo, X.; Wen, Y.; Yang, H. Rapid and selective detection of trace Cu2+ by accumulation- reaction-based Raman spectroscopy. *Sensors and Actuators B: Chemical* **2019,** *283*, 278-283.
19. Guo, Y.; Li, D.; Zheng, S.; Xu, N.; Deng, W. Utilizing Ag–Au core-satellite structures for colorimetric and surface-enhanced Raman scattering dual-sensing of Cu (II). *Biosensors and Bioelectronics* **2020,** *159*, 112192.

5. Biosensing application: Cytochrome c detection

Unlike the previous chapter, this section deals with a biological application of the optical fiber sensor shown in Chapter 3. Once we demonstrated that our nanospectroscopic approach was able for chemical sensing, we proposed to study the capabilities of the sensor for biological applications. For that reason, we decided to measure a protein, specifically the Cytochrome c (Cyt c), due to the relevance of such protein for medical applications, and to compare it with other nanospectroscopy-based platforms[1, 2]. The main results of this chapter are in this paper[3], where we show the most relevant results, such as the LoD achieved of 60 nM, an order of magnitude lower compared with[2]. As we will see and discuss in the section of results, an opposite behaviour was obtained, as we expected to observe a quenching in two specific wavelengths, but an increase in the absorbance spectrum at such wavelengths occurs.

In this chapter, we will explain first the main motivations for Cyt c detection, and then the steps to prepare the sensor will be shown. The results of the experiments will be discussed as well, focusing on the behaviour of the spectrum, the blank experiments carried out, and the measurements in a physiological environment. Finally, as we did in the previous chapter, we will compare the main features of our sensor with the state of the art.

5.1. Motivation: why measure Cytochrome c?

Cyt c is a multifunctional enzyme located in the membrane of the mitochondria that plays different roles in many biological functions. For this reason, the

information provided for such protein has a medical relevance, and many sensors of different technologies have been developed in the last decades to detect and quantify it[4].

Mainly, Cyt c has a crucial role in the mitochondrial electron transport chain as electron carrier[5, 6], and on the apoptosis process by generating reactive oxygen species (ROS)[7]. Regarding the last one, an excess of ROS production in the cells leads to the programmed death-apoptosis. Although the apoptosis is a regular process, it can be carried out by external factors as well, causing many human diseases, such as cancer, diabetics, cardiovascular problems, etc.[4, 8]. It is important to point out that in such cases, the Cyt c leaves the cells and is released to the human body, in the serum, or even in the blood circulation.

As we have commented, the detection of Cyt c has relevance for medical applications. One of these applications is to evaluate the cancer therapy usefulness and effectiveness[9, 10]. There are cancer therapies based on inducing the apoptosis processes in cancer cells, such as chemotherapy, γ-irradiation, or immunotherapy[4]. As the Cyt c reaches the serum of the patients, to quantify and monitor in real time this biomolecule gives us much information about the success or failure of therapy against cancer[11].

The detection of Cyt c provides us information that can be used for the diagnosis of several diseases at an early stage, as, for example, acute liver failure, myocardial infarction, etc[4, 12]. Because of Cyt c is released into the blood circulation, monitoring the concentration of such protein in blood can serve as a biomarker for different cardiovascular injuries or organ damages[13].

Therefore, as it exists a relation between many pathologies and treatments, the research based on the development of assays for Cyt c detection is increasing in recent times. Thus, it is necessary to create and investigate new sensors that allows not only a fast detection of such protein, but an economical and portable

device able to use it for POC applications. Thus, we think that our approach based on optical fibers and AuNPs allows us to develop biosensors with such features required.

5.2. Probe preparation

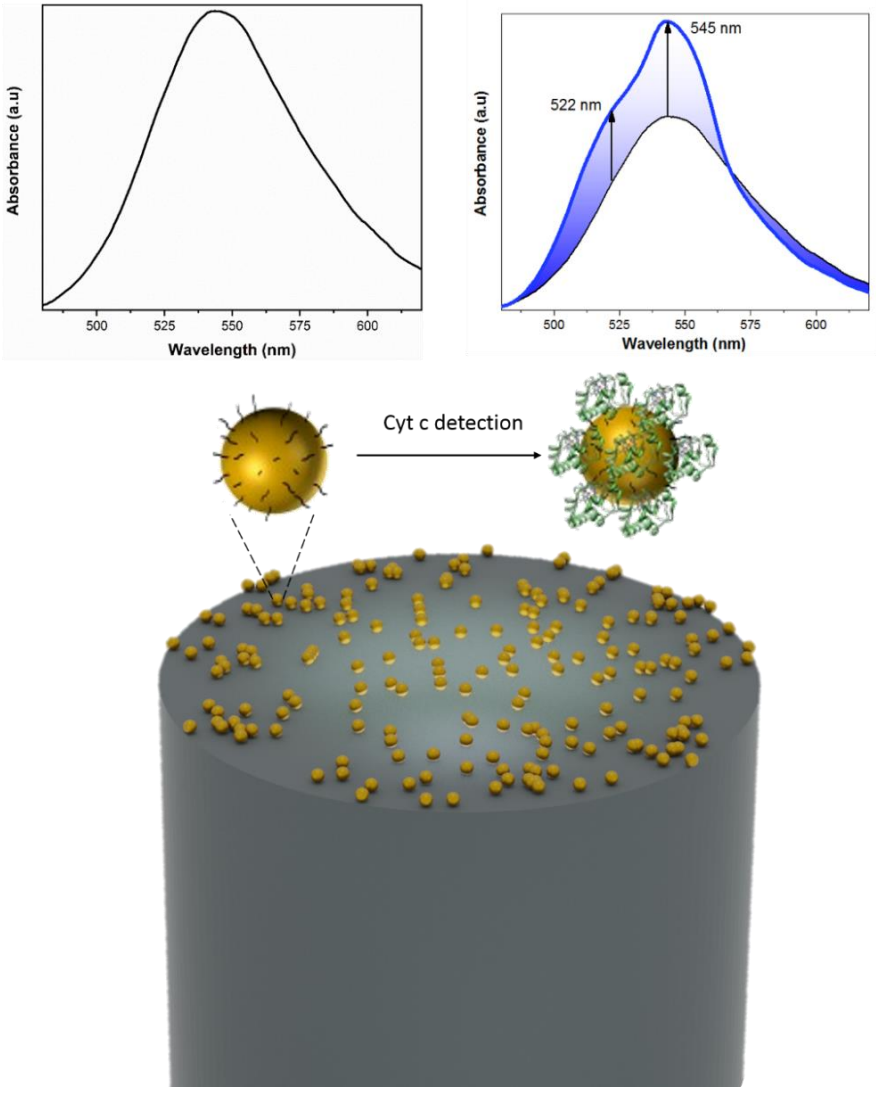

Figure 53. Graphical abstract of the Cyt c detection on the MMF facet. The graph shows the change in the spectrum when the protein is attached to the AuNPs.

As it was mentioned in the previous chapter, to trigger the nanospectroscopy between AuNPs and Cyt c, it is necessary to functionalize specifically the nanoparticles that are attached onto the MMF facet. As it has been demonstrated recently[14], the gap between the AuNPs and the protein is a crucial parameter in this case, since increasing such distance causes a deceasing in the effect of the Cyt c on the AuNPs spectrum. Figure 53 shows the general idea about the fiber sensor, which tries to make it understandable that functionalizing the AuNPs for Cyt c detection is a crucial step.

In this manner, to cause the nanospectroscopic effect, the AuNPs were modified chemically. Once the AuNPs were immobilized onto the MMF facet, the probe was immersed in 1mM 3-mercaptopropionic acid (MPA) solution for 120 minutes. The silane-functionalized MMF-AuNPs were washed with a solution of isopropanol-water (1:1) and were kept in MiliQ water. The chemical scheme of the fiber-based sensor after the functionalization is shown in Figure 54.

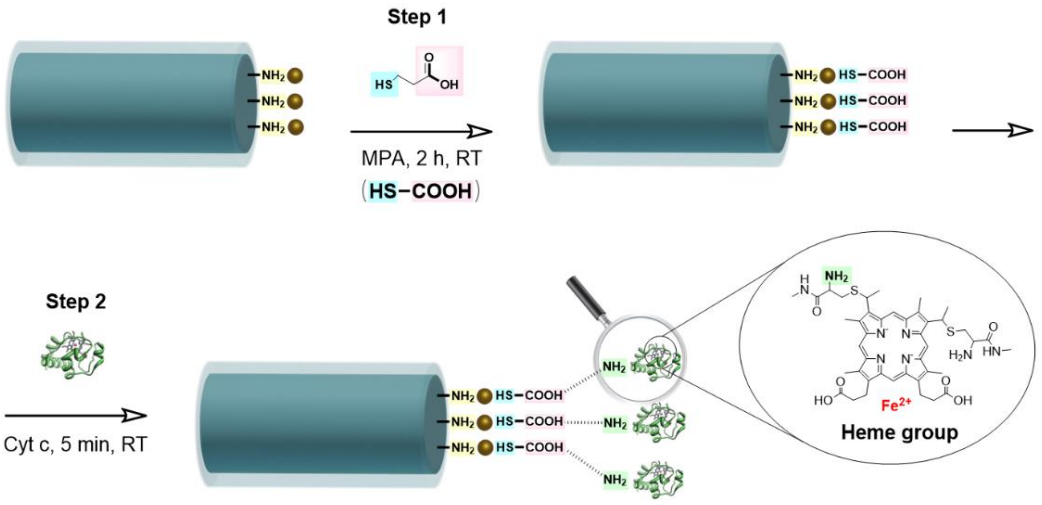

Figure 54. Scheme of the chemical functionalization process of AuNPs for Cyt c detection.

In Figure 55, the effect of the previous functionalization on the LSPR spectrum of AuNPs is shown. The blue line corresponds with the spectrum after AuNPs immobilization, and the black one corresponds with the spectrum after the MPA-based functionalization. As it can be observed, the aforementioned chemical functionalization has a negligible impact in the spectrum. It is important to point out that both spectra were recorded when the optical fibers were immersed in miliQ water, as they have to be compared under the same conditions, or, in other words, in the same refractive index.

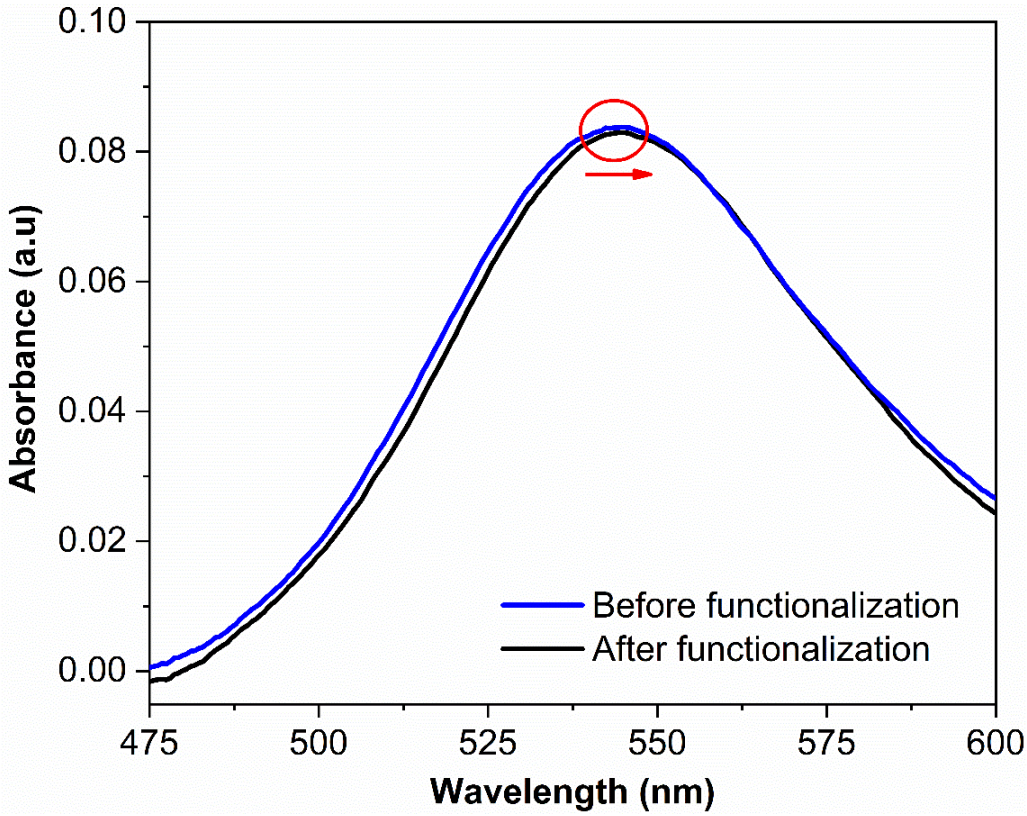

Figure 55. Absorbance spectra before (blue line) and after (black line) the functionalization process of AuNPs with MPA.

We have to point out that Cyt c appears in different forms, oxidized and reduced. The Cyt c was purchased in the oxidized form; however, we tried to detect the reduced form, as the absorbance band is more intense in the interested wavelength band. In fact, the reduced form can be obtained after a chemical process over the oxidized one. As we have explained in Chapters 2 and 4, the spectrum of AuNPs and Cyt c have to match in wavelength terms. To be sure that this condition is fulfilled, the absorption spectrum of the oxidized and reduced form of the Cyt c was obtained. .

To that end, the reduced form had to be prepared. This method was the same to prepare the Cyt c samples for the measurements, and it was as follows: First, it was prepared 0.1 M of sodium dithionite ($Na_2S_2O_4$) solution in phosphate buffered saline (PBS) buffer (0.01 M, pH 7.4). It was fresh for each experiment. Then, $Na_2S_2O_4$ (5 µL, 0.1 M) was added to the oxidized form of Cyt c aliquot (20 µL, 375 µM) into a 0.2 mL low protein binding tube. The sample was mixed and incubated for 5 min at room temperature (25 ºC approximately).

The absorbance spectra of the oxidized and reduced forms were recorded with a spectrophotometer. The absorbance spectrum of each form is depicted in Figure 56, where the differences can be observed clearly. As the oxidized form (see Figure 56a) has only one width peak, the reduced form (see Figure 56b) presents two narrower peaks, which matches with the AuNPs spectrum. In addition, it can be noticed that the peak around 550 nm is more intense than the peak placed at 520 nm.

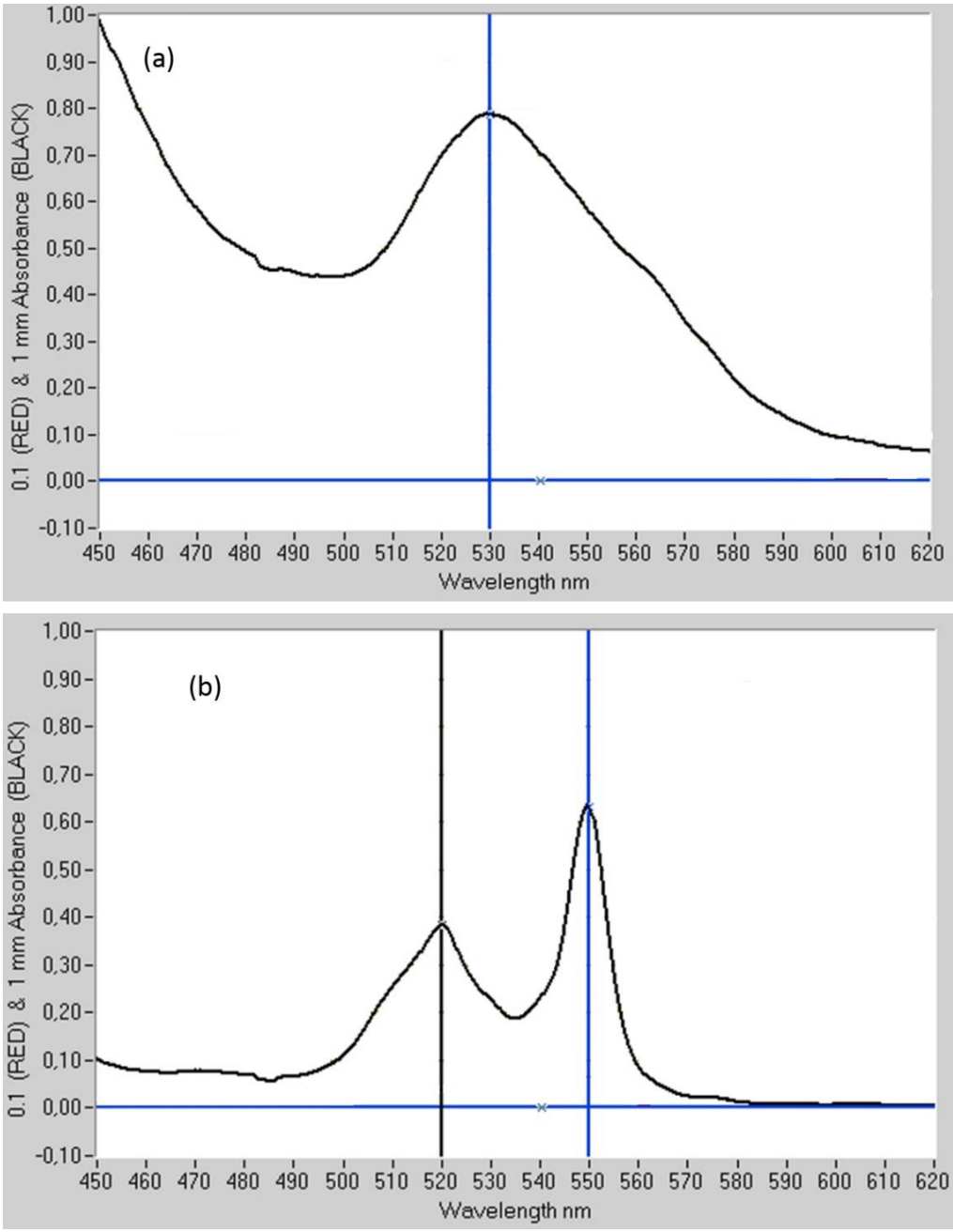

Figure 56. Absorbance spectra of the two forms of the Cyt c, (a) the oxidized (b) and the reduced form.

5.3. Results and discussion

The probes were immersed into aqueous solutions of 300 µL of final volume with different concentrations of Cyt c, working in the concentration range from 0.1 to 80 µM. In all experiments, the obtained spectrum from each concentration was recorded after 5 minutes of immersion of the optical probes into the solution. When the experiment was carried out, the solutions were protected from light. A photograph of a microwell plate where the solutions were spiked is shown in Figure 57. The colour of the solubility of the reduced form of Cyt c was dark red and brown-red as expected.

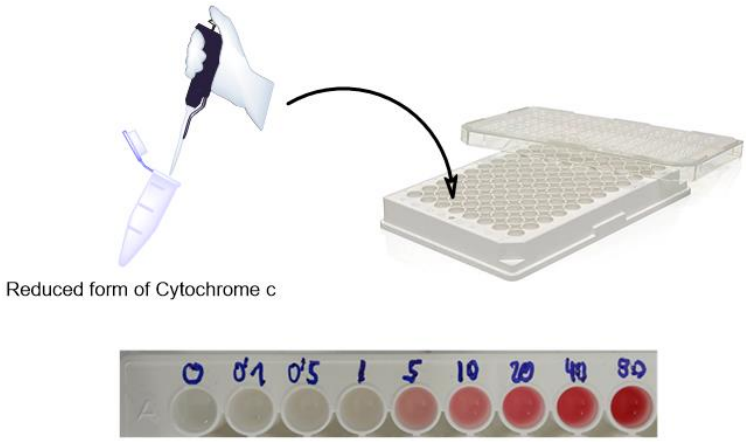

Figure 57. Concentrations of reduced Cyt c from 0 to 80 µM.

The binding of functionalized AuNPs with Cyt c allows the nanospectroscopic detection, as it can be observed in Figure 58. Figure 58a shows the spectra obtained in the concentrations measured. As the experiments were performed using the reduced form of Cyt c, the presence of its two characteristics peaks around 518 and 544 nm is observed as expected, which matches with the two peaks sown in Figure 56. To determine the effect of the Cyt c, the spectrum with no Cyt c, that means 0 M concentration, was subtracted to each other spectra and depicted in Figure 58b.

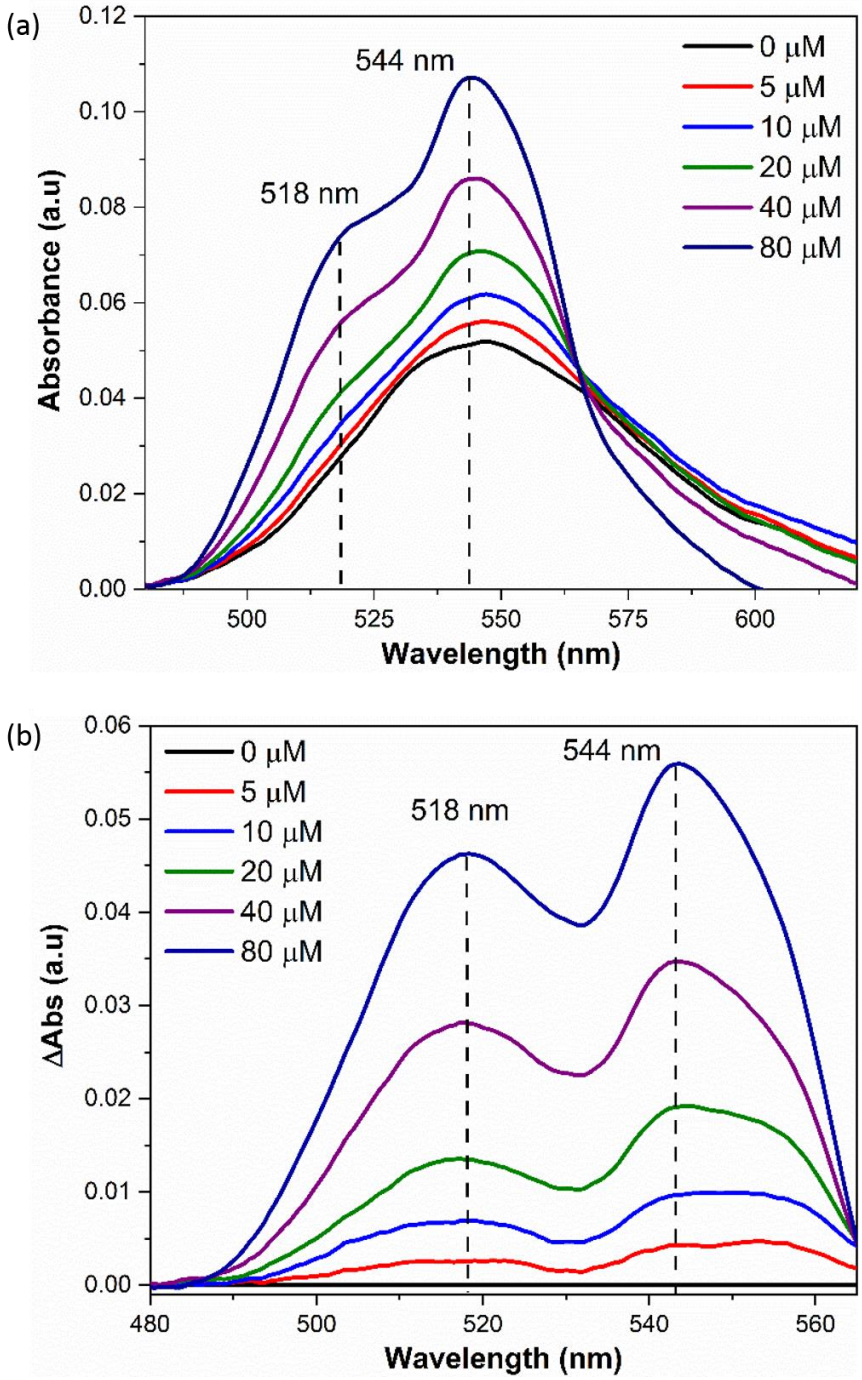

Figure 58. (a) Spectra of different Cyt c concentrations and (b) the spectra subtracting to each one the obtained spectrum when there is no Cyt c (0 μM).

As it can be observed in Figures 58a and b, the intensities of the two peaks (one at 518 nm and the other at 544 nm) grow as the concentration of Cyt c increases as well, but not by a shift in the AuNPs spectrum. In this manner, we demonstrated that the detection of Cyt C with MMFs by the nanospectroscopic effect. The calibration of the assay for Cyt c detection is shown in Figure 59, where each point was calculated using the following expression:

$$\Delta Abs(\lambda_i) = A_c(\lambda_i) - A_0(\lambda_i) \quad (17)$$

where $A_c(\lambda_i)$ is the absorbance intensity in the LSPR spectrum at a certain concentration (c) and wavelength (i), and $A_0(\lambda_i)$ refers to the absorbance intensity of 0 μM LSPR spectrum at a certain wavelength (i), being i = 518 or 544 nm in our case, or, in other words, in the absence of reduced Cyt c.

The sensor shows a widespread linear response from 0.1 to 80 μM, which implies a very easy calculation of the Cyt *c* concentration in all this range through the absorbance obtained. This linearity is obtained for both 518 and 544 nm wavelength peaks as it is shown in Figure 59, which corresponds with the dashed and with the continuous line respectively. The LoD for Cyt *c* is equal to 1 μM and 60 nM for the results obtained at 518 and 544 nm respectively, lower than the concentration reported previously[4] for patients with myocardial infarctions (0.8 μM). The LoD values were calculated at a signal-noise ratio of 3 (S/N = 3).

The maximum intensity of the first absorption band (518 nm) is weaker than the one of the second band (544 nm). This behaviour explains the sensitivity difference between both wavelength bands, being the 544 nm peak more sensitive than the 518 nm peak, as it can be observed by the LoD. The average relative standard deviation (RSD) that was calculated from the Cyt *c* calibration plot (obtained using at least three independent MMFs that were modified with functionalized AuNP@40nm) was around 9 %.

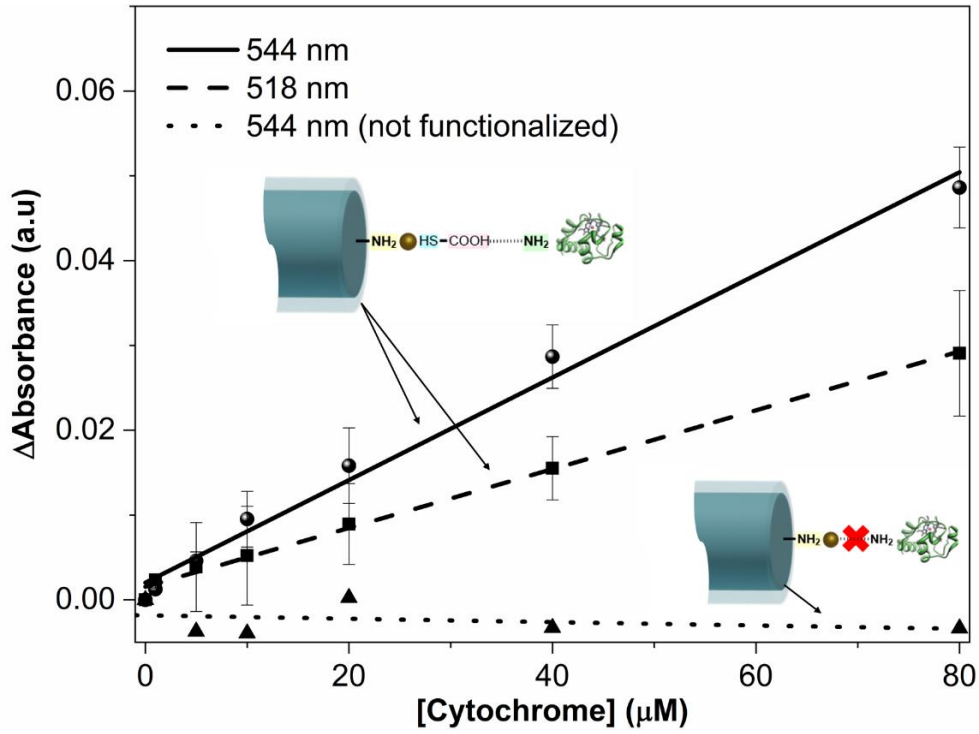

Figure 59. Calibration of the Cyt c measurements. The continuous, dashed and pointed lines (AuNPs were not functionalized) show the calibration at 544 nm, 528 nm and 544 nm, respectively. Error bars correspond to the standard error of 3 tests.

To confirm that the detection of Cyt c is due to the nanospectroscopic effect, a control experiment where AuNPs were not functionalized with MPA was carried out. The main idea was to prevent the binding between AuNPs and Cyt c, to prove that AuNPs and the protein have to be as close as possible to trigger the nanospectroscopy. To that end, the same experimental protocol and concentration range of Cyt c that in Figure 58 was performed. The calibration is depicted in Figure 59, which corresponds with the pointed line. The spectra are shown in Figure 60a. In both graphs, it can be observed that there is not a noticeable variation of the absorbance AuNPs spectrum when the probes were immersed in the Cyt c solution at different concentrations. This behaviour is opposite to the one observed in Figure 58, where the two peaks only appeared when Cyt c was in contact with functionalized AuNPs.

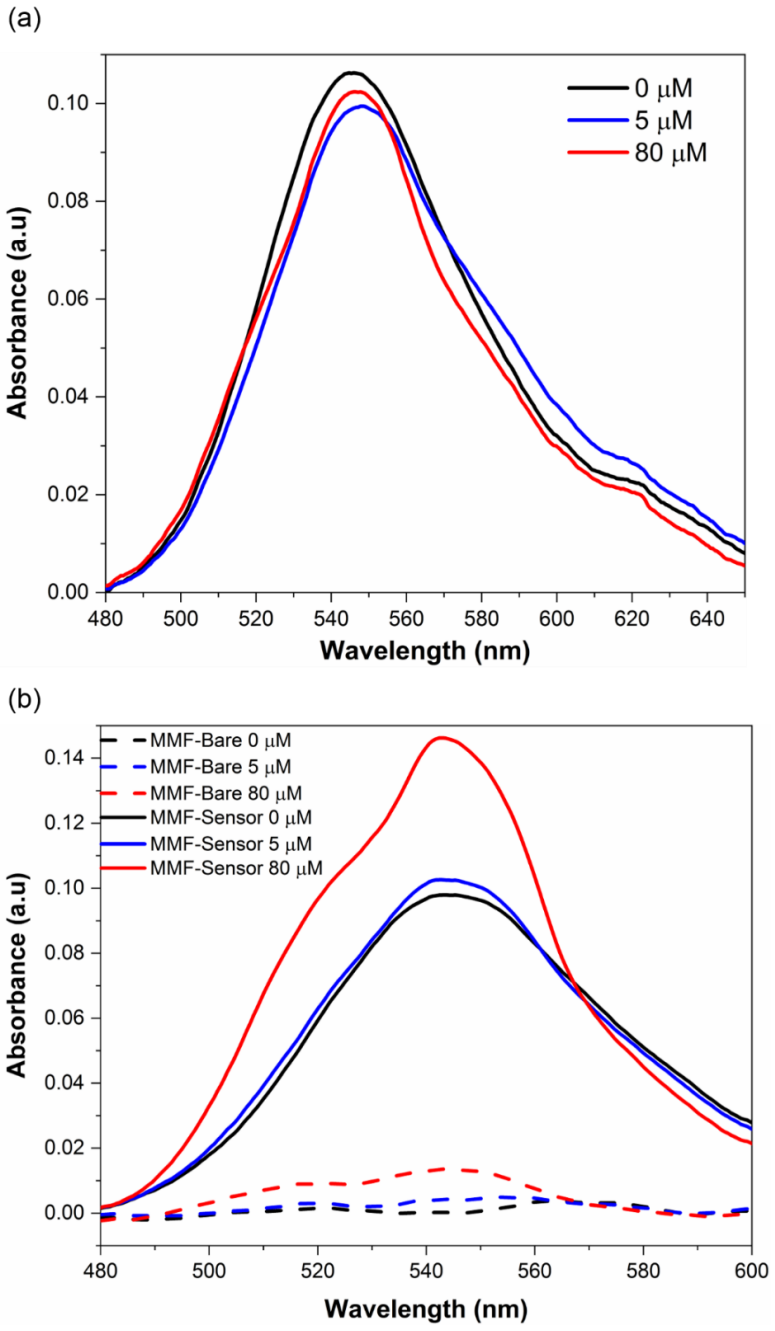

Figure 60. Spectra of the control experiments carried out when (a) the AuNPs were not functionalized and (b) when AuNPs were not immobilized onto the MMF facet (dashed line). The spectra with the continuous line in (b) correspond with the experiments when AuNPs are immobilized and functionalized.

This shows us that when AuNPs do not capture the Cyt c, and thus they are not close between them, no interaction is possible, since the distance between them is too long, and the AuNPs electromagnetic field does not disturb the Cyt c.

After this experiment, and with the aim to obtain information about if AuNPs affect in the absorbance amplification measured, an additional control experiment was done. In this case, a bared MMF was used, with no AuNPs attached onto the end face. The spectra that were recorded in the experiment are shown in Figure 60b, which corresponds with the dashed line. The results show a small increase in both 518 and 544 nm wavelengths. This suggests that the fiber is able to notice the Cyt c, but in a very weak way, being possible to detect the Cyt c in solution without any functionalization. Nevertheless, high Cyt c concentrations are needed (80 μM), which does not allow for a calibration of the system to lower concentrations. On the contrary, as we show, the functionalized AuNPs onto MMFs, which corresponds with the solid line in Figure 60b, favouring the amplification of the signal.

Unlike to what was previously reported[1, 2, 14], quantized dips were not observed, given that the obtained spectra actually show a progressive amplification of the absorbance, as can be observed in Figure 58. Higher Cyt c concentrations, higher absorbance intensities were found at 518 and 544 nm, which match the peaks of the reduced Cyt *c* absorbance band. This mismatching between the expected result and the one obtained has not been completely responded yet. However, two different hypotheses have been developed with the aim to explain this behaviour:

1. The first hypothesis is based on the last publication of Professor Lee[14]. As they demonstrated recently, the distance between the plasmonic structure and the analyte of interest has a crucial role. When such distance is in the subnanometer range, a quantum electron tunnel effect appears, which is strongly dependent on this gap[15, 16]. As the gap

decreases, the intensity of this quantum effect is higher, increasing the sensitivity and the interaction AuNP-target. As they comment, this quantum effect lives with the transfer of energy effect, which means that both phenomena are occurring at the same time, but they do not understand the root of such effect yet. Comparing our work with the shown in[14], AuNPs were modified with MPA ($HS(CH_2)_2COOH$) in both to capture the Cyt *c*, using the shorter linker of the $HS(CH_2)_nCOOH$ family, which corresponds with $n = 2$. This means that the linker distance of our sensors is 530 pm, as we show in Figure 61, and therefore, a quantum electron tunnel effect occurs. This could cause a progressive increase in the absorbance spectrum, but we cannot say for sure yet.

2. The Cyt c - AuNPs distance is around 600 pm, as can be observed in Figure 61. This may cause that the Cyt c - AuNP element would be observed as a unique element, and what we are seeing in the spectra would be a sum of the absorbance spectra of AuNPs and Cyt c. In other words, the proteins cover the AuNP and we observe the absorbance of the Cyt c - AuNP system, which increases as the number of proteins attached to the AuNP surface increases as well. So far, the question is, if this is true, why this is not observed in the other papers based on the nanospectroscopic phenomenon? Because such papers work with the dark field microscopy, and they only are able to observe the scattering from AuNPs, while our approach based on optical fibers allows us to observe a mixture of scattering and absorbance as we explained in Chapter 3, where the absorbance signal predominates over the scattering one. This hypothesis suggests a nanospectroscopic effect based on absorbance.

In any case, this work was performed at the final of the thesis, and therefore, both hypotheses have not been refuted yet. It is important to point out that the

relevance of this work stands on the experimental results obtained, although we will not able to understand the root of the effect yet.

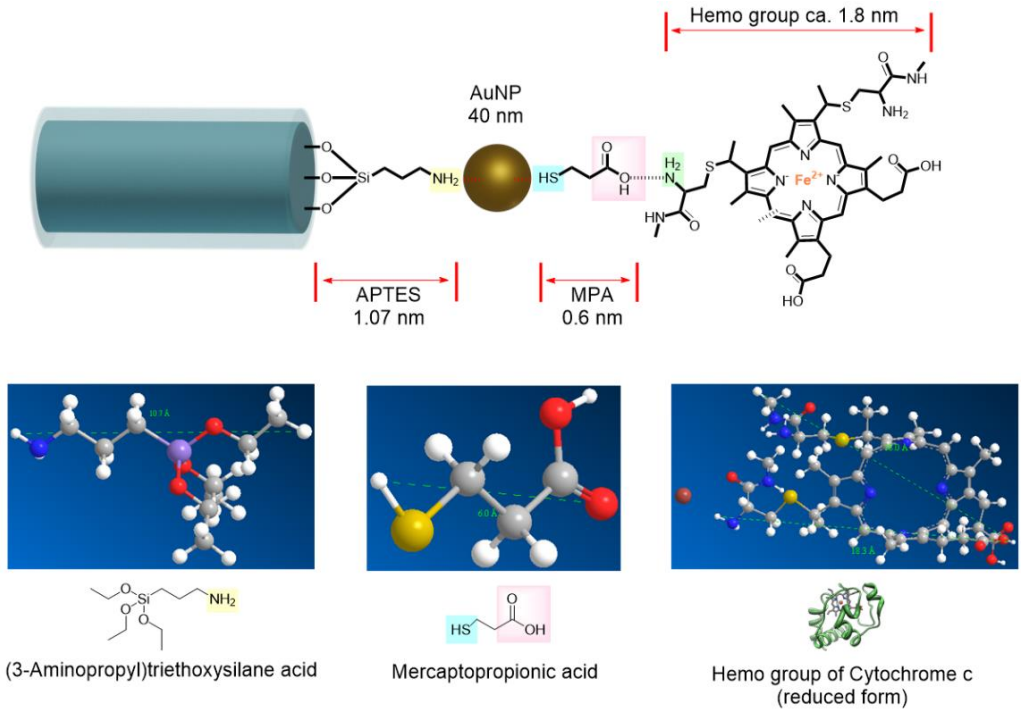

Figure 61. Chemical scheme of the MMF facet with AuNPs immobilized to it and functionalized with MPA. The distances among components are shown.

5.4. Physiological environments

In order to validate the sensor described in this chapter in a physiological environment, we performed an experiment but with the reduced Cyt c in bovine serum. As we explained in section 5.1 of this chapter, where the main motivations for Cyt c detection were shown, to quantify Cyt c in serum is very interesting because the Cyt c is released to the human body, and, thus, it is possible to detect it in serum. For that reason, we performed the identical experiment but in a bovine serum solution, and the results were compared with the calibration shown in Figure 59 that was conducted in a PBS solution.

The optical sensors were immersed into the buffered serum solution, which contained different concentrations of the reduced form of Cyt c, exactly the same concentrations that in previous experiments (see Figure 59 and the photograph in Figure 57). The results of such experiments are shown in Figure 62. As it can be observed, the calibration plot is very similar compared with the calibration obtained previously for buffered solutions. The error bars correspond with three different measurements. In addition, the LOD for the reduced Cyt c achieved is similar when the sensor measure in bovine serum, because of both calibration plots have almost identical slopes in both buffer and serum samples. In this manner, it is possible to demonstrate and validate the usefulness of the developed nanospectroscopy-based sensor for reduced Cyt c detection and quantification in serum samples.

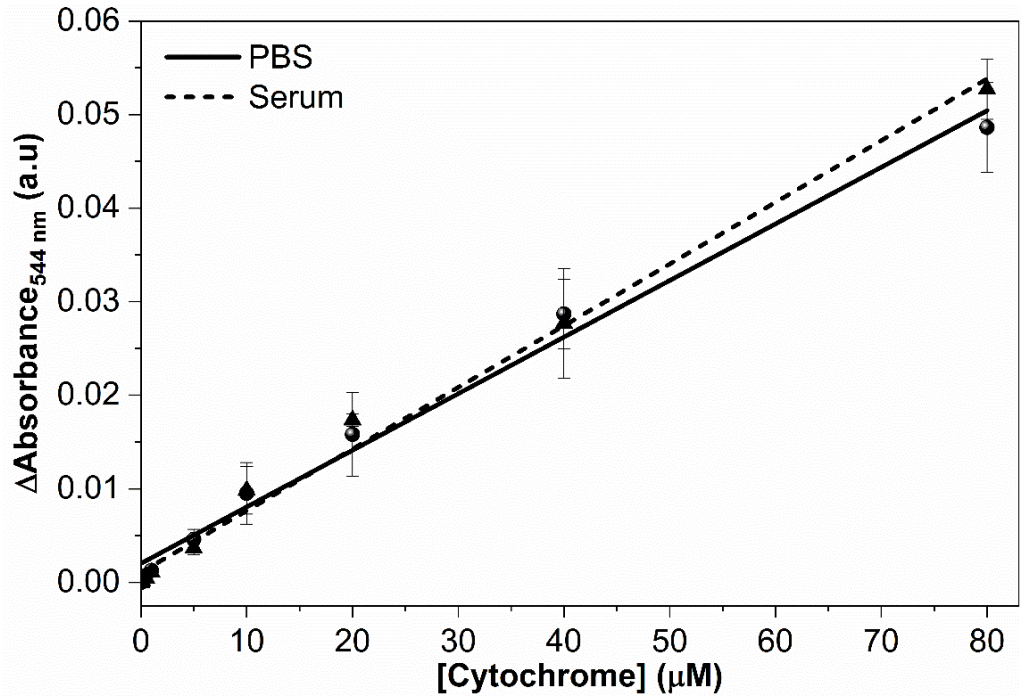

Figure 62. Calibration of the measurements of Cyt C in Serum (dashed line) compared with the results obtained in PBS (continuous line). Errors bars correspond with the standard error of 3 tests.

5.5. Performance of Cytochrome c sensors

The classical techniques and methods for Cyt *c* detection required expensive instruments or high time-consuming, such as Western blot or ELISA tests. For this reason, MMFs provide many advantages, such as the possibility to monitor in real time this protein and obtain faster analysis, which is basic for the development of POC sensors.

A summary of different sensors for Cyt c detection is shown in Table 4. As it can be observed in the table, the sensor proposed in this thesis shows a high performance compared with other works but, regarding the LoD, the sensors based on SERS show a better result. However, MMFs provide us advantages that other technologies cannot, such as the portability, due to the easy and simple interrogation system, which allows us to use the sensor shown in this chapter for POC applications, being more complicated for other techniques like based on Raman, Fluorescence or Electrochemistry.

With respect to the working range of our sensor, it can be observed in Table 4 that provides a shorter range compared with other works. However, as we explained in the first section of this chapter, the concentrations founded in our body when the Cyt c is released are much lower. In fact, a concentration of around 0.8 μM in the blood is found for myocardial infarctions. Depending on the application, a lower LoD is worth it, as in applications for diagnosis of diseases at an early stage. For these cases, the research based on PRET, SERS, and the one shown in this chapter offer good performance. However, in other cases, it could be more interesting to observe a wider working range, and the detectors based on Electrochemical or Electrochemiluminescence may represent a better solution.

Table 4. Comparison of detection performance of different methods for Cyt c detection.

Technology	**Year**	**Working range**	**Limit of detection**	**Reference**
Fluorescence	2016	0.1 to 40 μM	89 nM	[17]
Fluorescence	2015	4 to 24 μM	0.73 μM	[18]
Quantum dots	2019	2.0 to 150 nM	1.7 nM	[19]
Electrochemical	2018	10 to 215 μM	45 nM	[20]
Electrochemiluminescence	2020	10 nM-100 μM	2.5 nM	[21]
SERS	2019	0.044-9.95 μM	0.02 μM	[22]
SERS Fiber probe	2019	-	130 nM	[23]
PRET-Dark field	2007	5 to 100 μM	500 nM	[1]
Lab-on-fiber	**2020**	**1 to 80 μM**	**60 nM**	**[3]**

5.6. Summary

In this chapter, a biological application for the lab-on-fiber sensor has been shown, specifically for the Cyt c detection in its reduced form. For this end, the AuNPs immobilized on the fiber end face were modified by MPA. The detection method has been performed via nanospectroscopy, as it is based on changes in the AuNPs intensity, and not on a wavelength of resonance shift. Moreover, the system is able to detect the two peaks of the Cyt c absorption band, as we

have proven. The LoD of the sensor for Cyt *c* detection is equal to 1 μM and 60 nM for the results obtained at 518 and 544 nm respectively. Such results may permit to use of the sensor for real applications, as the concentration in blood for cardiovascular problems is around 0.8 μM.

Finally, the sensor was used not only in the buffer solution but in bovine serum, with a calibration plot similar compared with the one obtained in the buffer. Thus, we have demonstrated that our nanospectroscopic approach combined with optical fibers is able for biological applications as well.

References of Chapter 5

1. Liu, G. L.; Long, Y. T.; Choi, Y.; Kang, T.; Lee, L. P. Quantized plasmon quenching dips nanospectroscopy via plasmon resonance energy transfer. *Nat. Methods* **2007,** *4* (12), 1015-1017.
2. Choi, Y.; Kang, T.; Lee, L. P. Plasmon Resonance Energy Transfer (PRET)-based Molecular Imaging of Cytochrome c in Living Cells. *Nano Letters* **2009,** *9* (1), 85-90.
3. Ortega-Gomez, A.; Barroso, J.; Calatayud-Sánchez, A.; Zubia, J.; Benito-Lopez, F.; Basabe-Desmonts, L.; Villatoro, J. Cytochrome c detection by plasmonic nanospectroscopy on optical fiber facets. *Sensors and Actuators B: Chemical* **2021,** *330*, 129358.
4. Manickam, P.; Kaushik, A.; Karunakaran, C.; Bhansali, S. Recent advances in cytochrome c biosensing technologies. *Biosensors and Bioelectronics* **2017,** *87*, 654-668.
5. Hatefi, Y. the mitochondrial electron transport and oxidative phosphorylation system. *Annual review of biochemistry* **1985,** *54* (1), 1015-1069.
6. Koopman, W. J. H.; Verkaart, S.; Visch, H. J.; Vries, S. v. E.-d.; Nijtmans, L. G. J.; Smeitink, J. A. M.; Willems, P. H. G. M. Human NADH:ubiquinone oxidoreductase deficiency: radical changes in mitochondrial morphology?. *American Journal of Physiology-Cell Physiology* **2007,** *293* (1), C22-C29.
7. Kannan, K.; Jain, S. K. Oxidative stress and apoptosis. *Pathophysiology* **2000,** *7* (3), 153-163.
8. Uttara, B.; Singh, A. V.; Zamboni, P.; Mahajan, R. J. C. n. Oxidative stress and neurodegenerative diseases: a review of upstream and downstream antioxidant therapeutic options. *Current Neuropharmacology* **2009,** *7* (1), 65-74.
9. Eleftheriadis, T.; Pissas, G.; Liakopoulos, V.; Stefanidis, I. J. F. i. i. Cytochrome c as a potentially clinical useful marker of mitochondrial and cellular damage. Frontiers in immunology **2016,** *7*, 279.
10. Zhang, X.; Liao, N.; Chen, G.; Zheng, A.; Zeng, Y.; Liu, X.; Liu, J. J. N. A fluorescent turn on nanoprobe for simultaneous visualization of dual-targets involved in cell apoptosis and drug screening in living cells. Nanoscale **2017,** *9* (30), 10861-10868.
11. Sun, Y.; Ge, S.; Xue, J.; Zhou, X.; Lu, W.; Li, G.; Cao, X. Highly sensitive detection of cytochrome c in the NSCLC serum using a hydrophobic paper base-gold nanourchin substrate. *Biomed. Opt. Express* **2020,** *11* (12), 7062-7078.
12. Sakaida, I.; Kimura, T.; Yamasaki, T.; Fukumoto, Y.; Watanabe, K.; Aoyama, M.; Okita, K. J. J. o. g. Cytochrome c is a possible new marker for fulminant hepatitis in humans. *Journal of gastroenterology* **2005,** *40* (2), 179-185.

13. Ashe, D.; Alleyne, T.; Iwuoha, E. J. B. Serum cytochrome c detection using a cytochrome c oxidase biosensor. *Biotechnology and applied biochemistry* **2007,** *46* (4), 185-189.
14. Xin, H.; Sim, W. J.; Namgung, B.; Choi, Y.; Li, B.; Lee, L. P. Quantum biological tunnel junction for electron transfer imaging in live cells. *Nature Communications* **2019,** *10* (1), 3245.
15. Tan, S. F.; Wu, L.; Yang, J. K.; Bai, P.; Bosman, M.; Nijhuis, C. A. J. S. Quantum plasmon resonances controlled by molecular tunnel junctions. *Nature Communications* **2014,** *343* (6178), 1496-1499.
16. Zhu, W.; Esteban, R.; Borisov, A. G.; Baumberg, J. J.; Nordlander, P.; Lezec, H. J.; Aizpurua, J.; Crozier, K. B. Quantum mechanical effects in plasmonic structures with subnanometre gaps. *Nature Communications* **2016,** *7* (1), 11495.
17. Li, D.-Y.; Zhang, X.-M.; Yan, Y.-J.; He, X.-W.; Li, W.-Y.; Zhang, Y.-K. Thermo-sensitive imprinted polymer embedded carbon dots using epitope approach. *Biosensors and Bioelectronics* **2016,** *79*, 187-192.
18. Guo, T.; Deng, Q.; Fang, G.; Liu, C.; Huang, X.; Wang, S. J. B. Molecularly imprinted upconversion nanoparticles for highly selective and sensitive sensing of Cytochrome c. *Biosensors and Bioelectronics* **2015,** *74*, 498-503.
19. Cai, M.; Ding, C.; Cao, X.; Wang, F.; Zhang, C.; Xian, Y. Label-free fluorometric assay for cytochrome c in apoptotic cells based on near infrared Ag2S quantum dots. *Analytica Chimica Acta* **2019,** *1056*, 153-160.
20. Pashai, E.; Darzi, G. N.; Jahanshahi, M.; Yazdian, F.; Rahimnejad, M. J. An electrochemical nitric oxide biosensor based on immobilized cytochrome c on a chitosan-gold nanocomposite modified gold electrode. *International journal of biological macromolecules* **2018,** *108*, 250-258.
21. Wang, C.; Li, M.; Liu, D. Gold-Nanoparticle-Functionalized Cobalt–Nickel Phosphate 3D Nanoice Creams to Fabricate Stable and Sensitive Biosensors for the Cytochrome c Assay. *ACS Applied Materials & Interfaces* **2020,** *12* (31), 35385-35392.
22. Zhang, J.; Ma, X.; Wang, Z. Surface-Enhanced Raman Scattering-Fluorescence Dual-Mode Nanosensors for Quantitative Detection of Cytochrome c in Living Cells. *Analytical Chemistry* **2019,** *91* (10), 6600-6607.
23. Li, L.; Deng, S.; Wang, H.; Zhang, R.; Zhu, K.; Lu, Y.; Wang, Z.; Zong, S.; Wang, Z.; Cui, Y. J. N. A SERS fiber probe fabricated by layer-by-layer assembly of silver sphere nanoparticles and nanorods with a greatly enhanced sensitivity for remote sensing. *Nanotechnology* **2019,** *30* (25), 255503.

6. Conclusions and lines of future development

In this thesis, we have proposed a novel detection method involved in optical fiber sensors for biochemical applications. This work has opened a new research line in our research group, and all the work developed was new for all of us. Thus, each step forward helped to obtain new information and conclusions. The aim of this chapter is to show, first, the conclusions that we obtained during our investigations, and secondly, the future lines of work that can be performed to improve the research presented in this thesis.

6.1. Conclusions

The main conclusions are divided in three main groups: i) general conclusions; ii) the fabrication process explained in Chapter 3; and iii) the biochemical applications shown in Chapter 4 and 5.

- *General conclusions*
    - The combination of optical fibers and nanospectroscopy provides the development of sensitive, selective and low-cost sensors that may open a new generation of biochemical sensors for POC applications.
    - The nanospectroscopic approach allows to develop versatile sensors, as modifying the properties of the metal nanoparticles, such as the metal, size or shape, it is possible to select the resonance frequency of interest to match it with the resonance frequency of any target.

- The use of optical fibers as optical platforms provide, not only advantages related to the cost of the sensor, but the possibility to characterize the AuNPs immobilization in real time, and thus, extrapolate it to other surfaces, where monitoring the process is not possible.

- *Fabrication process*
  - Thanks to the information provided by the spectral characterization and the image analysis with SEM, we are able to increase the reproducibility of the manufacturing process. The reproducibility obtained was of 88 %, which is a significant value if we consider that the chemical immobilization is a random process.
  - The AuNPs immobilization process on the optical fiber end face shows three different behaviours with respect to the intensity of the recorded spectrum. The first behaviour corresponds to a linear increase, then, the intensity achieves a plateau, and finally, the observed tendency is a decrease.
  - The spectral behaviour relies on the aggregation of AuNPs. Thanks to the SEM images, we concluded that the different tendencies have a strong relation with the distribution of the AuNPs. As the number of single AuNPs decreases, or in other words, the number of aggregations increases, a gold layer can be formed causing the LSPR effect lost.
  - The immobilization of AuNPs can be optimized to perform faster by increasing temperature and having AuNPs concentrations. The impact of the core's diameter of the optical fiber relies on the time necessary to achieve the plateau, as the core is smaller, the plateau is achieved early, but the intensity obtained is lower, as the number of AuNPs that contribute to the total intensity is lower as well.

- *Biochemical applications*
    - We prove that the sensor developed in this thesis is able to measure for both, chemical and biological applications with a high performance.
    - In both applications, it is proved that when the target under study does not bind with the AuNPs and, therefore, they are not near between them, there is no variation in the intensity of the AuNPs, meaning, the nanospectroscopic effect is not triggered. Thus, in order to take advantage of this detection method, the sample has to be close to the electromagnetic field caused by the LSPR effect.
    - Regarding the Cu^{2+} sensor, the LoD measured was of 1 pM, 1000 times more sensitive compared with the ones based on nanospectroscopy but with a dark-field microscope as optical platform. The LoD is 242 fM under the signal-to-noise ratio of 3 (S/N = 3) criteria.
    - The selectivity of the Cu^{2+} sensor is proven. Other metal ions were measured with the identical experimental protocol, and the results of the Cu^{2+} stand out with respect the other ions.
    - The main limitation for the Cu^{2+} detector is the repeatability in the measurements, as we have shown that from the second measurement, it is not possible to achieve the same performance.
    - Regarding the Cyt c detection, the LoD obtained was of 1 µM and 60 nM for the results obtained at the resonance wavelengths of 518 and 544 nm respectively. Such results provide the use of this sensor for real applications, such as detection of cardiovascular diseases, where the concentration of Cyt c is around 800 nM.

- The experiments for the Cyt c detection were conducted in a buffer and in a bovine serum solution. The latter corresponds to a surrounding medium closer to real applications. The results in both solutions are very similar, which is an interesting output as it means that our sensor is able to measure in physiological environments with the same performance.

6.2. Lines of future development

The research of this thesis may open lines of development in the future. Thus, the aim of this section is to clarify and show the potential lines. Such lines are divided depending on if they are immediate improvements that can be applied in the work shown in this thesis, or, if they are, on the contrary, new researches lines.

6.2.1. Immediate improvements

The first improvement could be to understand the reason that the absorbance intensity increases when the Cyt c is detected. As we discussed and hypothesized this effect in Chapter 5 because of different reasons. Accordingly, the first objective has to be designing experiments to clarify this phenomenon. We propose to repeat the measurements detailed in Chapter 5 but modifying the length of the bound Cyt c - AuNPs, in order to obtain the impact of the length on the intensity variation of the spectrum. Thus, if the results with the optical fiber is similar that the one based on dark-field microscopy, we could determine that the physical effect is the same.

Another future improvement that can be developed is related to the repeatability of the Cu^{2+} detection. As we discussed in Chapter 4, the repeatability is a drawback of the sensor proposed. Such problem has a negative impact on the

use of the sensor for real measurements, as it limits the usefulness of the sensor. In order to apply the sensor to perform real time monitoring of copper in a certain river, the repeatability has to improve. To that end, one research line can be focus on improving the chemical bond in order to eliminate the copper attached to the AuNPs easily.

Once the characterization of the AuNPs immobilization has been developed and shown in Chapter 3, another interesting line could be to perform a massive manufacturing process of the sensor. The progress on 3D printers allows fabricating custom platforms, with the aim of designing an automatic protocol for the AuNPs immobilization on optical fibers.

Among the future direction lines, one of the most promising is the multiplexing. In the case of the nanospectroscopic approach proposed in this thesis, it is very interesting to take advantage of the possibility to cover the electromagnetic spectrum with different nanoparticles. The idea is simple: with the setup shown in the Appendix 1, but including a multiplexer, several fibers with different metal nanoparticles immobilized on the end face are able to detect different parameters in the same sample by nanospectroscopy.

6.2.2. Future directions

To integrate the sensor in a microfluidic channel including the multiplexing idea may open the possibility to manufacture sensors for POC applications massively. In addition, we could fabricate such devices with the aim to commercialize the sensor as a product. Thus, such devices based on three ideas, nanospectroscopy on optical fibers, multiplexing, and microfluidic channel, may help to develop miniaturize sensors to detect diseases in real time, which could be very useful in pandemic situations in order to produce fast detections, for instance.

Another promising future direction is to take advantage of the characterization in the AuNPs immobilization for biochemical applications. Instead of measuring by nanospectroscopy, a new approach could be to design labelled sensors with AuNPs and optical fibers. The general idea could be as follows: only the AuNPs attached to the analyte of interest will immobilize on the optical fiber surface. Thus, the intensity observed in the spectrometer due to the AuNPs immobilization could correspond indirectly with the number of analytes detected. As we have characterized this immobilization process, we are able to estimate the concentration, as to each AuNP would correspond one analyte. In this manner, a label sensor with a very low LoD could be developed, as the LoD would be given by the minimum number of AuNPs detected.

7. Publications of the author

In this section, the main contributions of the author published during the thesis are shown. They are divided in two groups, contributions related to the topic of this dissertation, and contributions that are the result of alternative research lines developed during the thesis.

7.1. Related to the thesis

Papers (sorted by year):

- J. Barroso*; **A. Ortega-Gomez***; A. Calatayud-Sanchez; J. Zubia; F. Benito-Lopez; J. Villatoro; Lourdes Basabe-Desmonts. *Selective ultrasensitive optical fiber nano-sensors based on plasmon resonance energy transfer*. **ACS Sensors**, 5 - 7, pp. 2018 – 2024, 2020.
- **A. Ortega-Gomez***; J. Barroso*; A. Calatayud-Sanchez; J. Zubia; F. Benito-Lopez; Lourdes Basabe-Desmonst; J. Villatoro*. Cytochrome c detection by plasmonic nanospectroscopy on optical fiber facets*. **Sensors and actuators B: Chemical**, 330, pp 129358, 2021.

Works submitted to national or international conferences (sorted by year):

- **A. Ortega-Gomez**, J. Barroso, F. Benito-Lopez, J. Zubia, J. Villatoro, L. Basabe-Desmonts. *Fiber optics sensing of copper ions in water based on plasmon resonance transfer energy*. **SPIE Photonics West 2019**, San Francisco, EEUU (2019), oral conference.
- **A. Ortega-Gomez**, J. Barroso, A. Calatayud-Sánchez, F. Benito-Lopez, J. Zubia, L. Basabe-Desmonts, J. Villatoro. *Detection of metal ions in water by*

nanospectroscopy on an optical fiber tip. **Optoel 2019**, Zaragoza, Spain (2019), poster.

- **A. Ortega-Gomez**, J. Zubia, J. Villatoro. *Highly reproducible LSPR-nanoprobe manufacturing process*. **Photonics North 2020**, Canada (2020), oral conference.
- **A. Ortega-Gomez**, J. Barroso, A. Calatayud-Sánchez, F. Benito-Lopez, J. Zubia, L. Basabe-Desmonts, J. Villatoro. *Fiber optic biosensor by plasmon resonance energy transfer*. **OSA Advanced Photonics 2020**, Montreal, Canada (2020), oral conference.
- A. Calatayud-Sánchez, **A. Ortega-Gomez**, J. Barroso, J. Zubia, F. Benito-Lopez, J. Villatoro, L. Basabe-Desmonts. *Ultrasensitive plasmonic sensors on optical fibers end-face*. **μTAS 2020**, online, poster.
- **A. Ortega-Gomez**, J. Barroso, A. Calatayud-Sánchez, F. Benito-Lopez, J. Zubia, J. Villatoro, L. Basabe-Desmonts. *Copper ions sensor nanospectroscopy-based by Multimode Optical Fiber*. **Europtrode 2021**, Warsowia, Poland (2021), oral conference.
- A. Calatayud-Sánchez, **A. Ortega-Gomez**, J. Barroso, F. Benito-Lopez, J. Villatoro, L. Basabe-Desmonts. *Plasmon Resonance Energy Transfer (PRET)-based bionanosensors on glass: PRETSURF*. **Europtrode 2021**, Warsowia, Poland (2021), oral conference.
- J. Barroso, A. Calatayud-Sánchez, **A. Ortega-Gomez**, F. Benito-Lopez, J. Villatoro, L. Basabe-Desmonts. *Novel sensing platforms based on plasmon resonance energy transfer (pret)*. **Europtrode 2021**, Warsowia, Poland (2021), poster.
- **[INVITED TALK]** A. Calatayud-Sánchez, Raquel Catalan-Carrio, **A. Ortega-Gomez**, J. Barroso, J. Zubia, F. Benito-Lopez, J. Villatoro, L. Basabe-Desmonts. Plasmon resonance energy-transfer-based fiber-optic platform for ultrasensitive sensing. **SPIE 2021**, San Francisco, EEUU (2021).

7.2. Related to other research lines

Papers (sorted by year):

- J. Amorebieta, G. Durana, **A. Ortega-Gomez**, R. Fernández, J. Velasco, I. Sáez de Ocáriz, J. Zubia, J. E. Antonio-López, A. Schülzgen, R. Amezcua-Correa, J. Villatoro. *Packaged multi-core fiber interferometer for high-temperature sensing.* **Journal of Lightwave Technology**. 10, pp. 2328-2334, 2019.
- M Azkune, **A Ortega-Gomez**, I Ayesta, J Zubia. *Refractive-Index Profile Reconstruction in Graded-Index Polymer Optical Fibers Using Raman Spectroscopy.* **Materials**, 13, 2251, 2020.
- **[INVITED PAPER]** J. Villatoro, J. Amorebieta, **A. Ortega-Gomez**, J. E. Antonio-López, J. Zubia, A. Schülzgen, R. Amezcua-Correa. *Composed multicore fiber structure for direction-sensitive curvature monitoring.* **APL Photonics**, 7, pp. 70801, 2020.
- J. Amorebieta, **A. Ortega-Gomez**, G. Durana, R. Fernández, J. E. Antonio-López, A. Schülzgen, J. Zubia, R. Amezcua-Correa, J. Villatoro. *Highly sensitive multicore fiber accelerometer for low frequency vibration sensing*. **Scientific Reports**, 10, pp. 1-11, 2020.
- J. Amorebieta, **A. Ortega-Gomez**, G. Durana, R. Fernández, J. E. Antonio-López, A. Schülzgen, J. Zubia, R. Amezcua-Correa, J. Villatoro. *Compact omnidirectional multicore fiber-based vector bending sensor*. **Scientific Reports.**

Works submitted to national or international conferences (sorted by year):

- J. Villatoro, **A. Ortega-Gomez**, J. Zubia, J. E. Antonio-López, A. Schülzgen, R. Amezcua-Correa. *Ultrasensitive vibration sensor based on an asymmetric*

multi-core optical fiber. **Optical fiber sensors (OFC)**, Lausanne, Switzerland (2018), poster.

- J. Amorebieta, G. Durana, **A. Ortega-Gomez**, R. Fernández, J. Velasco, I. Sáez de Ocáriz, J. Zubia, J. E. Antonio-López, A. Schülzgen, R. Amezcua-Correa, J. Villatoro*. Strongly coupled multi-core fiber-based interferometer for high temperature sensing*. **SPIE Optics + Optoelectronics**, Prague, Czech Republic (2019), talk.
- J. Amorebieta, **A. Ortega-Gomez**, G. Durana, R. Fernández, J. E. Antonio-López, A. Schülzgen, J. Zubia, R. Amezcua-Correa, J. Villatoro. *Twin cascaded multicore fiber interferometer for optical sensing with enhanced sensitivity*. **Optoel 2019**, Zaragoza, Spain (2019), poster.
- J. Zubia, M. Azkune, **A. Ortega-Gomez**, I. Ayesta, E. Arrospide, G. Durana, I. Bikandi. *Measuring the polymer optical fiber refractive index with a confocal Raman microscope*. **Optoel 2019**, Zaragoza, Spain (2019), poster.
- **[INVITED TALK]** J. Zubia, M. Azkune, **A. Ortega-Gomez**, I. Ayesta, E. Arrospide, G. Durana, I. Bikandi. *A new method for measuring the refractive index profile on POFs with a confocal Raman microscope.* **The 28th International Conference on Plastic Optical Fibers**, Yokohama, Japan (2019).
- J. Amorebieta, **A. Ortega-Gomez**, G. Durana, R. Fernández, J. E. Antonio-López, A. Schülzgen, J. Zubia, R. Amezcua-Correa, J. Villatoro. *Highly sensitive orientation and amplitude discerning vector bending sensor based on asymmetric multicore fiber*. **OSA Advanced Photonics**, Montreal, Canada (2020), talk.

Appendix 1. Optical setup used in the experiments

All the experiments shown in this thesis related to the optical fibers were conducted with the setup depicted in Figure 63 (see photographs in Figure 64). Such set-up allows measuring the absorbance from AuNPs immobilized in the facet of the optical fiber. The setup consists of a simple light-emitting diode (LED), a fiber optical coupler (FOC), and a spectrometer. As it can be appreciated, simplicity, portability, and versatility are the most relevant features of this setup. Regarding the versatility, it was demonstrated with the experiments shown in Chapter 2 about the impact of the optical fiber in the AuNPs immobilization process. In this case, only by modifying the FOC it was possible to measure different optical fibers. Thus, two MMFs with a core of 105 µm and 50 µm of diameter (FG105LCA, Thorlabs) and (FG050LCA, Thorlabs) respectively, were used with their corresponding FOCs, (TM105R5S1A, Thorlabs) and (TM50R5S2A, Thorlabs) respectively. The other fiber used in Chapter 2 was a SMF that works in the visible range with a diameter of 2.5 µm (460HP, Thorlabs) and the FOC used was (TW560R5F2, Thorlabs).

The LED (MCWHL5) was selected in order to match its operating range with the resonance wavelength of the AuNPs. Thus, the LED was a white light source that emits from 400 to 700 nm. The spectrum of the LED is depicted in Figure 65. The working principle of the setup is as follows: The LED injects the light to the optical system, and it arrives at the end face of the optical fiber through the FOC. The facet of the optical fiber act as a low reflectivity mirror, and passes again through the FOC, arriving finally at the spectrometer (Avantes, mini2048-VI25).

To obtain the LSPR spectrum from the AuNPs attached on the optical fiber facet, the following expression is applied:

$$A = -log\left(\frac{S-D}{R-D}\right) \tag{18}$$

where S is the recorded spectrum when AuNPs are immobilized, R corresponds with the spectrum before the AuNPs immobilization, or in other words, when there are no AuNPs onto the optical fiber facet, and finally, D is the recorded spectrum when the LED is switched off.

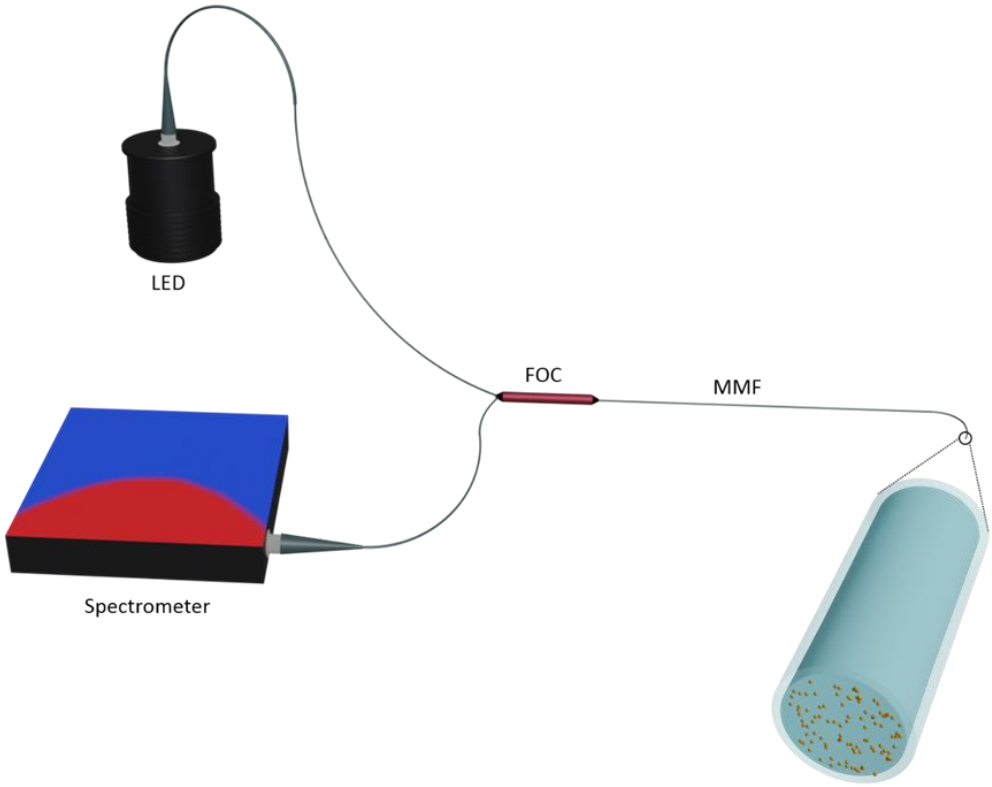

Figure 63. Scheme of the setup used for the experiments conducted in the thesis.

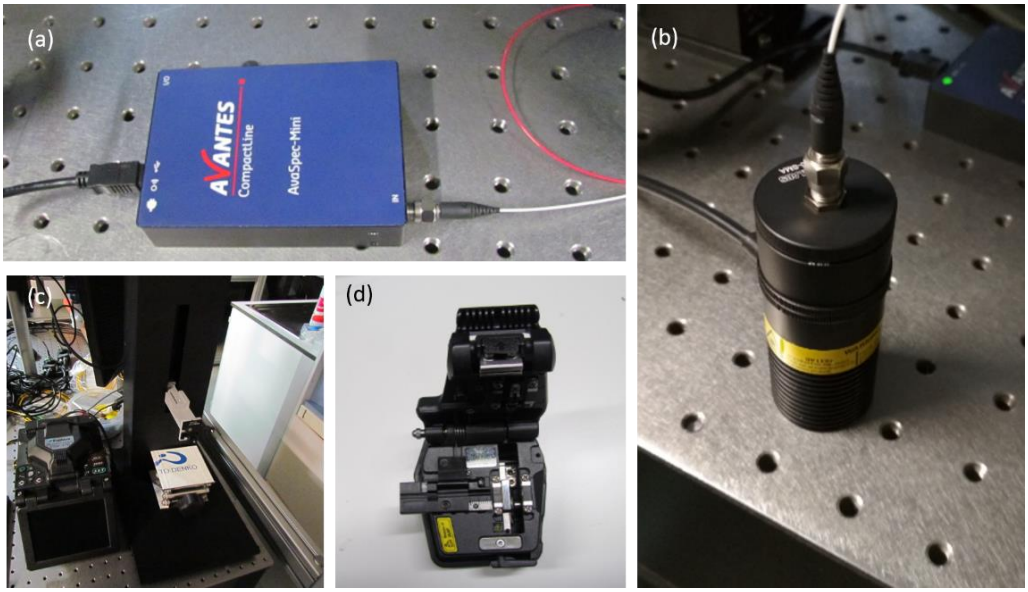

Figure 64. Photographs of the parts used in the optical setup. (a) The spectrometer, (b) LED, (c) splicer and (d) cleaver.

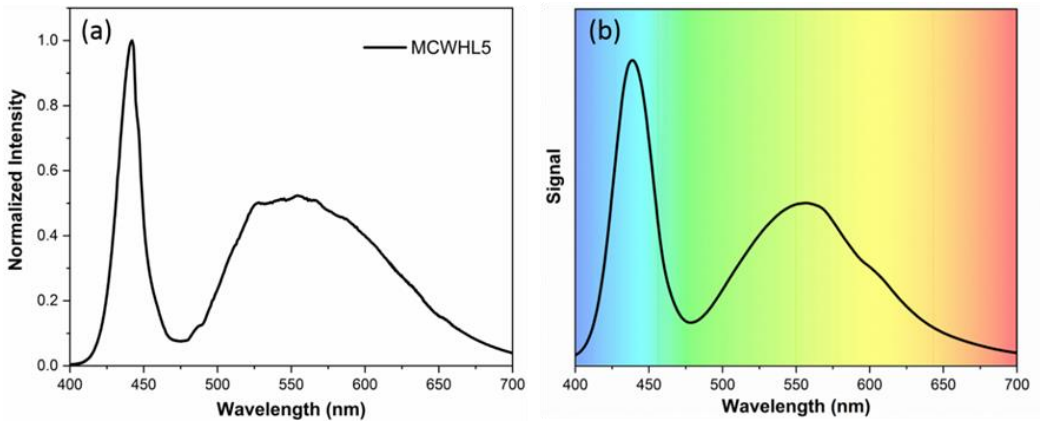

Figure 65. (a) Spectrum of the LED purchased from Thorlabs (Germany). (b) Reflection spectrum that was recorded with the bare fiber without any AuNPs attached to its facet.

Appendix 2. X-ray photoelectron spectroscopy

X-ray photoelectron spectroscopy (XPS) measurements were done in order to demonstrate the complexation of Cu^{2+} ions by AuNPs-TMSen. Due to problems in the XPS setup and the size of the optical fiber, the experiment was conducted in a slide of glass. In order to be sure about the reliability of the results in this glass slide, such slides were chemically modified with the same protocol followed to modify the optical fibers. The modified slides were immersed with milliQ water of 10^{-4} M of $CuCl_2$ for 5 minutes. Then, the slides were rinsed with isopropanol:water 1:1, let it dry and measured. The equipment utilized for XPS was a SPECS (Berlin, Germany) system equipped with a Phoibos 150 1D-DLD analyser. In addition, the monochromatic radiation source Al Kα (1486.7 eV) was used.

First, an initial analysis was conducted to determine the elements in the sample (wide scan: step energy 1 eV, dwell time 0.1 s, pass energy 80 eV). Then, it was carried out a deeper analysis of the detected elements (detail scan: step energy 0.08 eV, dwell time 0.1 s, pass energy 30 eV) with an electron beam angle of 90º. Finally, spectra were processed with the Casa XPS 2.3.16 software. As s conclusion, we can determine that the XPS signals obtained in the experiment demonstrated the presence of Cu^{2+} ions only after the incubation with the metal salt solution.